Departament d'Enginyeria Mecànica
UNIVERSITAT POLITÈCNICA DE CATALUNYA

Detection of Failure Mechanisms of Tool Steels by means of Acoustic Emission Technique

by

Eva Martínez González

Supervised by:

Dr. Jordi Romeu Garbí

A Thesis submitted for the

Degree of Doctor of Philosophy of Mechanical Engineering

in the

Escola Universitària d'Enginyeria Tècnica Industrial de Barcelona,

Mechanical Engineering Department

Universitat Politècnica de Catalunya (UPC)

September, 2013

ôIn theory, theory and practice are the same

In practice, they are notô

Albert Einstein

TABLE OF CONTENTS

ABSTRACT

This thesis is focused on the calibration of the Acoustic Emission (AE) technique to detect and identify damage mechanisms in tool steels. The AE measurement procedure has been calibrated for two mechanical tests: fracture test (three-point bending test) and indentation test (spherical indentation).

Fracture tests cause cracks due to tensile stress. The damage begins with the nucleation of cracks (cracking carbides and local plastic deformation) and afterwards, the cracks spread through the metallic matrix following the broken carbides. This research proposes a filtering process to detect each stage of fracture: the cracking of carbides (nucleation), the stage where the crack passes through to the steel matrix and final catastrophic failure.

Spherical indentation tests enable the creation of a more complex distribution of stresses in an affected part of the specimen. Applying low level loads, an elastic field was created in the specimen under the ball indenter. Nevertheless, AE activity was detected in this elastic field, and these signals were related to the breaking of carbides located in the zone of maximum shear stress. An important feature of this test is that the cracking of carbides takes place without plastic deformation, and therefore the damage signals were clearly identified with carbide breakage.

In both tests, carbide breakage was confirmed by means of AE as the cause of nucleation of cracks in tool steels. AE made it possible to identify the carbide breakage and the propagation of cracks through the metallic matrix and predict the final fracture of the specimen in bending tests. This thesis proposes a new acquisition and filtering configuration in fracture tests to eliminate spurious signals due to contact damage between the specimen and machine supports, as a methodology for identifying different damage mechanisms in small-sized specimens based on certain AE waveform features. From the standpoint of research into materials, coupling the proposed AE setup in each test significantly improves the tests, since it permits the evolution of the damage to be identified during the loading cycle. The laboratory results obtained endorse the possible use of AE in preventive maintenance in the tool-shaping industry.

ACKNOWLEDGMENTS

Firstly, I would like to express my gratitude to Dr. Jordi Romeu, director of my thesis and chief of the Laboratori of Acoustic and Mechanical Engineering (LEAM), for his continued support and help in the fulfillment and finalization of this research work. Your insistence and encouragement have been essential during this time, and I thank you for your never-ending knowledge, motivation and attention. I appreciate that a few years ago you invited me to be part of your research group. Thank you for all the conversations that we have had, they always helped me to see another point of view.

I would also like to acknowledge the CTM (Technological Center of Materials) the opportunity to work in their facilities. And especially to the people I have had the pleasure to work with. I would like to express my gratitude to Dr. Daniel Casellas, chief of the Materials Technology Area at the CTM for his trust in me and in the Acoustic Emission technique. I would like to thank my colleagues in experimentation at the CTM, with very different scaled points of view: ónanoô in case of Nuria Cuadrado, ómicroô of Dra. Giselle Ramirez and ómacroô of Dra. Ingrid Picas. Notably, I would thank novel Dra. Ingrid Picas, who spent with me most of the hours in the lab. We shared the hardest moments of experimentation, those in which the hours pass without any results, and the best moments when we understood the ócalkô of carbides.

I appreciate José Martínez Jecquier of NDT Ingenieros S.A. for the conversations about acoustic emission and the required equipment. Thank you for your time, patient and support whenever I need them. Also, I would like to express my gratitude to Dr. Adrian Pollock of Mistras Group, who responded to an unusual request, who helped me in a bad moment and shared with me his passion for acoustic emission. Thank you for taking time to help me and tell me who is who in the small family of AE.

I want to thank my fellows of the EUETIB, with whom I share my day to day. They always encouraged me to advance with the thesis listening to me in my bad and good moments.

Finally, I would like to thank all those numerous people, whose names are not mentioned, but whose support is greatly appreciated. All these people alien to my professional world that now they know what Acoustic Emission is.

Sincere thanks to all of you,

Eva Martinez

GLOSSARY OF SYMBOLS

a	Radius of contact between ball indenter and specimen in spherical indentation test
A	Amplitude
AE	Acoustic emission
AET	Acoustic emission technique
AHSS	Advanced high strength steels
$AF_{i,j}(k)$	Average amplitude in the frequency domain of the signal, where i where i is related with the time segment, j with the origin of the source and k defines the frequency segment.
AR	Aspect ratio
AR_i	Amplitude ratio i, is the ratio of $AT_{2,j}$ to $AT_{3,j}$
$AT_{i,j}$	Average amplitude in the time domain of signals, where i where i is related with the time segment and j with the origin of the source.
CLSM	Confocal laser scanning microscope
CM	Confocal microscope
$CNTS$	Counts
D	Duration
D_{max}	Maximum diameter

D_{min}	Minimum diameter
DDT	Duration discrimination time
DT	Destructive testing
E	Youngôs modulus
ECD	Equivalent diameter
En	Energy
f	Frequency
Fe_{α}	Alpha iron or ferrite
Fe_3C	Iron carbide or cementite
FHCDT	First hit discrimination time
$H_{i,j}$	Refers to a classification of the signals, where *i* is related with the time segment and *j* with the origin of the source.
HRC	Hardness Rockwell C
HV1	Hardness Vickers
k	Define the frequency segment of a signal
K_{1C}	Fracture toughness of carbides
LEFM	Linear elastic fracture mechanism
NDT	Non-destructive testing
OM	Optical microscope
p	Indentation stress
p_0	Mean contact pressure
p_{γ}	Indentation stress that generate plastic deformation
P	Load
P_c	Critical load

P_γ	Load at yield point
PM	Powder metallurgy
r_0	Radius of circular cracks in spherical indentation test
R	Indenter ball radius
ReT	Rearm time
RMS	Root mean square
RT	Rise Time
S1	Sensor 1
S2	Sensor 2
S3	Sensor 3
SBR_j	Spectral Bands Ratio i, is the ratio of $AF_{i,j}(1)$ to $AF_{i,j}(2)$ for i=1
SF	Shape factor
t	Time
Thr	Threshold
TS_i	Time segment i
wt%	Weight percent
ε	Strain
$\mathring{\sigma}$	Applied normal stress
$\mathring{\sigma}^R$	Bending strength
$\mathring{\sigma}^{RC}$	Carbide tensile fracture stress
τ	Applied shear stress
τ^{RC}	Carbide shear fracture stress
υ	Poissonôs ratio
γ	Sphericity

LIST OF FIGURES

LIST OF TABLES

Chapter 1: Introduction and overview

1.1. Introduction

Tool steels are widely used in the manufacture of tools for punching, cutting, shaping, stamping, cold extruding, etc. These are repeatedly subjected to high stress during service. These steels must exhibit very high strength, hardness and wear resistance. These properties are antagonistic with high fracture resistance or toughness. Thus, tool steels are very sensitive to fracture if stresses during service or manufacture exceed those which the microstructure can support.

Hardness

Tool steels are, in general, high carbon content steels that are hardened by heat treatment consisting of quenching and tempering. Higher steel hardness is obtained by quenching in the martensite phase, which is a supersaturated solution of alpha-iron (Fe_α). They are usually alloyed with other elements to improve their mechanical properties. In the quenching treatment the alloyed elements form carbides [1-3].

Carbides are very hard substances embedded in the mass of the steel in form of precipitations. The presence of carbides in the steel structure is ensured when the content of dissolved carbon in austenite increases above the required solubility limit for subsequently forming enough martensite during the hardening treatment. The supersaturated carbon solution diffuses to form other carbides during tempering. By adding alloying elements such as chromium, molybdenum, vanadium, tungsten, titanium, etc., the iron carbide (Fe_3C) is transformed into other harder carbides. The level of hardness depends on the nature of the carbides present.

Wear resistance

Another important feature of tools is the period of time during which their working parts are maintained in good condition. Therefore, it is crucial to delay the progressive wear of tools in service. Wear resistance is a difficult phenomenon to analyze given the large number of influencing factors, for example:

- the amount of carbides present in the steel structure,
- hardness after quenching and tempering,
- the type of friction (dry or wet) between the tool and the material being worked,
- the frictional coefficient between both materials,
- the distribution, hardness, shape and volume of carbides.

Toughness

Toughness means the ability of the material to absorb energy and undergo plastic deformation without fracturing. This energy, in the case of tools, has to be compensated more elastically than plastically, to prevent permanent deformations. This accuracy means that heavy-duty tools have a higher yield point if they have to work under important loads.

The toughness depends on the structure and chemical composition of the steel. A high carbon content and a large amount of carbides implies high hardness and wear resistance, but significantly reduces toughness after heat treatment.

1.1.1. Fracture mechanisms of cold-work tool steels

Material fracture is the separation of the solid into two or more parts. Tool steels are very sensitive to fracture if the stresses exceed those which the microstructure can endure. The fracture process can be divided into three stages:

i) crack formation (nucleation),
ii) crack growth (propagation) and
iii) final fracture.

The fracture can be ductile or fragile. Both are produced when the stress exceeds the maximum resistance of the material, but the damage mechanisms occurring prior to the fracture are different. Normally, the fractured surfaces show a combined ductile and brittle fracture.

A ductile fracture is characterized by generalized plastic deformation preceding the final fracture. The cracks advance slowly while the applied stress is increased (established cracks). Some of the energy from stress concentrations at the crack tips is dissipated by plastic deformation before the crack propagates. Due to that, this fracture presents great energy absorption. By contrast, brittle fracture is characterized by rapid crack propagation without any appreciable plastic flow previous to fracture and the energy absorption is very scant.

A ductile fracture is a strain-controlled fracture that occurs due to the deformation-induced nucleation and growth of micro-voids around the hard particles. The ductile fracture resistance of

tool steels tends to be low due to the high hardness of the martensitic matrix obtained during the heat treatment and the large density of carbides, as is stated above, are very hard and brittle particles built into the tool steel microstructure. Operating loads within the recommended limits and below the proportional tensile or shear strength of properly process tool steels do not initiate ductile fracture. However, factors such as overloads, stress concentrations, surface flaws or the non-uniform distributions of coarse carbides may significantly reduce the resistance of a tool steel and this type of fracture can appear.

A brittle fracture is a stress-controlled fracture that occurs with little or no plastic deformation. Frequently, the stresses that cause a brittle fracture are well below those expected to form ultimate tensile strengths. A brittle fracture may be initiated by cleavage cracks in the hard particles or in their boundaries, which in turn lead to unstable cleavage crack propagation in matrix structures with low toughness (Figure 1.1).

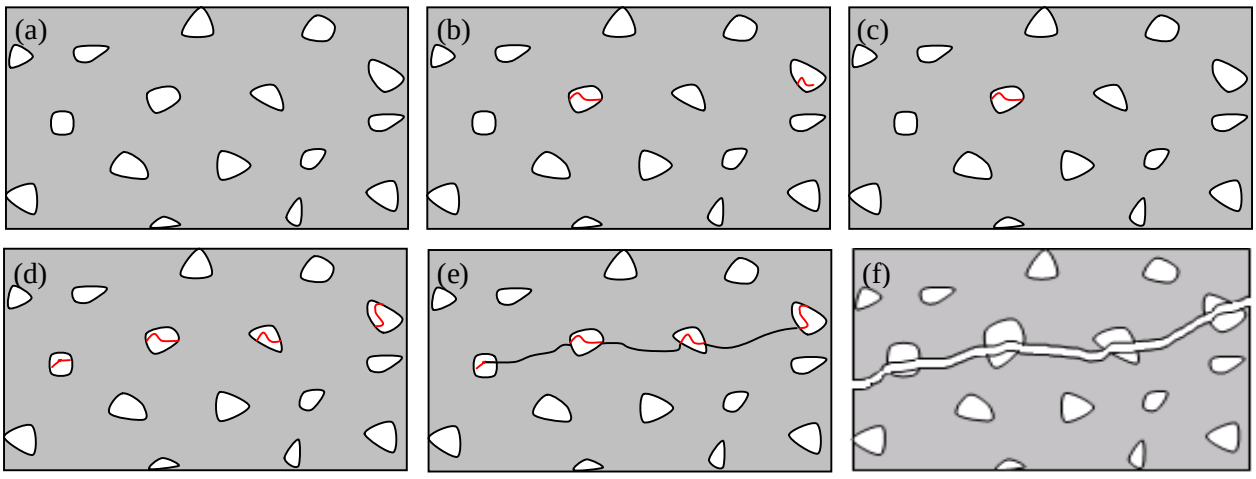

Figure 1.1. Schematic representation of a tool steel fracture: (a) schema of the material composition (carbides embedded in the metallic matrix), (b) cleavage of a carbide, (c) and (d) cracks of more carbides, (e) propagation of a crack in the metallic matrix following the cracked carbides and (f) final fracture of the specimen.

Moreover, polycrystalline metal fractures may be transgranular or intergranular (Figure 1.2), depending on whether the crack propagates through the grains or follows their boundaries [4].

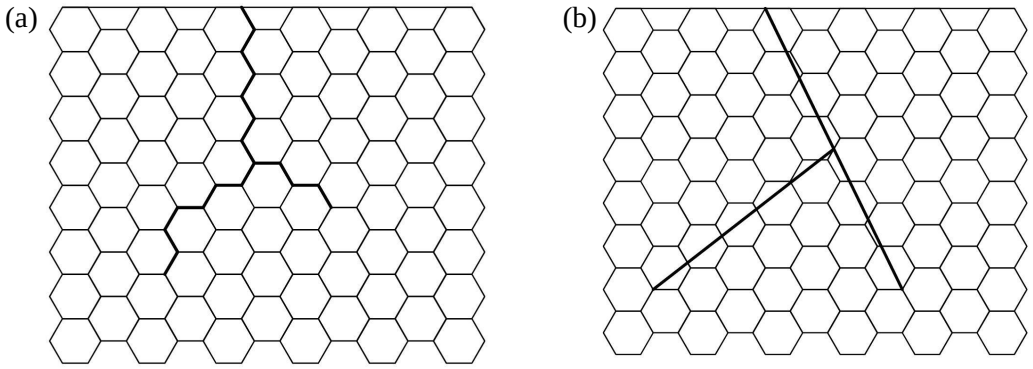

Figure 1.2. Schematic representation of: (a) an intergranular crack and (b) a transgranular crack.

Intergranular fractures are related to the size of the grains, with phosphorous segregation on the austenitic crystals boundaries and precipitation of cementite in the grain boundaries. Thus, in the heat treatment it is desirable to obtain a fine grain austenitic matrix and a homogeneous dispersion of carbides. In tool steels, and other high carbon steels, the most common mechanism of brittle fracture is intergranular cracking along the austenitic grain boundaries initiated in the broken carbide or in its decohesion (Figure 1.2(a)).

Therefore, the fracture resistance of these materials is related to the size of the dispersed particles in the martensitic matrix. Two types of particles which influence the fracture are: carbides and inclusions (nonmetallic elements that are introduced into the steelmaking process). Their large size, high densities or non-homogeneous distribution contribute to premature failure of the tools. The size and shape of these particles also play an important role in resistance, for example, elongated particles or flattened shapes introduce anisotropy into the properties of steel [5,6]. Likewise, irregular shapes can act as stress concentrators.

1.1.2. Conventional methods for the failure mechanisms study

To improve the mechanical performance of materials and components a study of fracture mechanics is important. With this aim, several mechanical tests can be performed. These tests are classified into Destructive Tests (DT)) and Non-Destructive Tests (NDT), depending on whether the specimen is modified or not during the test, respectively. Normally, both are required in combination for the study of a material.

Some of the most common NDT are listed below with their limitations [7]:

- *Visual inspection, microscopy and surface analysis*. It can be relatively easy to apply if the expected defect is on the previously polished surface of the specimen. But it is more difficult when the flaw is inside the specimen, and this must be cut so that the flaw appears on the new free surface.
- *Liquid penetrants:* This technique reveals discontinuities open to the surfaces of solid and nonporous materials. Indications of a wide variety of discontinuity sizes can be found regardless of the configuration of the test object and regardless of the discontinuity orientation. The liquid penetrants seep into various types of minute surface openings by capillary action. The cavities of interest may be very small and often invisible to the naked eye.
- *Electromagnetic methods* based on the electromagnetic properties of a material. These techniques are widely used for identification or differentiation purposes in a wide variety of physical, structural and metallurgical conditions in electrically-conductive ferromagnetic and non-ferromagnetic metals.
- *Radiographic Testing.* This is based on the test objectõs attenuation of penetrating radiation ï either electromagnetic radiation with a very short wavelength or particulate radiation (X-

rays, gamma rays and neutrons). Different portions of an object absorb different amounts of penetrating radiation due to differences in density and variations in the thickness of the test object with differences in absorption characteristics caused by variation in composition. This variation in the attenuation of the penetrating radiation can be monitored by detecting the nonattenuated radiation that passes through the object. It is a very costly inspection method.

– *Ultrasonic testing*. In this technique ultrasonic wave beams are introduced into a material for the detection of surface and subsurface discontinuities. These waves travel through the material with some energy loss (attenuation) and are reflected and refracted at the interfaces. The echoes are then analyzed to define and locate discontinuities.

All these methods can be combined with destructive testing to inspect the damage occurring in the material. Depending on the mechanical test and inspection method, two situations can arise:

a) The specimen must be modified to inspect and evaluate the damage. In this case, only the final flaw can be evaluated but not its evolution.
b) The specimen can be inspected without being destroyed (for example, for surface flaws or using techniques that allow the interior of the material to be inspected). In this case, it is possible to load the specimen, stop the test, evaluate the damage generated and re-load it again to repeat the strategy as often as necessary to ascertain the evolution of the flaws during the test. Obviously, it is a long and arduous process.

Another NDT method which is not as common is the Acoustic Emission (AE) method. It is based on the detection of stress waves produced by sudden internal changes in stressed materials. The sudden movement generates waves that radiate out into the test object and can be detected on the surface of the specimen. This technique is ideally applied during a controlled loading test

since the increasing flaws are the source of the stress waves; thus it is possible to identify the flaws in the sites where they are produced.

1.1.3. Acoustic Emission

1.1.3.1. Overview

In many technical articles or commercial presentations, AE is described as a new technique. In actual fact, very few technologies can be advertised as ñnewò, and most of them have been known and used since ancient times in a primeval state. The novelty probably lies in the increase in present knowledge, the way in which these technique are applied or the areas in which they are actually used. This is the case of AE, which is apparently a new emerging technique within NDT. But it has been used and known since the earliest civilizations which used it as a forecasting tool. It is logical, since many natural phenomena are audible; for example, water in freezing, earthquakes or a broken branch, *etc*. Probably, one of the first practical uses of AE was made by pottery makers to assess the structural stability of ceramic pieces, paying attention to the sounds emitted during the cooling process in the even.

The first documented observation of AE in metal was during twinning of pure tin as early as 2600 b.C. The first text documenting this phenomenon was written by the Arabian philosopher and alchemist Abu Musa Yabir al-Sufi Hayyan (721-815 a.C.); his latinized name was Gerber. His publication describes that tin (*Jupiter*) emits a loud noise, and he also described iron (*Mars*) as ñsounding muchò during forging [8].

Historic texts exhibit many references and observations of this phenomenon, but the first modern technique studies date from 1950, when the German engineer Joseph Kaiser presented his thesis at Munich University [9]. He studied the sounds produced in metallic materials

submitted to tension. In his thesis, he presented the work now known as ñKaiser Effectò [10], a fundamental principle in the study of damage to materials. Since then, different works, studies and publications have been written due to the large number of applications and situations permitting the use of this technique. Between 1960 and 1980, despite equipment limitations, several pioneer researchers such as Dunegan [11], Pollock, Wadley, Scruby, Birchon, Schofield, Beattlie, Proctor, Harris and Ono issued considerable scientific production in order to make progress in this field [12]. Some of them, who are currently still active, are members of working groups on AE and specialized journal editors. The works that they have written are currently being revised due improved equipment which permits the forwarding and validation of the previous theories.

But it is from the late 1990s that AE was reborn through the emergence of a number of interesting research studies in this field from different areas. The growing interest in AE is due, in part, to the significant advances that have taken place in microelectronics and computer-assisted analysis techniques in recent years. Powerful storage technologies and the analysis of big data are necessary.

There are several lines of research related to AE with important scientific production. On reviewing the technical publications of recent years, interest is distributed into the following areas:

- Development of sensors, equipment and acquisition systems.
- Research and application of AE in the study of materials (metals, polymers, composites, ceramics, construction materials, biomaterials, *etc.*)
- Search for new applications and the adequacy of their techniques: biomedical engineering, medical diagnosis of certain conditions, *etc*.

- Large structures: bridges, railway structures, pressure vessels, *etc*.
- Study of AE waves.
- Application of AE as a preventive maintenance tool in machines or in their elements.

1.1.3.2. The AE technology

The term ácoustic emissionô is used to define both a physical phenomenon and an NDT technology. AE is commonly defined as transient elastic waves produced by a sudden redistribution of stress within in a material [13]. When a structure is subjected to an extreme external stimulus (change in pressure, load, temperature, *etc.*), internal modifications take place (such as the growth of cracks, local plastic deformation, corrosion, phase transformations, *etc.*). These sources (events) release energy in the form of stress waves into the material, which then propagates as an elastic wave through the material.

For instance, if a pencil is slightly submitted to bending until fracture, the fracture of wood fibers can be perfectly heard. The noise is caused by the stress waves that propagate through wood and air. In this case, the waves are generated at frequencies within the audible range. There are some even less audible acoustic emission examples, such as wood fracture, ice cracking, tearing of paper, etc. Normally, AE signals are inaudible. Rapid stress-releasing events generate a spectrum of stress waves starting at 0 Hz which usually fall off at several MHz. The most interesting sources released energy of between 1 kHz and 1 MHz [14].

AE or AET (Acoustic Emission Technique) such as NDT is based in this phenomenon. In this test, waves generated by an AE source are detected by means of the appropriate sensors attached to the surface that convert the surface movements into electrical signals. With the right

equipment and setup, motions with the accuracy of picometers (10 -12 pm) can be detected. Figure 1.3 shows a schematic principle of the technique.

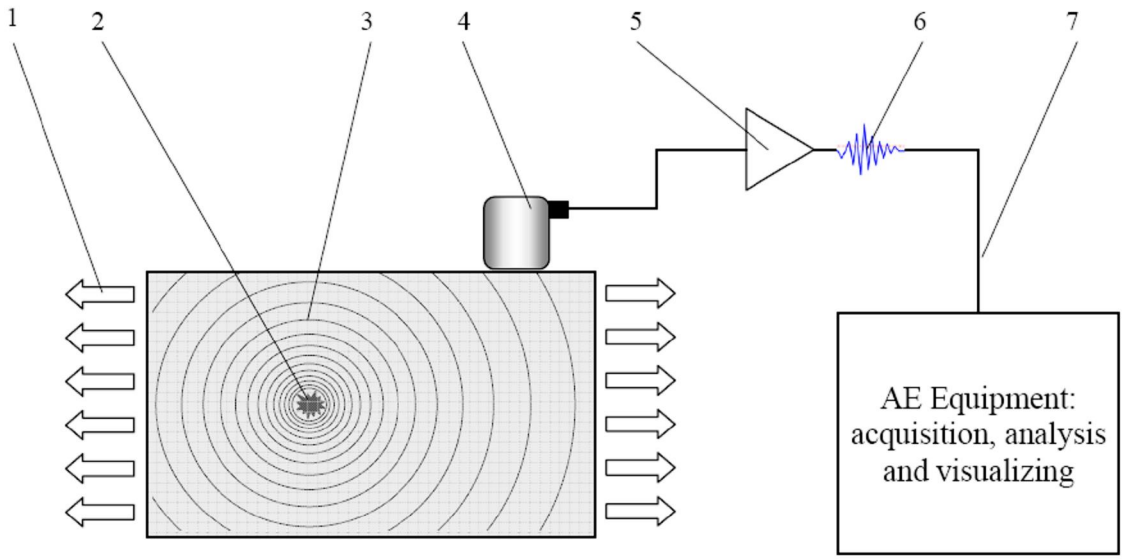

Figure 1.3. Schematic principle of AE wave detection: 1. Stimulus; 2. Growing discontinuity (AE source); 3. Structure or specimen; 4. AE waves; 5. AE transducer; 6. Pre-amplifier; 7. Output signal.

The three major uses of the AE technique are: i) source location, ii) characterizing of materials (mechanical performance and damage evaluation) and iii) health monitoring of structures and machines [15-18].

AE can be related to an irreversible release of energy and it can also be generated from sources not involving material failure, including friction, cavitations and impact.

Other NDT (radiography, ultrasounds, eddy currents, *etc.*) detect geometrical discontinuities, introducing some form of energy into the studied structure. In contrast, in AE the self-generating flaws emit stress waves that can be detected at a certain distance by the appropriate sensors, and the characteristics of the acquired signals are useful evaluating the damage that is occurring within the material.

1.1.3.3. Characteristics of the AE technology

The principal characteristics of the AET are as follows:

- It is a ópassiveô technique; the flaw itself generates the AE wave that can be detected. One of the most advantages of AE is this point, since it permits the test to be executed with minimum effects on the service of the studied part, since no energy is introduced into the system.
- It detects distant AE sources; the maximum distance depends on the material properties.
- It is sensible to the growth of flaws and changes in the material structure, instead of the presence of geometric flaws.
- It is non-invasive.
- It can be applied during service.
- It permits the location of growing discontinuity.

And the main limitations of the technique are:

- As the flaw itself generates the AE signals, their intensity cannot be controlled and the test is unrepeatable.
- Stable discontinuities do not generate AE signals, and so they are undetected by AET.
- Some materials do not emit AE when the previous load applied is exceeded; this is an important phenomenon known as the Kaiser Effect [9-10].
- This method is very sensitive to process noises; before attempting an AE test it is essential to eliminate the unwanted signals.

1.2. Research objectives

The main objective of this thesis is to calibrate the methodology for detecting initiation and propagation damage and cracks in tool steel specimens by means of AE. For the purpose of adapting the AE technique to the study of mechanical behavior in tool steels, the cracks in the specimens are induced by two loading conditions using: i) fracture (three-point bending) tests and ii) spherical indentation tests. Both are normal mechanical tests for the study of fragile materials. AE must be useful in detecting initial damage in the specimen and the critical damage stage that provokes its fracture. This main objective is based on some partial objectives referred in the following paragraphs.

An obstacle for the successful and regular use of the AE method in mechanical tests is noise discrimination. The working conditions of the test machines produce AE signals that are not related to the degradation of the specimen but they are detected by the AE equipment. Unwanted noise, which is associated with the moving parts of the machines and the hydraulic loading system of the test machines, must be systematically distinguished from sounds associated with specimen damage.

A second difficulty that must be resolved in this thesis is related to the small dimensions of the specimens. The mechanical tests are performed with very small specimens due to the high resistance of the studied materials, where the location AE techniques and the discrimination of the signals are confused due to the quasi-instant quantity of wave reflections that are added to the signal. The thesis proposes a methodology for acquiring and analyzing the signals that minimizes the effects of the waveform distortions.

The results reported in this research will provide a technical basis for the effectiveness of the AE method as a complementary diagnosis method during the laboratory testing of these tool steels which will allow the tests results to be fine-tuned.

1.3. Justification

The use of Advanced High Strength Steels (AHSS) in structural automotive components has been increased over the past few years to satisfy the more stringent regulations regarding low CO_2 emissions and high safety performance in vehicles. The high fracture strength of AHSS (from 600 to around 1500 MPa) makes it possible to manufacture lightweight parts with high crash-resistance. Conversely, the high yield stress of AHSS is a main inconvenience during cold forming and cutting processes, since the high loads which are required cause accelerated wear and the premature fracture of the tools [19]. Thus, the development of new tool materials that combine high wear resistance and fracture toughness is required to fully exploit the potential of AHSS. Within this framework, a proper tool steel microstructural design is needed, taking into account the influence of the micro constituents on the fracture event. The size, shape and distribution of the primary alloy carbides embedded in the matrix, as well as their chemical composition and mechanical properties are studied in order to optimize the mechanical response of tool steels [20]. Furthermore, tool failure during the industrial process is expensive due to the high cost of tools and the unproductive time needed to replace them. Thus, AET is a technique which could be used in preventive maintenance of these tools.

AE is a powerful tool for the study of materials, and is specially useful due to its extreme sensitivity to small changes within the material and its ñin-serviceò information. Nonetheless, the

technique has not been widely used in the study of tool steels. It is therefore necessary to address the applicability of the technique in these materials.

This research presents an experimental application of the AE method for identifying fracture mechanisms in tool steels during fracture and contact tests.

Bending tests permit the application of a controlled load to the specimen in order to damage it. During the test the specimen is submitted to tensile stress. Applying different loads, damage severity in the specimen can be controlled. The three-point bending test is useful because the maximum tensile stress is produced on one of the surfaces of the specimen. It permits the observation of the side with the most damage in the microscopy, and it is not necessary to cut the specimen to observe the broken carbides, possible plasticity or incipient cracks. This test makes it possible to correlate the AE signals obtained with the observed damage in the specimen for different load levels.

With the spherical indentation test, an elastic field is generated in the specimen. It is thus possible to crack some carbides without propagating cracks within the material. This enables the isolation of the carbide crack from other mechanisms.

1.4. Thesis overview

The remainder of this thesis is organized into six chapters which are briefly described in the following lines:

- *Chapter one* is an introduction to the thesis. It contains general information about tool steels damage mechanisms and their detection. The objectives and justification of this thesis are also presented.
- *Chapter two* is related to steel characterization by means of the three-point bending test. This chapter is subdivided in three parts: i) identification of initial damage in specimens with a typical AE setup, ii) experimental procedure for eliminating background noise and problems due to reflections and iii) the results of identifying the damage mechanism, including the identification of nucleation and crack growth by the steel matrix, and demonstration of the order in which they occur and the stress level that takes place.
- *Chapter three* explains the results obtained with a spherical indentation test to identify the cracking of carbides due to shear stress.
- *Chapter four* contains a discussion of the key findings in this study.
- *Chapter five* presents suggestions for future research.

1.5. References

[1] Martínez Baena, M.A. and Palacios, J.M.; Algunas consideraciones sobre los aceros de herramientas, su utilización y tratamiento térmico. *Tratamientos Térmicos*, Nr.83, pp. 34-47, June 2006.

[2] Donald R. Askeland. *Ciencia e ingeniería de los materiales.* Ed. Paraninfo, 2001. ISBN 9788497320160.

[3] William D. Callister Jr. *Materials science and engineering: an introduction.* 8th ed. John Wiley & Sons Ltd., 2009. ISBN-10: 0470419970.

[4] F.J. Gil Mur and J.M. Manero Planella. *Metalografia.* Barcelona: Edicions UPC, 2005. ISBN: 8483018047.

[5] Okolovich, G.A.; Tool steels for cold working dies. *Metal science and heat treatment*, Vol. 48, Nr. 5, pp. 233-239, 2006.

[6] G.A. Roberts, G. Krauss and R. Kennedy. *Tool steels.* 5th ed. Metal Park (OH, USA): ASM International, 1998. ISBN: 978-0-87170-599-0. pp. 325-327.

[7] Gary L. Workman and Patrick C. Moore (eds.). *Nondestructive testing Handbook, volume 10.* 3th ed. Columbus (OH, USA): ASNT, 2012. ISBN: 978-1-57117-187-0.

[8] Drouillard, T.F.; A history of acoustic emission. *Journal of Acoustic Emission.* Vol. 14. Nr. 1, pp. 1-34, 1996.

[9] Kaiser, J. *Untersuchungen uber das auftreten gerauschen beim zugersuch (An investigation into the occurrence of noises in tensile test or a study of acoustic phenomena in tensile test)*. PhD. Dissertation Technische Hoschuschule Munchen. Munich (Germany).

[10] PATENSCHRIFT Nr. 852771 (1952) ñMaterialprüfverfahrenò. Dr. Ing. Joseph Kaiser.

[11] Dunegan, H.L.; Harris, D.O.; Tetelman, A.S.; Detection of fatigue crack growth by acoustic emission techniques. *Materials Evaluation.* Vol. 28, Nr. 10, pp. 221-227, Oct. 1970.

[12] Halford, K.M. and Worden, K.; Special issue guest editorial on acoustic emission. *Journal of Strain Analysis*, Vol. 40, Nr. 1, Editorial, 2005.

[13] CEN. *EN 13554:2002* Non-destructive testing. Acoustic emission. General principles. April 2002.

[14] Scruby, C.B.; An introduction to acoustic emission. *Journal of Physics E: Scientific Instruments.* Vol. 20, Nr. 8. pp. 946-953, 1987.

[15] Ono, K.; Current understanding of mechanism of acoustic emission. *Journal of Strain Analysis.* 2005, Vol. 40, Nr. 1, pp. 1-15, 2005.

[16] Christian U. Grosse and Masayasu Ohtsu (eds.) Acoustic emission testing. Basics for research-application in civil engineering. Germany. Springer: 2008. ISBN: 978-3-540-69895-1.

[17] Steel, J.A. and Reuben, R.L.; Recent developments in monitoring of engines using acoustic emission. *Journal of Strain Analysis*. Vol. 40, Nr. 1, pp.45-57, 2005.

[18] Sikorska, J.Z. and Mba, D.; Challenges and obstacles in the application of acoustic emission to process machinery; *Proceedings of the Institution of Mechanical Engineers, Part E: Journal of Process Mechanical Engineering*, Vol. 222, pp. 1-19, February 2008.

[19] Advanced High Strength Steel (AHSS) Application Guidelines Version 3. International Iron & Steel Institute. Committee on Automotive Applications, 2005. Online at www.worldautosteel.org

[20] Casellas, D.; Caro, J; Molas, S.; Prado, J.M.; Valls, I.; Fracture and toughness of carbides in tool steels evaluated by nanoindentation. *Acta Materialia*, Vol. 55, Nr. 13, pp.4277-4286, August 2007.

Chapter 2: Characterization of tool steels by three-point bending test

2.1. Introduction

The interaction between the two main constituents of tool steel microstructures: the primary carbides and the metallic matrix, determines their mechanical properties and hereby, the performance of tools working in industrial applications. A proper comprehension of micro-mechanical mechanism leading to damage in the microstructure prior to failure comprises the identification, localization and quantification of the phenomena being involved in the process when a certain load is applied.

Carbides play an important role determining the mechanical response of these steels since they act as fracture initiation sites. Cracks nucleate form broken primary carbides and grow through the metallic matrix until they attain the critical size for failure [1,2]. Thus, an increase of carbides mechanical properties is expected to raise fracture and fatigue resistances of tool steels. This is why Casellas et al. [3] used nanoindentation techniques to determine the mechanical properties (i.e. hardness, Youngôs Modulus and fracture toughness) of primary carbides embedded in several tool steels. However, as shown by Picas et al. [4], the fracture strength of carbides not only depends on their mechanical properties, but also on their shape, arrangement

and presence of internal defects. Accurate data on the primary carbides fracture strength in tool steels will bring valuable knowledge to light, concerning the global mechanical response of tools. The onset stresses for crack nucleation and growth in tool steel microstructures are rather unknown. To fill this gap of knowledge, this research has used the AE technique during fracture tests (three-point bending tests) in order to cope with the difficulty to identify the applied stresses related to the nucleation and growth of cracks. The three-point bending tests permits easily visualize by microscopy the most stressed surface; this is an advantage over the tensile test which has been more widely monitored by AE.

Fukaura et al. [5] and Yokoi et al. [6] are amongst the few authors who employed this technique to determine the progression of internal damage in tool steels. Fukaura [5] applied AE to determine the stress level at which carbides start to break in a tensile test. Their work showed the relationship between the characteristic AE wave parameters and material damage evolution. The main problem of their work was to relate the AE information with damage in the specimen; since during tensile tests damage occurs inside the specimen. However, as these authors indicated, the use of relatively low frequency sensors (375 kHz) might have had introduced some limitations that could have been avoided by the bending test to their predominant frequency, and correlated continuous low frequency signals to plastic deformation events, while sudden high frequency signals to fracture events. Yokoi [6] determine that carbide cracking could successfully be detected by AE; in his work, the signals started at a certain applied load and the event rates continually increased until reaching the fracture stress. These authors stated that no continuous AE signals existed but that numerous burst emission at close intervals were recorded instead. Yamada and Wakayama [7] observed a rapid increase in cumulative AE energy prior to the final fracture of cermets samples and attributed this phenomenon to the to the main crack formation. They also distinguished two types of AE signals: one was a burst-type signal with

high frequency and the other was a low frequency and continuous-type signal. The former was considered to be emitted form micro-cracking while the latter was due to plastic deformation of the binder phase.

The following sections of this chapter show the results obtained during three-point bending tests monitored by AE. Each of the sections presents a point of view of the problem, showing the results in sequential order as the research advanced. Section 2.2 shows the simplest monitored procedure of bending test in order to identify the initial damage and its evolution. Section 2.3 proposes a new AE filtering process and procedure for monitoring the three-point bending tests that permits to refine the results. Finally, section 2.4 present a classification of AE signals that permits to identify different damage mechanism during the bending test.

2.2. Analysis of fracture resistance of tool steels by means of AE

2.2.1. Introduction

Aimed to a better understanding the role of the microstructural constituents (primary carbides and metallic matrix) in the fracture mechanisms of tool steels, this section is focused on the application of AE in monotonic bending tests to determine the stress levels at which damage appears.

2.2.2. Experimental procedure

2.2.2.1. Specimens

Two commercially available tool steels were selected: DIN 1.2379 (equivalent to AISI D2) and a tool steel named as UNIVERSAL (developed by ROVALMA S.A.). The chemical composition of both can be found in Table 2.2.1. The DIN 1.2379 tool steel shows a ledeburitic microstructure with primary carbides formed during solidification by the eutectic reaction $\Rightarrow \gamma + M_7C_3$ [8]. In UNIVERSAL steel two types of primary carbides are present, one type is M_7C_3 but shows higher Vanadium and Tungsten content than those found in DIN 1.2379, and the second type is MC Vanadium rich and shows increased hardness and toughness values compared to the other types. Properties of these carbides can be found in reference [3]. Carbides in DIN 1.2379 have elongated shapes and are dispersed in the matrix forming bands along the forging direction. In the meanwhile, primary carbides of UNIVERSAL steel are more equiaxed and homogeneously distributed in the matrix [1].

Table 2.2.1. Chemical and mechanical properties of materials DIN1.2379 and UNIVERSAL

Steel	C	Cr	Mo	V	W	HRC
1.2379	1.5 - 1.6	11.0 - 12.0	0.6 - 0.8	0.9 - 1.0	-	60 - 62
UNIVERSAL	0.9 ï 1.2	6.8 - 8.5	-	2.5 ï 3.0	1.1 ï 1.4	60 - 62

Prismatic specimens with dimensions 50x8x6 mm were extracted from forged billets, with the longitudinal axis parallel to the forging direction. The obtained samples were heat treated by quenching in oil and tempering up to a hardness of 60 - 61 HRC (heat treatments can be found scheduled in [3]).

2.2.2.2. *Monitored AE flexion fracture test.*

A three point bending test was used to evaluate the mechanical behavior of specimens. The surface exposed to tensile stress was grinded and polished, and the edges were rounded in order to avoid stress concentration effects. Tests were carried out in a universal testing machine in air at room temperature and the load rate was fixed at 1 mm/s.

Two small magnetic AE sensors were disposed alongside the specimens in order to detect the AE signals. The sensors had a fixed resonance frequency of 700 kHz (VS700D, Vallen System Gmbh). Two pre-amplifiers with a gain 34dB of the same brand were used (EAP4). Signals were recorded and analysed using the Vallen System Gmbh AMSY5 analyser. During the measurements, digital filters of 95-850 kHz were applied.

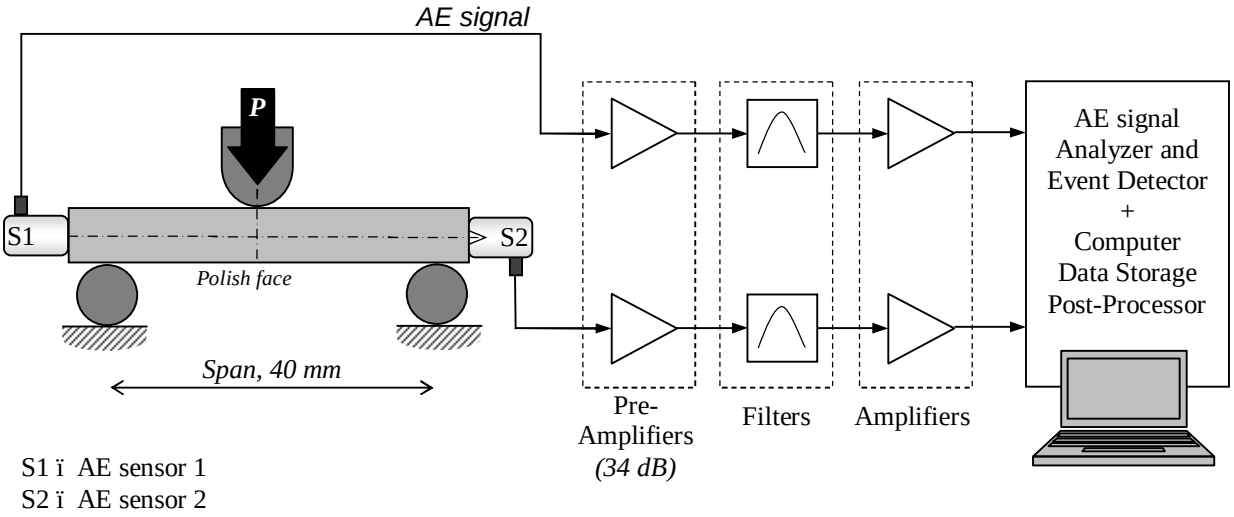

Figure 2.2.1. Diagram of the experimental setup.

2.2.2.3. *Test procedure.*

For each type of tool steel, several bending tests were first carried out up to the end (breakage of the specimen) in order to define the typical AE signal pattern in the fully run test. Later, the tests were paused upon significant changes of the AE signals. However, a maximum load of 70% of the material fracture strength was applied so as to prevent the sensors from being damaged as a consequence of the sudden specimen break. DIN 1.2379 and UNIVERSAL characteristic fracture strength values were determined by Picas et al. and can be found in [1]. At each halt, the surface subjected to tensile loading was examined by means of Optical and Confocal Microscopy (OM and CM) to identify the potential sources in the microstructure responsible for the detected changes in AE signals.

2.2.3. Results and Discussion

The results obtained in the fully run tests are displayed in Figure 2.2.2 and 2.2.3 for DIN 1.2379 and UNIVERSAL respectively. They show the correlation between the applied stress and the AE signal intensity as a function of time.

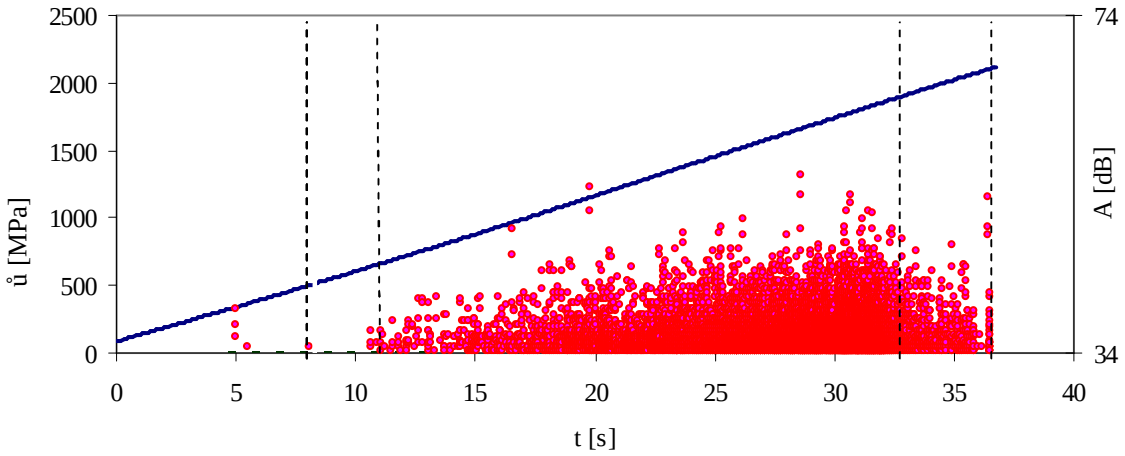

Figure 2.2.2. Bending test results, steel DIN 1.239. Blue line: stress vs. time; red points: EA signals vs. time.

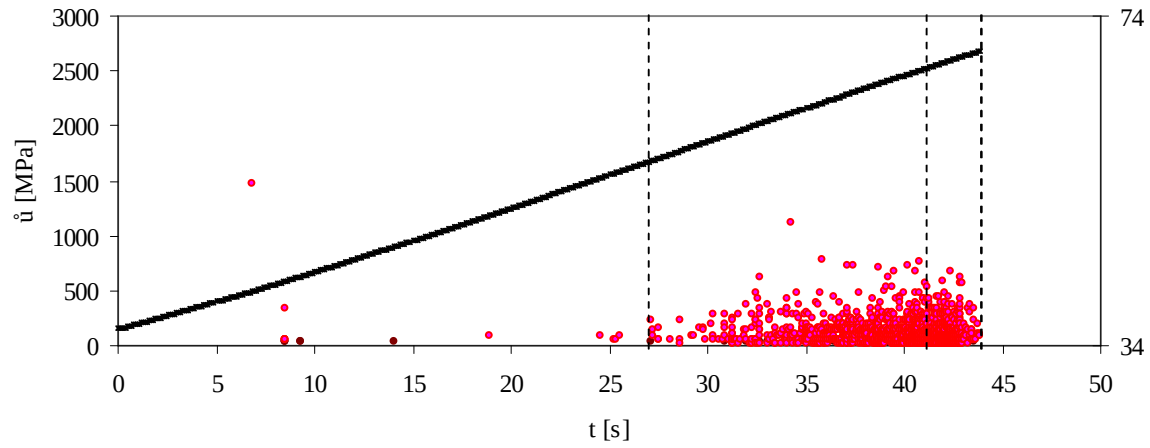

Figure 2.2.3. Bending test results, steel UNIVERSAL. Blue line: stress vs. time; red points: EA signals vs. time.

Both DIN 1.2379 and UNIVERSAL show a similar pattern with regard to the captured AE signals. Three different zones can be distinguished:

First zone

During the first stage of the test, AE signals are almost inexistent. The reason is that the material is under elastic deformation and neither the carbides nor the matrix show fracture or plastic deformation. In other words, once the noise is filtered out, the absence of AE signals can be associated with material linear behavior.

Nonetheless, the detection of a few isolated AE signals could presumably be caused by the fracture of some carbides or a material chip off due to polishing; even though no certainty can be given at this point.

Second zone

In this zone appear the first AE signals. In the DIN 1.2379 they start at approximately 11 s and in the UNIVERSAL at 27 s, which correspond to a stress level of 640 MPa and 1700 MPa respectively. The signals increase gradually in intensity and abruptly in number. During this stage, several broken carbides can be discerned in the steels microstructure. As shown in Figure 2.2.4 and 2.2.5 for DIN 1.2379 and UNIVERSAL respectively, the amount of broken carbides increases considerably with the rising stress. In some cases a small area of plastic deformation appears.

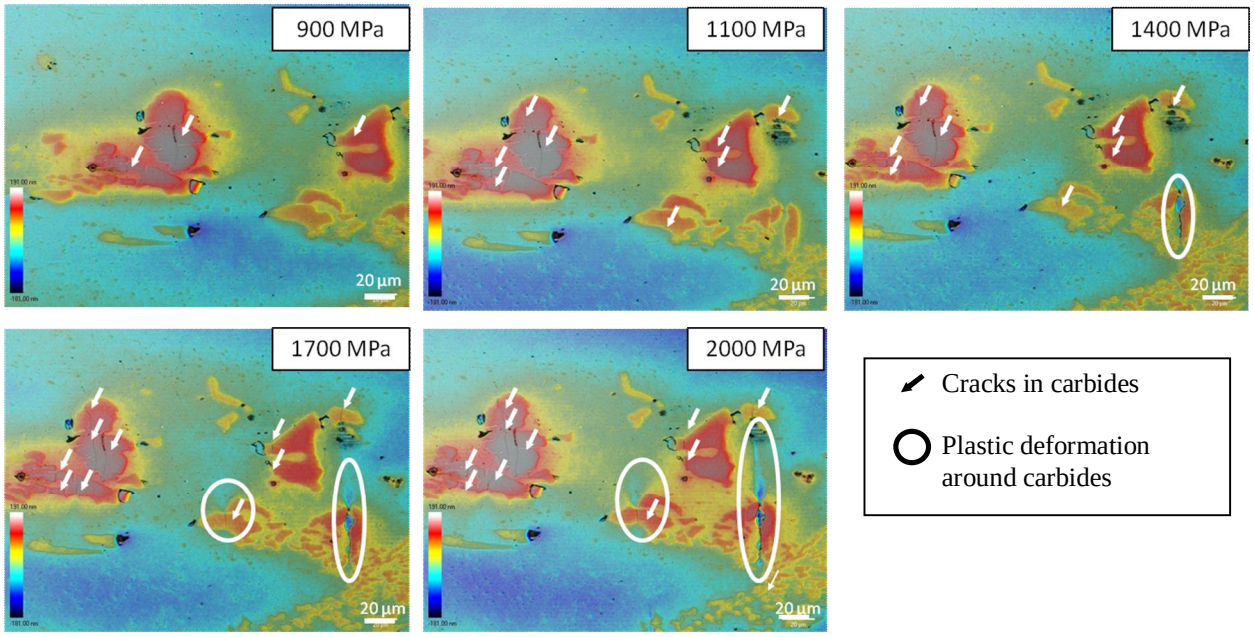

Figure 2.2.4. Example of broken carbides observed by means of CM in the tensile stressed surface of DIN 1.2379 specimens.

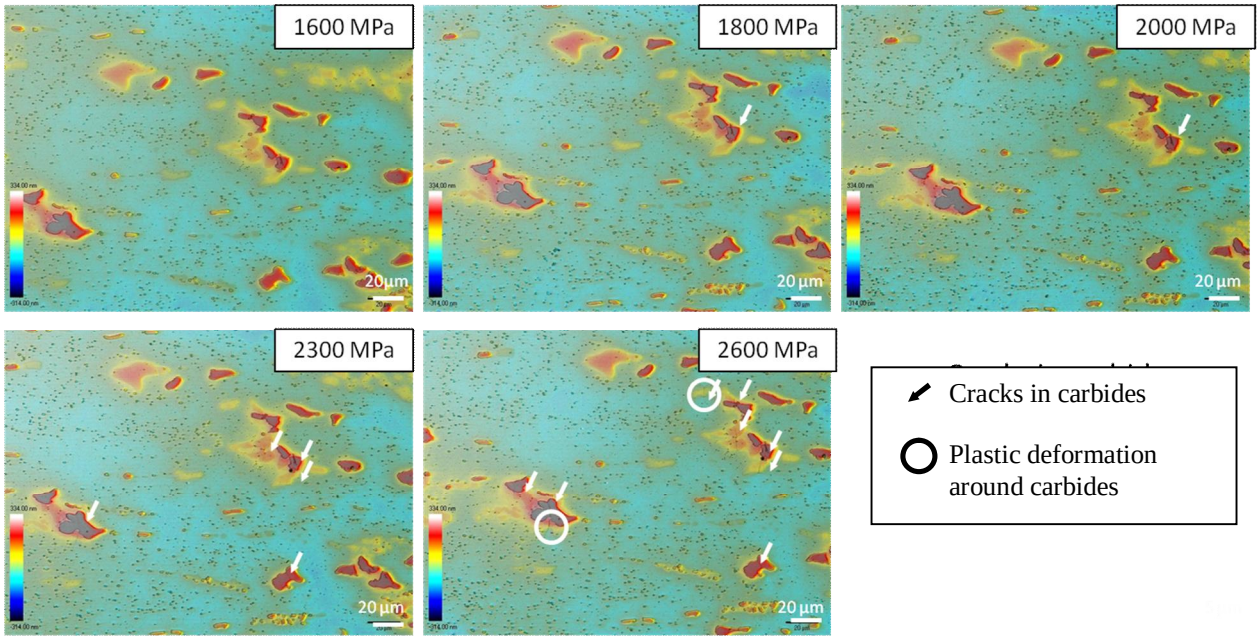

Figure 2.2.5. Example of broken carbides observed by means of CM in the tensile stressed surface of UNIVERSAL specimens.

Third zone

The amounts of registered signals, as well as the cumulated energy, considerably increase. The intensity does not increase but in opposition, the average value shows a slight decrease. At these stress levels, a high number of carbides are found to be fractured, the plastically deformed areas have spread and deepened and even small cracks are observed in the matrix, as shown in Figure 2.2.6. At this point, the test has been stopped to prevent the sensors from damage due to the sudden specimen breakdown. As shown by Picas et al. [1], the number of broken carbides and matrix cracks is expected to keep growing up to coalesce the ones with each others, leading to the final fracture.

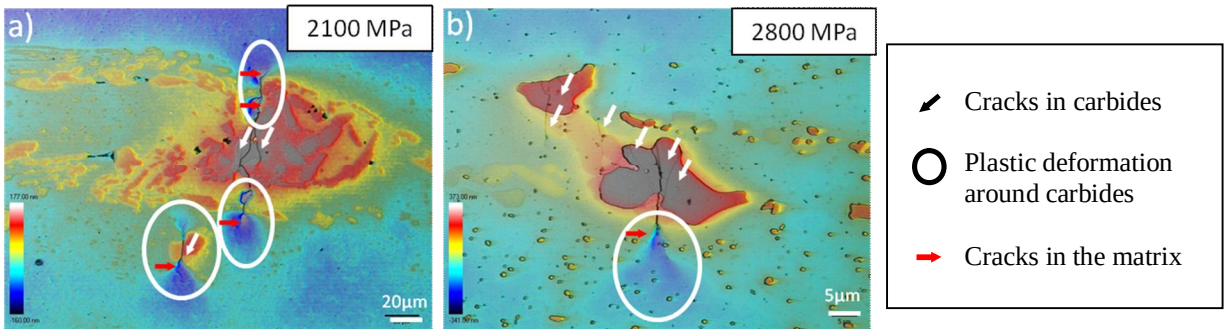

Figure 2.2.6. Broken carbides, plastically deformed areas and small cracks in the matrix can be identified by means of CM in the tensile stressed surface of specimens: a) DIN 1.2379 at 2100 MPa and b) UNIVERSAL at 2800 MPa.

In this study, the stress level at which carbides are found to start breaking in DIN 1.2379 is 640 MPa, which is around the 20 % of the fracture strength determined for this material [1]. In the case of UNIVERSAL, the signals that point out breakage of carbides appears from 1700 MPa, which corresponds to approximately the 45 % of the fracture strength of this material [1]. Such results can be explained by the lower fracture toughness of primary carbides in DIN 1.2379, as has been previously evaluated by Casellas et al. [3], and the elongated shape and

arrangement in bands (in which local stresses can be higher) of carbides in DIN 1.2379, as has been stated by Picas et al [1].

Some of the results presented here show agreement with those obtained by Yamada and Wakayama [7] with Ti(C,N)-based cermets. Basically, two types of AE signals can be identified: a high frequency burst-type signal and a lower frequency continuous type. The first type could be attributed to the carbide micro-cracking processes while the continuous type could be related to plastic deformation in the matrix. Although this theory is consistent with the results obtained in this study, additional research is required to ascertain these correlations.

2.2.4. Conclusions

According to the experimental results obtained by means of coupling AE to bending tests, and the microstructural observation of two different tool steels, the following conclusions can be drawn:

- AE is an appropriate experimental tool to detect carbide cracking in tool steels microstructure.
- An experimental relationship has been established between the fracture of carbides and the obtained AE signal. The stress levels at which carbides were broken were determined by AE and experimentally confirmed by microstructural inspection.
- The tool steel with the highest broken carbide content induces the highest quantity of AE signals with more temporal dispersion.

2.2.5. References

[1] Picas, I.; Cuadrado, N.; Casellas, D., Goez, A.; Llanes, L.; Microstructural effects on the fatigue crack nucleation in cold work tool steels, *Procedia Engineering, Fatigue 2010*, April 2010, Vol.2, Nr.1, pp. 1777-1785.

[2] Berns, H.; Broeckmann, C.; Weichert, D.; Fracture of hot formed ledeburitic tool steels. *Engineering Fracture Mechanics,* Nov. 1997, Vol.58, Nr. 4, pp. 311-325.

[3] Casellas, D.; Caro, J.; Molas, S.; Prado, J.M.; Valls, I.; Fracture toughness of carbides in tool steels evaluated by nanoindentation. *Acta Materalia,* Aug. 2007, Vol. 55, Nr. 13, pp. 4277-4286.

[4] Picas, I; Hernandez, R; Casellas, D; Valls, I; Strategies to increase the tool performance in punching operations of UHSS. R. Kollek (Ed.), 2010, Proc IDDRG, Graz, Austria 325-334.

[5] Fukaura, K., Ono, K.; Acoustic emission analysis of carbide cracking in tool steels. *Jorurnal of Acoustic Emission,* 2001, Vol.19, pp.91-99.

[6] Yokoi, D.; Tsujii, N.; Fukaura, F.; Effects of tempering temperatures and stress amplitude on low-cycle fatigue behavior of a cold work tool steel. *Materials Science Research International,* Vol. 9, 216-222.

[7] Yamada, K. and Wakayama, S., AE monitoring of microdamage during flexural fracture of cermets. *Proceedings EURO PM2009- Hardmetals & Cermets*, 247-252.

[8] Metals Handbook ï Metallography, Structures and Phase Diagrams, ASM International, Vol. 8, p.402, USA 1978.

2.3. Filtering of acoustic emission signals for the accurate identification of fracture mechanisms in three-point bending tests

2.3.1. Introduction

In order to characterize the mechanical behavior of a material, monitoring the test with AE becomes a tool for understanding what is happening to the material throughout the whole test. However, acquired AE signals depend on several factors such as the type of mechanical test, the material under consideration and its type of damaging mechanisms, surface roughness, *etc.* Moreover, these signals are usually contaminated by background noise that can be classified according to its origin: the one inherent to the measurement chain (including both mechanical and electrical origin) and the one that appears as a consequence of the mechanical process being evaluated. Any noise, despite its origin, impairs the correlation between the failure mechanism and AE data. Therefore, the interpretation of the AE signals may produce an erroneous evaluation of the real damage. As a result, it is essential to apply some kind of filter in the acquisition and analysis of data, especially in the case of seeking the incipient origins of flaws.

Some methods have been proposed to extract the signals related to relevant sources of AE based on: i) time domain features [1,2], ii) frequency domain features [2,3] or iii) localization of the origin of the AE signal and relating this position with a possible real source of damage [4, 5]. In all cases, the filtering process uses characteristics of the waveform (Figure 2.3.1) as: duration (*D*), amplitude (*A*), energy (*En*), rise time (*RT*), frequency (*f*), *etc.*, or a combination of them. It is accepted that damage signals are of higher amplitude and higher frequency than those relative to noise, which, in general, present lower amplitude, more duration, higher rise time and more absolute energy/signal strength than a crack or damage signal [5]. As a result, most of the usual

filtering processes are based on these general features of the signals [1-3]. However, when AE is attempted on a laboratory scale, on small specimens, the waveform is overly deformed due to the reflections produced in the surfaces and the results of the filters are less effective than in big structures.

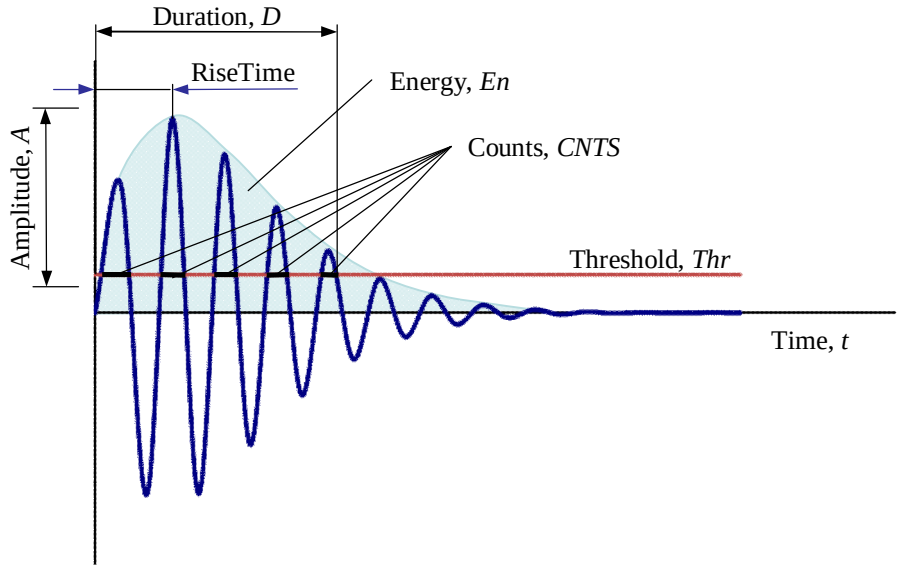

Figure 2.3.1. AE signal features.

Many research studies on damage mechanisms for fragile materials use the bending test to identify the beginning of each damage mechanism [6-10] (for example, in tool steels, cracking of carbides, decohesion between carbides and the metallic matrix, plastic deformation, growth of cracks, *etc.*). The bending test generates damage in a small area of the stressed specimenôs surface that can be controlled by microscopy, but it is difficult to detect the beginning of the damage mechanism with precision. The use of this test in a stepwise loading mode and comparing the AE signals with the observed damaged surface with a microscope facilitates the relating of the signalôs features with the mechanism that generates them [10,11]. However, AE signals caused by the deformation of the specimen at the upper and lower supports (background noise due to the mechanical process) have the potential of masking the AE signals related to the

damage mechanism; therefore preventing the detection of the applied stress at which the fracture mechanism takes place.

The purpose is to develop a signal filtering process capable to discriminate between AE signals emitted by natural damage mechanisms in specimens from others caused by the interaction of the specimen with the supports necessary to carry out the mechanical test. This enables to filter all AE signals not related to the damage mechanisms under investigation. The novelty of this type of filtering is that it extracts information only from the first cycles of the signals instead of from their whole length. The filtering process is applied to a three-point bending test of a cold work tool steel DIN 1.2379 in order to determine the onset stresses for the acting damaging mechanisms involved in the fracture process.

2.3.2. AE Sources in the three-point bending test

In three-point bending tests the most stressed area and in which damage and final failure takes place is the centre of the specimen (Figure 2.3.2.).

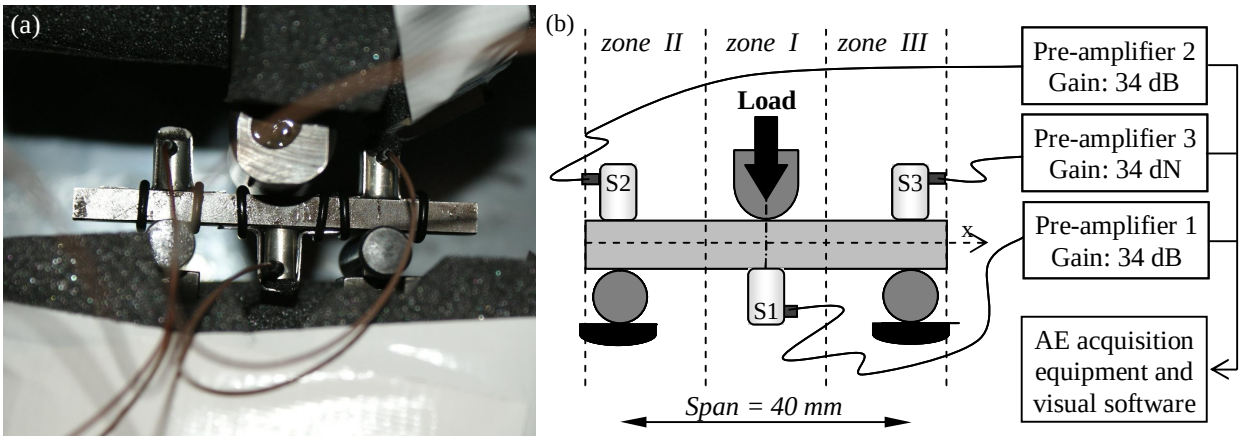

Figure 2.3.2. Experimental setup of the three-point bending test: (a) Image of the mounted specimen and (b) schematic setup.

However, the AE signals emitted by natural damage generated in the microstructure as a result of the mechanical test are affected by both the background noise due to the measurement chain and the mechanical process.

The background noise related to the measurement chain in this kind of test can be reduced by using general measures conventionally employed in AET. These measures include the careful assembly of the acquisition system, which involves protecting the sensors, fixing the cables to avoid that they move and selecting the correct threshold to limit the quantity of signals reaching the sensors. Another common practice consists in applying a low frequency filter with the aim of cutting out vibration and machine noises.

Mechanical process background noise is mainly due to the high contact pressure at the specimen surface directly in contact with the supports of the bending fixture. These zones in the specimen can be severely damaged during the test, and they also generate AE signals. This spurious noise can be eliminated with a lineal location processor. In figure 2.2.2, the signals produced in zone II or III correspond mainly to this type of noise. The main problem occurs in the zone of interest (zone I), where the generated AE signals have two next damage origins: i) the contact pressure between the upper central support and the specimen (noise signals) and ii) the stress state induced in bending (signals of interest). The elimination of this kind of spurious signal has been attempted by different AE filtering processes, such as:

a) To raise the threshold before or during the test. This procedure is not valid if the measurement deals with the nucleation of incipient cracks in the microstructure, because the energy released is very low [12] and valid AE signals could be excluded.
b) To study the relationship between the duration and amplitude of the signals. Swangson filters define some combinations of values to identify noise signals [11,13]. It is a filter strongly

dependent on the threshold and the waveform. In small specimens, the distorted waveforms make these filters unsuitable.

c) The use of master-slave or guard technique. Master sensors are mounted near the source of interest and enclosed by others called slaves or guard sensors. If any signal arrives first to a guard sensor, it is rejected [14]. This is useful only if the source of the signals is isolated.

d) Some studies are based on frequency domain features in order to determine the damage severity or to identify different damage mechanisms [10,15], but they are not used to filter background noise (except low frequencies or noises with clear frequency predominance). In the case of small specimens, multiple reflections produce change of modes that distort the characteristics of the frequency domain.

2.3.3. De-noise filtering process

Although during the test, possible sources of background noise were identified and isolation mechanisms were applied (as detailed in Method section 2.3.4), the raw data acquired still contain noise signals. The de-noise process developed in this thesis deals with the elimination of the AE signals which are emitted by: i) residual environmental noise (measurement chain noises) and ii) AE signals related with the contact between supports and the specimen (mechanical process noise). As mentioned before, the waveforms in small laboratory specimens are quickly distorted, especially if they are made of a metallic material with low attenuation (Figure 2.3.3).

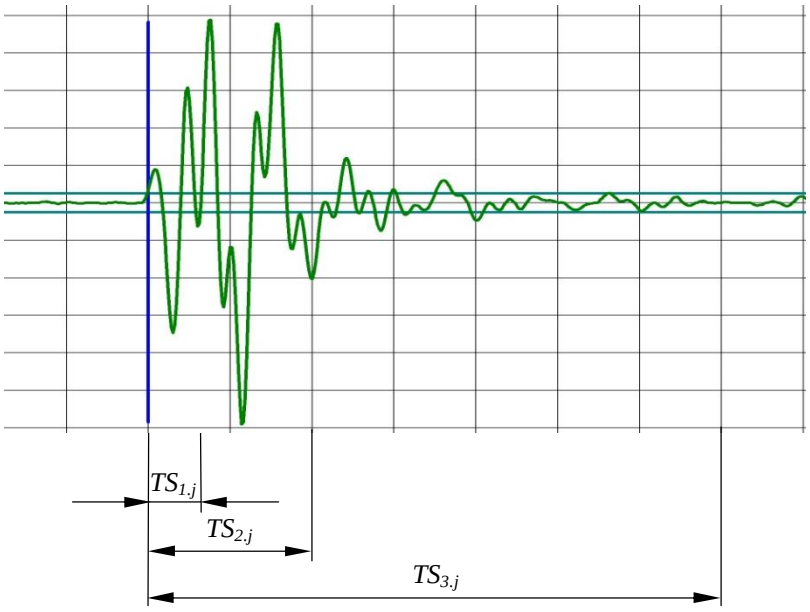

Figure 2.3.3. Measured signal waveform with time segment definition.

Therefore, the use of parameters related to AE wave shapes could be confusing to classify signals. Taking into account the small size of the specimens used in this study (as shown in section 2.3.4.2), only the very first cycles of the waveform carry information about the source (the rest of cycles must be discarded as they are affected by boundary reflections). This initial segment of waves is defined as TS_1 (Figure 2.3.3) and its features were analyzed to identify the main characteristics of signals originated in zones II or III (Figure 2.3.2), corresponding to damage due to supports and specimen surfaces. Then, the signals originated in the central area of the specimen (zone I) with similar characteristics to those of zones II and III were eliminated. This filter leaves AE signals exclusively related to micro-structural damage generated as a result of the applied load during the bending test. Figure 2.3.4 presents a schematic diagram of the filtering applied in this work and the algorithm is summarized as follows:

- Time segment definition: Each signal is divided into three time segments (Figure 2.3.3): i) Signal segment 1, TS_1, ii) signal segment 2, TS_2, with a length of three times TS_1, with the

aim to include the peak amplitude of the signal, and iii) signal segment 3, TS_3, including the full length of the signal excluding pre-trigger. TS_2 and TS_3 are used to clearly identify burst from continuous signal types. Continuous signal types are related to background noise and plasticity mechanism [16].

- Origin of hits: Using linear location algorithms, the hits are classified according to their origin in the range of zones I, II and III (Figure 2.3.2). The location in the *x*-zone is an event builder constructed with an *x*-sensor defined as normal and others defined as guard sensors. The velocity of propagation and the distances between sensors are detailed in Method section 2.3.4.
- Initial classification of the signals: according to the time segment definition and signal origin, the signals are defined as $H_{i,j}$ where i = 1é 3 refers to the time segment and j = 1é 3 refers to the origin of the signal.
- Time domain features: the average amplitude of each time segment ($AT_{i,j}$) for all signals is obtained by the Root Mean Square (RMS) method.
- FFT features:
  i) Two frequency segments (k) were defined between 95 ï 450 kHz (k = 1) and 450 ï 850 kHz (k = 2); in accordance with the sensor response.
  ii) $AF_{i,j}(k)$: average amplitude in the frequency domain of the signal.
- Definition of decision variables:
  i) Amplitude Ratio (AR_i) defined as the ratio of $AT_{2,j}$ to $AT_{3,j}$; to identify burst type signals from continuous ones.
  ii) Spectral Bands Ratio (SBR_j): is the ratio of $AF_{i,j}(1)$ to $AF_{i,j}(2)$ for i=1. This indicator allows the clustering of signals according to the energy distribution in the frequency segments previously defined.

- Criteria for discrimination of the measurement chain for background noise: to reject signals which present a continuous waveform. In this particular case, after observation, the threshold of AR_i > 6 dB gives good results.
- Classifying damage mechanism: Identify appropriate features capable of clustering signals. For this study: the correlation between SBR_j and $AT_{1,j}$.

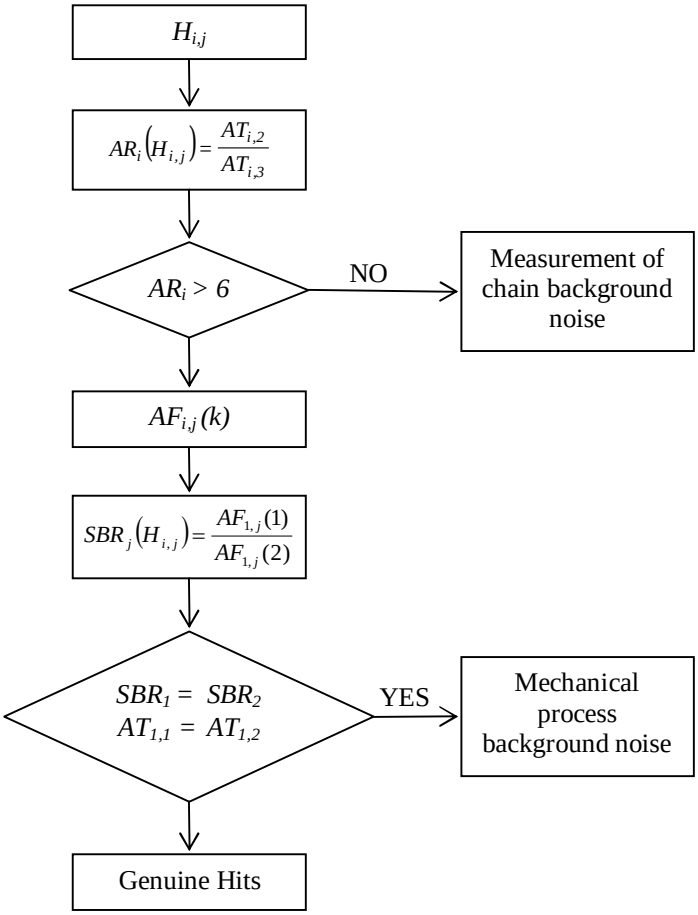

Figure 2.3.4. Block diagram of the analysis of acquired data.

2.3.4. Method

The filtering process is applied to the acquisition data obtained in a monotonic three-point bending test. To correlate and identify AE signals with specimen damage a Confocal Microscope (CM) is used to inspect the microstructure of the samples.

2.3.4.1. *Experimental procedure*

The three-point bending test is carried out in a universal testing machine with a constant span length of 40 mm using an articulated fixture to minimize torsion effects. The displacement rate applied was 0.1 mm/min and the test took place at room temperature. The set-up is schematized in Figure 2.3.2.

2.3.4.2. *Specimens*

Cold work tool steel DIN 1.2379 specimens were used. They had a prismatic shape (length = 50 mm, width = 8 mm and thickness = 6 mm) with the forging direction oriented parallel to the long axis of specimens. Samples were mechanically ground and their corners were rounded to avoid stress concentration and remove any defect introduced during sample preparation. The face subject to tensile stress during the bending test was carefully polished to a mirror finish using colloidal silica particles measuring approximately 40 nm.

The goal of the three-point bending test coupled to AE analysis in this tool steel is to obtain accurate data regarding damaging mechanisms at the initial stage of fracture. Picas et al. [17] reported that breakage of primary carbides determines the onset for crack nucleation and propagation in tool steels under monotonic conditions. Thus, AE signals emitted by carbide failures were sought. In order to verify that the breakage of carbides generates different signals with respect to those caused by contact pressure at upper and lower supports, the three-point bending test was also performed with a spring steel DIN 55Cr3 . This is a martensitic steel with no large primary carbides embedded as in DIN 1.2379, that is why no AE activity was expected related to their breakage. The chemical composition and hardness of 1.2379 and 55Cr3 are summarized in Table 2.3.1.

Table 2.3.1. Chemical and mechanical properties of tested materials: 1.2379 and 55Cr3.

Steel	C	Cr	Mo	V	Mn	HRC
1.2379	1.5 - 1.6	11.0 - 12.0	0.6 - 0.8	0.9 - 1.0	-	60 - 62
55Cr3	0.55	0.85	-	-	0.85	43 - 45

2.3.4.3. *AE Measurements*

Figure 2.3.2(b) shows the AE acquisition set-up. The equipment was an AMSY-5 (Vallen System, GmbH) equipped with four channels and connected to a computer with VisualAE software (Vallen System, GmbH). The test was monitored using three small resonant-type sensors firmly attached to the specimen. One sensor (S1) was mounted in the center of the tensile face, and the other two (S2 and S3) were on the opposite side. All of them were aligned with the three supports of the bending fixture. The sensors present a resonant frequency centered on 700 kHz, but their response is relatively flat until 450 kHz and between 550 to 800 kHz. To guarantee enough acoustic transmission, silicone grease was introduced between the plate of the sensor and the surface of specimen. The three (central and roller) supports were covered with a PVC film with a thickness of 0.15 mm, to minimize the frictional noises with the specimen during the test.

Some preliminary measurements of the background noise were conducted in order to determine the threshold level. In this case, four sensors were attached to the specimen and the upper anvil assembly. As AE activity was detected with amplitudes below 30 dB, the threshold level was fixed at 34 dB.

The propagation velocity through the specimen was determined using two simulated AE events: a Hsu-Nielsen source (pencil lead break) and digital signals sent through the sensors. Acquisition parameters and event builder parameters are summarized in Table 2.2.2.

Table 2.3.2. Acquisition and post-processing parameters.

Parameter	Value
Sample rate	10 MHz
Threshold, *Thr*	34 dB
Rearm Time, *ReT*	0.0512 ms
Duration Discrimination Time, *DDT*	0.050 ms
1st Hit Discrimination Time, *FHCDT*	0.08 ms
Time segment 1, TS_1	3.2 μs
Time segment 2, TS_2	10 μs
Time segment 3, TS_3	50 μs

2.3.5. Results and discussion

Figure 2.3.5 shows the cross-plot correlation of SBR_j versus $AT_{1,j}$ for the two steels during the three-point bending test. Figure 2.2.5(a) plots the results of 1.2379 and it shows a clear common area for hits in zones I, II and III (superimposed on the graph). Hits located in zones II and III can only occur due to contacts with the rolling supports. Hence, hits located in zone I with similar characteristics of SBR_j versus $AT_{1,j}$ to those of zones II and II are assumed to be generated by the contact of the specimen with the upper central support. The signals with a different relationship between SBR_j and $AT_{1,j}$ are only located in zone I and correspond to the relevant signals for the test (natural damage in the microstructure as a result of the applied stress). The

sources of these hits are carbide breakage and crack nucleation and propagation from them. The events located in zone II and III with higher amplitude (80-85 dB) correspond to the movement of the supports due to the displacement of the load device when the test was finished (encircled in Figure 2.3.5(a)).

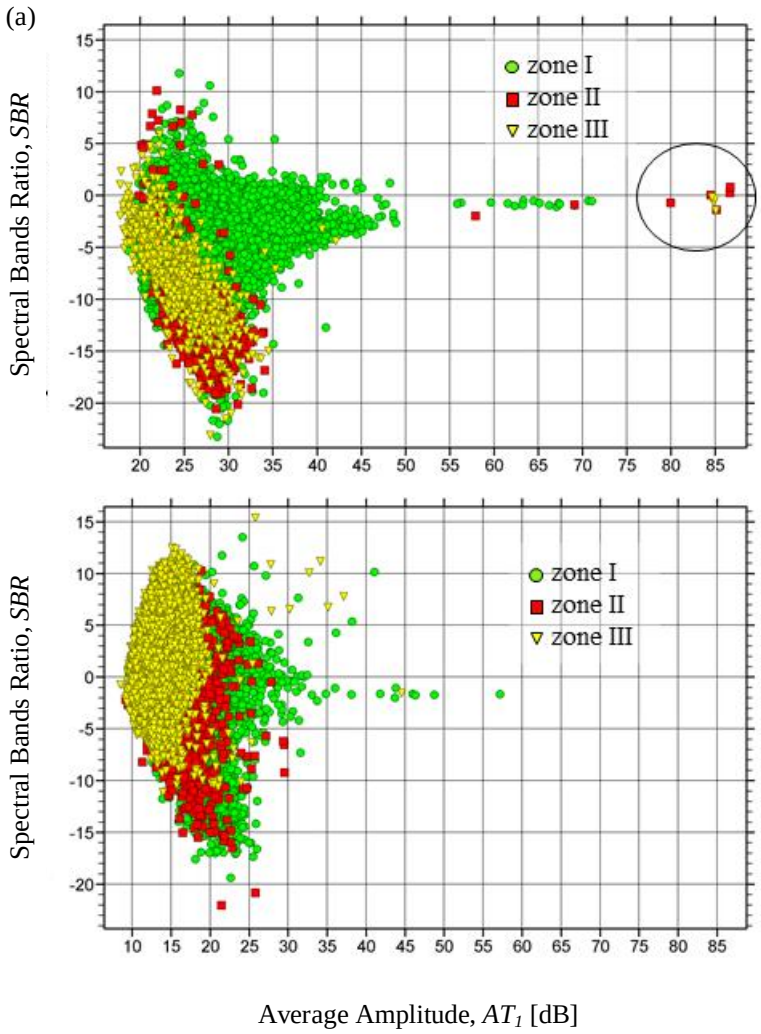

Figure 2.3.5. SBR_j vs $AT_{1,j}$ crossplot, classified for each zone, during the three-point bending test for two steels: (a) DIN 1.2379 and (b) DIN 55Cr3.

The spring steel specimens were employed to check the results of the clustering process, as shown in Figure 2.3.5(b). The located hits in each zone of the specimen have similar characteristics in reference to the relationship between SBR_j and $AT_{1,j}$. In this case, the

predominant source of AE was that generated by contact pressure between supports and specimens surface. Nevertheless, a larger quantity of hits was located in zone I (Figure 2.3.5(b)) ï central support was double force that the rolling supports and some damage occurred in the center of the specimen that was related to plastic deformation taking place in the microstructure. The similar results for both steels, with one common mechanism of damage, permit the identification of the characteristics of the contact pressure damage signals. So, the relationship SBR_j - $AT_{1,j}$ becomes an indicator of damage in the supports during the bending test.

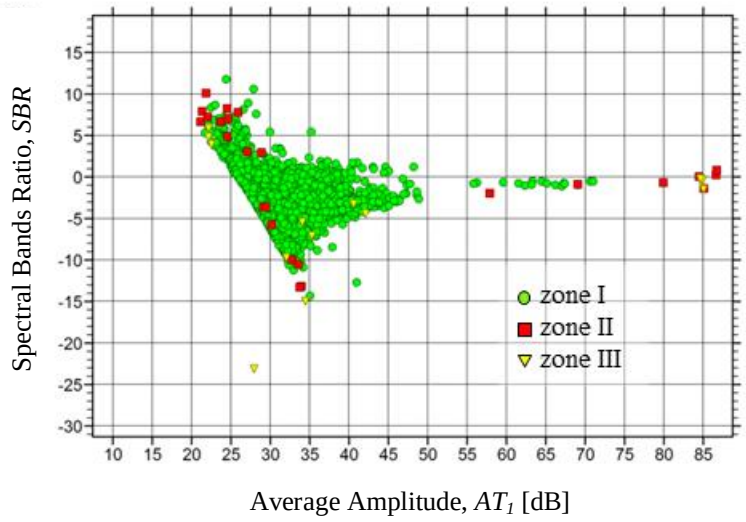

Figure 2.3.6. (a) SBR_j vs $AT_{1,j}$ crossplot with applied filter for DIN 1.2379 specimen (Green hits originated in zone I, yellow in zone II and red in zone III during the three-point bending test) and (b) cumulative hits during the bending test comparing raw data without filtering (■-line) with filtered data (●-line).

Having identified the characteristics of the signals corresponding to damage generated at contacting points of the surface, signals measured in 1.2379 steel with identical features of 55Cr3 steel were removed (Figure 2.3.6) from the raw data. Figure 2.3.8(a) presents cumulative hits that first arrived to S1 during the test and compares results for un-filtered (■-line) and

filtered data (●-line) of a 1.2379 specimen. The filtering process eliminates an important quantity of undesirable hits, in this case around of the 60% of the signals.

Figure 2.3.8(b) shows in more detail data plotted in Figure 2.3.8(a) and it can be observed that the hits located in zone I according to the filtered data (●-line) begin later than with unfiltered data (■-line). Results of micro-structural inspection of 1.2379 at zone I at a stress level below 800 MPa show no damage (see Figure 2.3.7(a)), while above 800 MPa carbides have already broken (Figure 2.3.7(b)). Note that if the data is not filtered, the conclusion could be that carbide cracking begins at around 650 MPa, while in reality it occurs at more than 800 MPa in this specimen. This result points out the importance of extracting relevant signals to evaluate the onset stresses for damage in the microstructure of a specimen. Comparable results were obtained by Fukaura and Ono [18] testing a JIS SKD11, equivalent to a 1.2379, in a tensile test without the problem of pressure contacts.

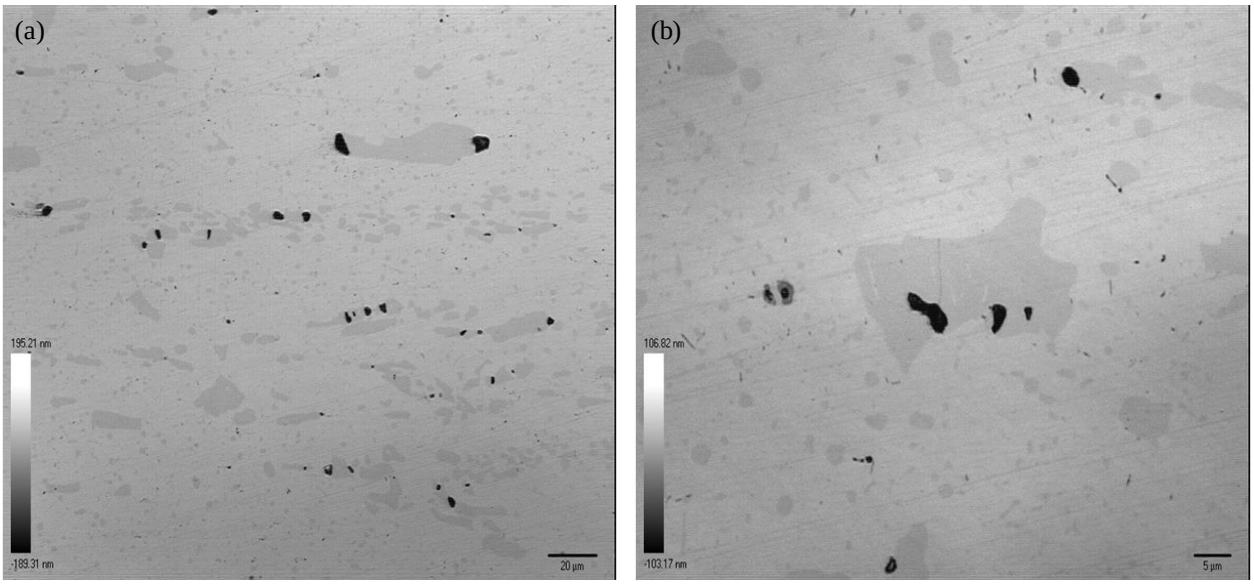

Figure 2.3.7. Microscope images of the maximum tensile surface (a) at 790 MPa without breakage of carbides and (b) at 900 MPa applied stress.

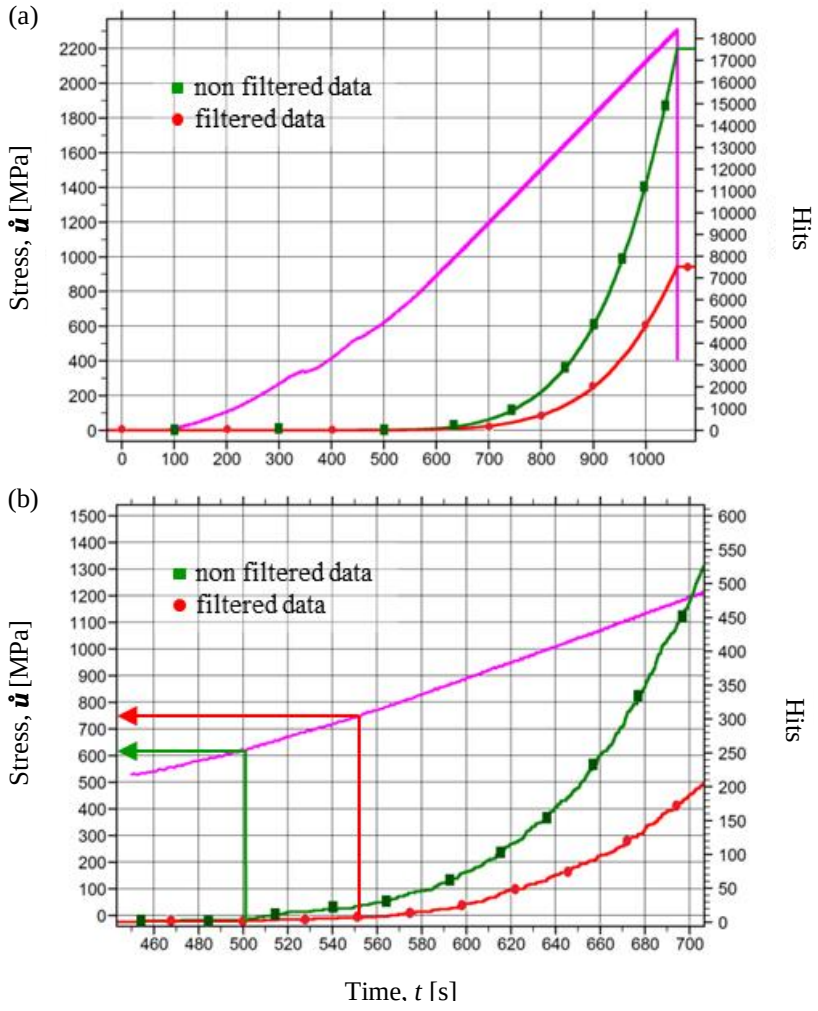

Figure 2.3.8. (a) Cumulative hits during the bending test comparing raw data without filtering (■-line) with filtered data (●-line) and (b) amplified detail of figure (a).

The signals located in zones II and III were also correlated with the micrographic images, as shown in Figure 2.2.9 in case of 1.2379. It can be seen that damage generated due to contacts with the rolling supports can be very different from specimen to specimen, and even in one single specimen and if applied stresses are similar. In Figure 2.3.9(a) there is virtually no damage, in Figure 2.3.9(b) the damage is visible and in Figure 2.3.9(c) the damage is severe (presenting scratches, cracks and even some broken carbides). Such differences may probably be explained due to relative movements of specimens and lower rolling supports during the test.

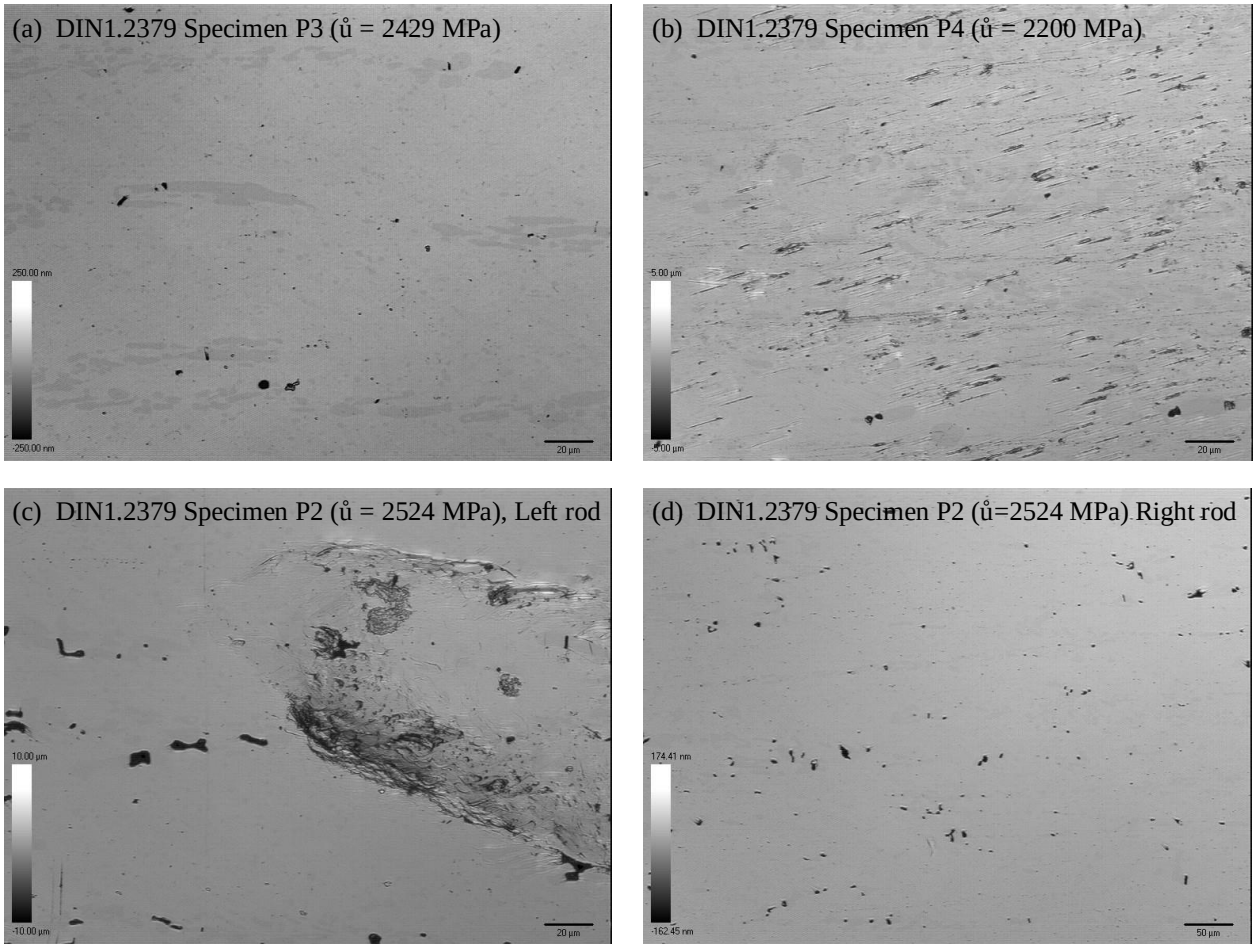

Figure 2.3.9. Confocal images of the contact surface of some DIN 1.2379 specimens at rod contact area: (a) practically non-existent damage in specimen P3, (b) specimen-P4 presents some damage (c) and (d) specimen-P2 presents severe damage and low damage in each rod respectively.

Figure 2.3.10 shows the cumulative unfiltered hits that reach S2 and S3 first for two different specimens. In both cases the cumulative number of hits increases exponentially during linear load increase. At the beginning of the tests, with low loads, there is no damage to the specimen and practically no hits are getting to sensors S2 or S3. When damage is generated in the surface of the specimen in contact with rolling supports, some hits appear and grow continually until the load is removed. Moreover, the total number of hits in these sensors is related to the severity of the damage induced in the specimen. Specimen P3 presented low damage on the contact surface (Figure 2.3.9(a)) and similar results were observed in both contact surfaces in zone II and III.

The number of hits related to contact damage is presented in cumulative form in Figure 2.3.10(a). S1 and S2 present equal behavior and a similar total number of hits. Instead, specimen P2 presents two different behaviors at the contact area; at one area (in zone II) severe contact damage were observed (Figure 2.3.9(c)), while at the other roller support contact area there is almost no damage (Figure 2.3.9(d)). The sensor mounted at the closest position to this damaged surface was S2 with more than 400 hits (Figure 2.3.10(b)), while signals with first arrival to S3, mounted near the non-damaged surface, only presented 60 hits. It allows stating that there is a strong relationship between this cluster of signals and the observed contact damage.

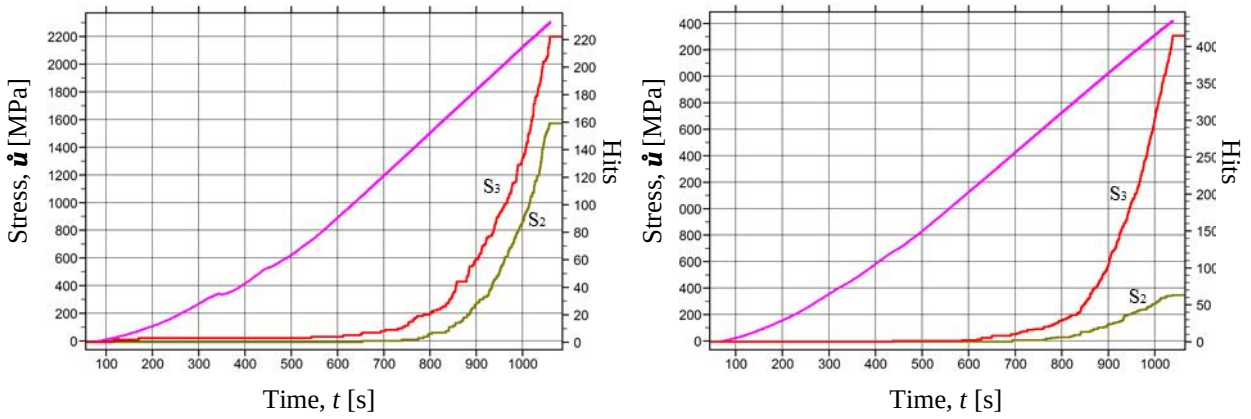

Figure 2.3.10. Cumulative hits originating in zones II and III and maximum stress during a three-point bending test of DIN 1.2379 specimens: (a) specimen P3 (practically non-existent damage) and (b) specimen P2 with different damage severity in the contact with lower rolling supports.

2.3.6. Conclusions

The technique of acoustic emission measurements has been successfully applied to detect and identify the fracture mechanisms in steels with high hardness levels (higher than 44 HRC, as a tool steel and a spring steel) by means of three-point bending test. The main difficulty from the AE measurements point of view is the coexistence of useful AE signals generated during the

fracture events with spurious signals related to damage in the contact surfaces of the specimen with upper central and lower supports that do not account for the specimen fracture process. Specifically, it is found that the signal caused by the damage induced by the supports is stronger at the beginning than that caused by the cracking of carbides and crack propagation, which is the real fracture mechanism in the studied steels. The coexistence of both signals seriously hampers the proper identification and evaluation of the fracture mechanisms.

Aimed at overcoming such uncertainty, a filtering protocol is proposed based on the first segment of the waveform, which detects and filters the AE signal distortions caused by reflections. Taking advantage of the characteristics of frequency features, the proposed filtering analysis provides the main parameters only for the first segment of time. The analysis permits to successfully identify the different origins of AE signals generated during the bending test that are: background noises, damage at the contact area between the specimen and the supports and the fracture process leading to specimen failure. The filtering process is applied to the analysis of fracture mechanisms in a tool steel. It allows for an accurate determination of the stress level that triggers carbide cracking, that is 800 MPa for the studied DIN 1.2379 steel. Such value was experimentally confirmed by surface inspection of tested samples. The use of unfiltered signals would erroneously set this carbide fracture stress level at 650 MPa, which represents an error of close to 20%. It would give bad data to tool steel makers for the microstructural design of tool steels and induce to misunderstandings to the tool user when trying to correlate the micromechanical properties of the tool steel to the macroscopic behavior of industrial tools.

2.3.7. References

[1] Volodin, T.V.; Khasanov, O.L.; Konovalov, S.V.; Volodin, V.L. and Zuev, L.B.; Acoustic emission in steel failure. *Steel in Translation*, 2010, Vol. 40, Nr. 12, pp. 1041-1046.

[2] Hrairi, M.; Statistical signal processing and sortinf for acoustic emission monitoring of high-temperature pressure components. *Experimental Techniques*, 2009, Vol. 33, Nr. 5, pp. 35-43.

[3] Surgeon, M. and Wevers, M.; Modal analysis of acoustic emission signals from CFRP laminates. *Non-Destructive Testing & Evaluation International (NDT&E International)* , 1999, Vol. 32, pp. 311-322.

[4] Richard D. Finlayson. *Acoustic emission testing, Handbook of non-destructive evaluation.* New York (USA). McGraw-Hill: 2000.

[5] Sison, M.; Duke Jr., J.C.; Lozev, M.G. and Clemeña, G.G.; Analysis of acoustic emission from a steel bridge hanger. *Research in Nondestructive Evaluation*, 1998, Vol.10, 123-145.

[6] Hall, D.J.; Booth, S. and Evans, W.T.; Use of acoustic emission to identify oxide fracture modes. *Materials Science and Technology*; 1990, Vol. 6, pp. 53-55.

[7] Kaphle, M.R.; Tan, A.; Thambiratnam, D.; Chan, T.H.T.; Damage quantification techniques in acoustic emission monitoring. *In WCEAM2011 6th World Congress Engineering Asset Management,* 2nd ï 5th October, 2011, Cincinatti, OH, USA.

[8] Trebacz, H. and Zdunek, A.; Three-point bending and acoustic emission study of adult rat femora after immobilization and free remobilization. *Journal of Biomechanics*, 2006, Vol. 36, pp. 237-245.

[9] Han, Z.; Luo, H.; Cao, J.; Wang, H.; Acoustic emission during fatigue crack propagation in a micro-alloyed steel and welds. *Materials Science and Engineering A (Structural Materials: Properties, Microstructure and Processing)*, Sept. 2011, Vol. 528, Nr. 25-26, pp. 7751-7756.

[10] Martinez-Gonzalez, E.; Picas, I.; Casellas, D.; Romeu, J.; Analysis of fracture resistance of tool steels by means of acoustic emission. *Journal of Acoustic Emission.* 2010, Vol. 28, pp. 163-169.

[11] ElBatanouny, M.K.; Larosche, A.; Mazzoleni, P.; Ziehl, P.H.; Matta, F.; Zappa, E.; Identification of cracking mechanisms in scaled FRP reinforced concrete beams using acoustic emission. *Experimental Mechanics,* 2012, pp. 1-14.

[12] Pollock, A.; Material brittleness and the energetics of acoustic emission. *Proceedings of the SEM annual conference (Society of Experimental Mechanics Inc.).* June 7-10, 2010, Indianapolis, Indiana (USA).

[13] Fowler, T.J.; Blessing, J.A.; Conlisk, P.J.; Swangson, T.L.; The MONOPAC system. *Journal of Acoustic Emission.* 1989, Vol. 8, Nr. 3, pp. 1-8.

[14] Miller, R.K. and McIntire, P.; *Nondestructive testing handbook: acoustic emission*. Columbus (OH, USA). ASNT: 1987, pp.24.

[15] Nam, K. and Mal, A.; Characteristics of elastic waves generated by crack initiation in aluminium alloys under fatigue loading. *Journal of Materials Research.* June 2001, Vol. 16, Nr. 6, pp. 1745-1751.

[16] Wevers, M. and Lambrights, K.; Applications of acoustic emission for SHM: a review. *Encyclopedia of structural health monitoring (Encyclopedia of SHM).* John Wiley & Son, Ltd., 2009.

[17] Picas, I.; Cuadrado, N.; Casellas, D., Goez, A.; Llanes, L.; Microstructural effects on the fatigue crack nucleation in cold work tool steels, *Procedia Engineering (Proc.Eng.), Fatigue 2010,* April 2010, Vol.2, Nr.1, pp. 1777-1785.

[18] Fukaura, K. and Ono, K. Acoustic emission analysis of carbide cracking in tool steels. . *Journal of acoustic emission.* 2001, Vol. 19, pp. 91-99.

2.4. Discrimination of different fracture phenomena by means of AE

2.4.1. Introduction

From the standpoint of section 2.3, this section is focused on the detection in real time of the elastic wave signals generated during monotonic three point bending tests, and which can be related to initiation and growth of cracks in the microstructure. In order to classify the different signal spectrum characteristics generated by tool steels of different microstructural features, this study deals with two tool steels with different size, geometry and distribution of primary carbides in the metallic matrix.

2.4.2. Experimental procedure

2.4.2.1. Materials

Two different cold work tool steels were considered in this study. The first type is a conventional ledeburitic high-carbon, high-chromium tool steel DIN 1.2379 (AISI D2). The second is a special grade of cold work tool steel developed by ROVALMA S.A., named HWS, which in comparison to the aforementioned 1.2379 has lower carbon and chromium content but more vanadium. 1.2379 is obtained by ingot metallurgy routes while HWS is produced by powder metallurgy (PM). The main alloying elements found in their chemical composition are shown in Table 2.4.1.

Table 2.4.1. Main allowing elements in the chemical composition of the studied steels (in wt%).

Steel	C	Cr	Mo	V	W
1.2379	1.5 - 1.6	11.0 - 12.0	0.6 - 0.8	0.9 - 1.0	-
HWS	0.9 - 1.2	6.8 ï 8.5	-	2.5 ï 3.0	1.1 ï 1.4

Prismatic samples were extracted from forged and annealed commercial bars parallel to the forging direction. Heat treatment was applied to the samples of each material in order to get a hardness level of 60 ï 62 HRC, as summarized in Table 2. The bending strength, σ_R, of these materials was reported by Picas et al. [1], and the fracture toughness, K_{IC}, was determined as specified in the ASTM E 399-90 standard. These values are also shown in Table 2.4.2.

Table 2.4.2. Heat treatment applied to the studied materials and obtained hardness, bending strength (σ_R) and fracture toughness (K_{1C}).

Steel	Austenitizing (quench in oil)	Tempering	HRC	σ_R [MPa] [1]	K_{1C} [MPa·m$^{1/2}$]
1.2379	1050 ºC for 30 min	550 ºC for 2 h (x2)	60 - 62	2847 ± 96	28
HWS	1060 ºC for 35 min	540 ºC for 2 h (x3)	60 - 62	4382 ± 111	21

2.4.2.2. Specimens

Samples dimensions were w = 8 mm, h = 6 mm and l =120 mm (Figure 2.4.1). Samples were mechanically ground and their corners were rounded to avoid stress concentrations and to remove any defects introduced during sample preparation. Faces subject to tensile stress during three point bending tests were carefully polished to a mirror-like finish using colloidal silica particles with approximately 40 nm sizes.

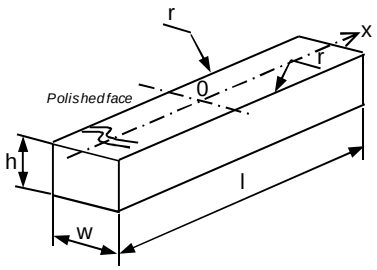

Figure 2.4.1. Schema of the samples used in this study.

2.4.2.3. Microstructural inspection and fracture tests

Microstructural inspection of the samples was carried out using a Field Emission Scanning Electron Microscope (FE-SEM). Fracture tests were performed by means of three point bending tests with a constant span length of 40 mm in a universal testing machine, using an articulated fixture to minimize torsion effects. The applied displacement rate was 0.01 mm/min. 5 samples of each material were monitored until final fracture, while 3 samples were analyzed by means of stepwise loading, as illustrated schematically in Figure 2.4.2(a). After each load step, the surface subjected to tensile loading (Figure 2.4.2(b)) was examined by means of Confocal Microscopy (CM) in order to relate each type of AE characteristic signal pattern to the generated damage in the microstructure.

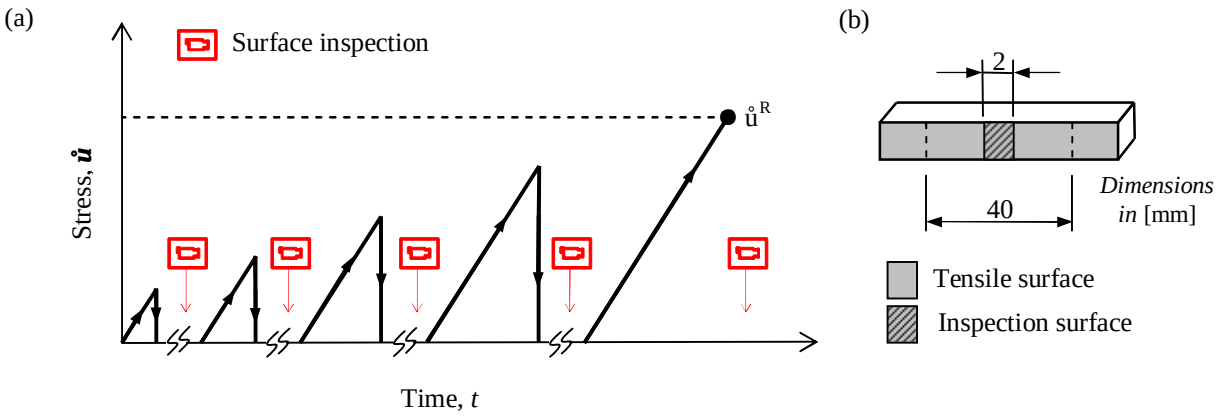

Figure 2.4.2. (a) Stepwise loading to final fracture of the sample, $\mathring{u}^R$. (b) Schema of the micrographically inspected zone of samples.

2.4.2.4. AE monitoring

Waveforms of the AE signals emitted during the test were detected and recorded with a Vallen System. Three miniature AE sensors were attached to the specimen opposite to each pin of the bending fixture (S1, S2 and S3 in Figure 2.4.3). The diameter of the sensor face was 3 mm. Sensor S1 acted as signal sensor in the middle of the tensile face, while S2 and S3 acted as guard sensors to avoid frictional noises. The sensors arrangement permits a linear localization, using the delta-t between S2 and S3 to locate the source, but only when S1 was the first hit. The sensors were resonant type (VS700D) with a frequency range between 100 ï 800 kHz and a peak frequency on 600 ï 800 kHz (flat range). Three 34 dB pre-amplifiers (AEP4) and a four channel systems (AMSY-5) were used (Figure 2.4.3). Signal frequency filtering was carried out by the pre-amplifiers and the AMSY-5 board. The filter was a band-pass type and it was set in the range of 95 - 850 kHz. The acquisition threshold was fixed at 34 dB and signals with zero duration and/or zero rise time were removed. A very short signal acquisition time (4 μs) was chosen in order to avoid capturing noise caused by wave rebounding due to surface walls and concatenated hits.

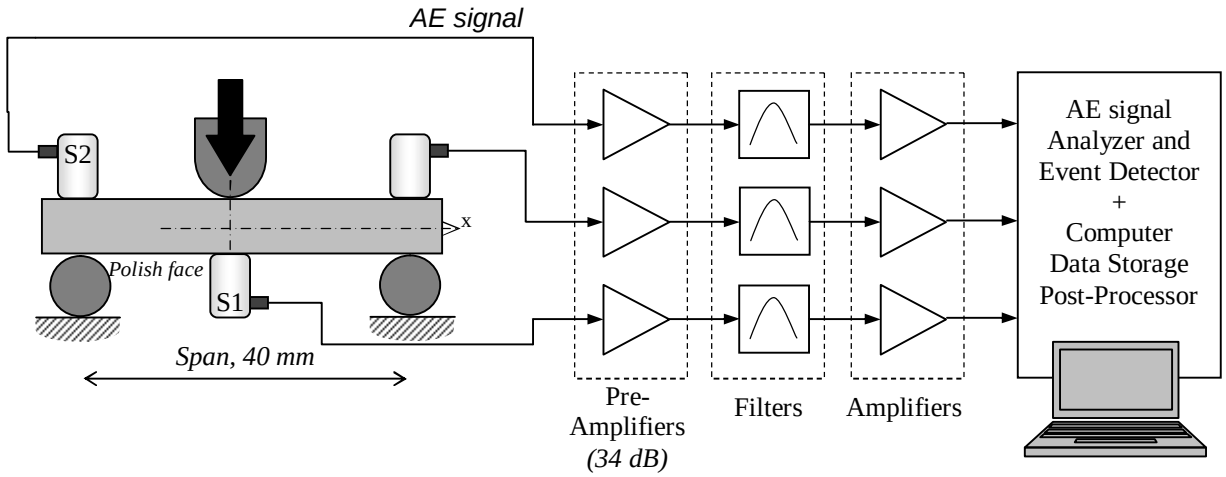

Figure 2.4.3. Experimental set-up for the AE monitored bending test.

2.4.2.5. AE noise signals

The three channels detected signals from very small events in the sample as the load increased during the test. AE sources were linearly localized with respect to the center of the sample (x axis in Figure 2.4.1 and Figure 2.4.3) by their different capturing times in the sensors. The acquired signals came from three main sources: (a) friction, (b) damage in those zones of the specimen directly subjected to the contact pressures exerted by the bending fixture pins and (c) damage at the center of the tensile face of the specimen as a result of the stresses applied. Sources (a) and (b) were removed during analysis as they were related to noise phenomena following the procedure described in section 2.3.3. Only (c) signals were taken into account, directly reflecting the evolution of damage in the microstructure. The area of interest comprised the interval from x = -15 mm to x = 15 mm (Figure 2.4.3). Any AE signal not located in this interval was filtered out using linear location. Recording exclusively events located in this

interval, the delta-t between S2 and S3 was used to locate the source but only when S1 was the first hit.

2.4.2.6. Analysis of AE waveforms

According to Fukaura and Ono [2], the waveforms related to cracks in carbides and cracks in the matrix can hardly be distinguished because they both correspond to crack opening types. Classifying the sources of AE signals by means of standard signal features; i.e. amplitude, rise time, duration, etc., was not possible in this work because waveforms were highly distorted already after a few micro-seconds (see the example in Figure 2.4.4 produced by a pencil lead break on the specimen surface). Such distortions were caused by reflections, changes of modes, etc., specially accentuated due to the small specimen dimensions and the low attenuation of the material.

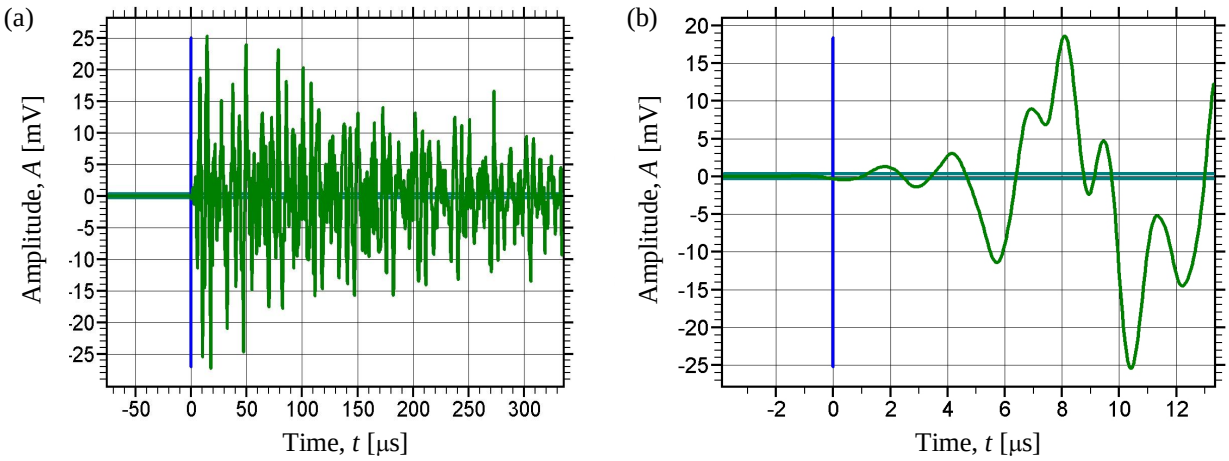

Figure 2.4.4. (a) Waveform produced by a Hsu-Nielsen source (when the graphite enclosed in a lead pencil breaks). (b) Zoom of the initial cycles of this artificial source.

2.4.3. Results

2.4.3.1. Microstructural analysis

In Figure 2.4.5 the microstructure of the steels studied can be observed. The microstructure of 1.2379 was markedly anisotropic, with large carbide stringers forming bands in the metallic matrix (Figure 2.4.5(a)). The primary carbides of this steel were rather large and had irregular morphologies. HWS showed the typical microstructure of PM steels with very small spherical carbides distributed in the matrix with no preferred orientation (Figure 2.4.5 (b)).

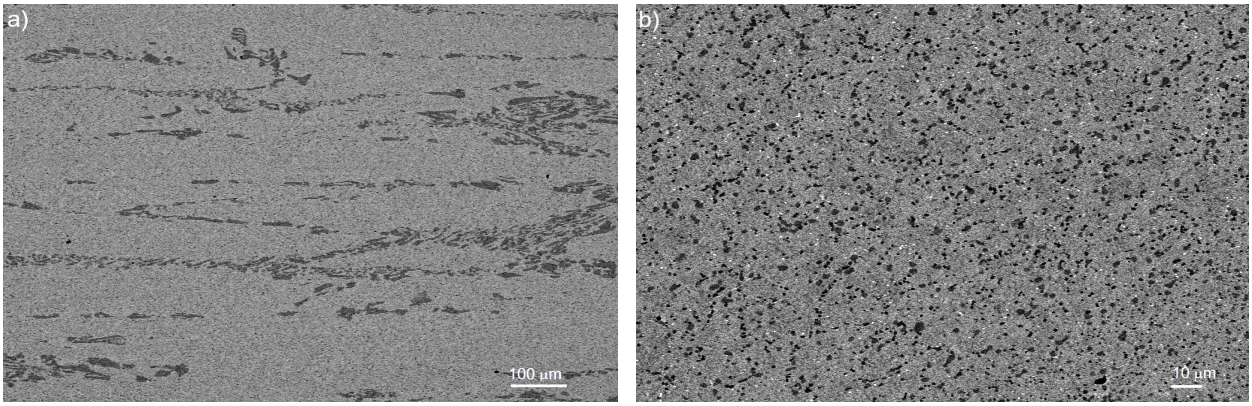

Figure 2.4.5. Microstructure of the studied tool steels: (a) 1.2379 and (b) HWS.

2.4.3.2. Identification of characteristic AE signal patterns in bending tests of 1.2379 under monotonic loading

Fig. 2.4.6 shows AE results from the bending tests under monotonic loading for 1.2379. This diagram plots the cumulative number of hits as a function of the stress applied and the location of each signal on the sample surface (with respect to the centre of the sample). As can be seen, the highest amount of signals was generated at the centre of the sample (x = 0, where the applied stress was the highest during the three point bending test), and the quantity of emitted signal continuously increased with the applied stress.

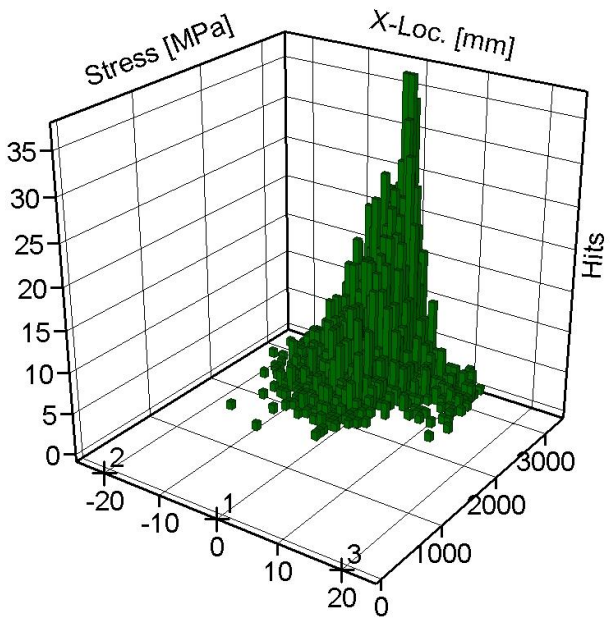

Figure 2.4.6. Cumulated number of hits in function of the stress applied during the bending test and the location of the signals at the sample surface (the x axis (X-Loc.) refers to the position of the signal with respect to the center of the specimen, the y axis refers to the applied stress and the z axis to the cumulated number of registered hits).

A closer examination of the AE signals allowed them to be classified into two categories depending on the characteristics of their spectra. As shown in Figure 2.4.7(a), the first type of signal (Type 1) had a peak frequency (F_{max}) centered at 280 kHz, while the F_{max} of the second type (Type 2) was around 660 kHz. Figure 2.4.7(b) shows that at the beginning of the test, no AE activity was detected. At a certain applied stress level, a Type 1 AE signals started to be recorded (●-line). These were burst-type signals, and the hit rate increased along with the applied stress. Later, as the stress increased, Type 2 signals started to appear (■-line). These signals also increased in number with the applied stress, but at the moment of final fracture they were less numerous than the Type 1 signals.

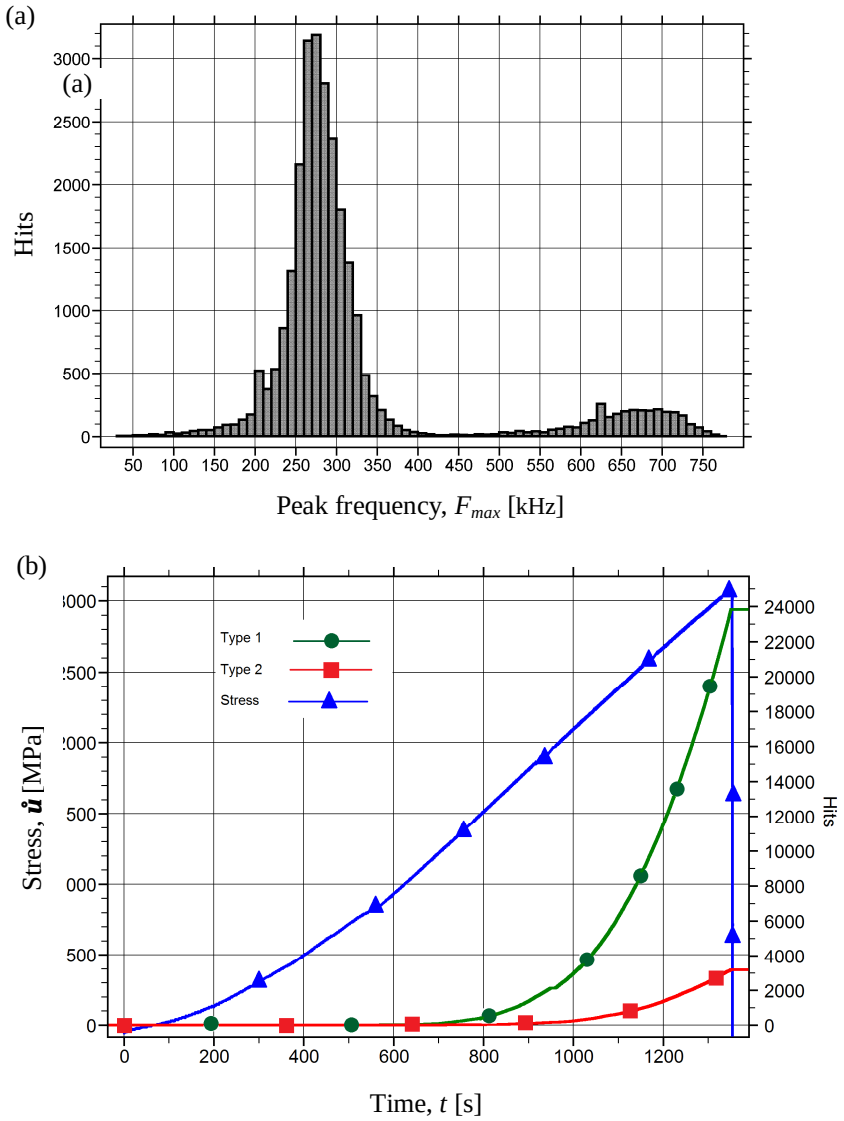

Figure 2.4.7. (a) Number of located hits on the interest length of specimen vs. peak frequency (F_{max}) for the two signals registered; (b) Cumulated number of hits vs applied stress during a monotonic bending test in which two different types of AE signals could be identified.

2.4.3.3. Relationship between AE signals and micro-damage during bending tests of 1.2379 under monotonic loading

Stepwise bending tests made it possible to inspect the tensile surface of the samples at different increasing stress levels, and to correlate the registered AE data (specifically, the two different identified signal types) with the micro-damage observed in the microstructure.

Figure 2.4.8(a) shows the cumulated number of hits as a function of the applied stress, during the first step in the loading. This test was stopped at 800 MPa, as soon as the first signals were detected. These signals answered to the same pattern as those of Type 1 identified before. However, no damage could be observed at the sample surface, as shown in Figure 2.4.9(a); likely something happened at the microstructure but it could not be detected yet.

The next test was stopped at 2200 MPa, when a higher quantity of AE signal was detected. Practically all signals responded to the Type 1 characteristics previously identified, and a few Type 2 signals were first detected (Figure 2.4.8(b)). In this case, the first cracks were observed in the microstructure and they were located at primary carbides (Figures 2.4.9(b) and 2.4.9(c)). However despite many carbides being broken, none of the cracks thus nucleated were observed to have started propagating through the metallic matrix surrounding the broken carbide.

The last load step at 2600 MPa revealed a notable increase of Type 2 signals, even though the number of Type 1 signals had not ceased to increase (Figure 2.4.8(c)), along with the number of broken carbides in the sample. Inspection of the surface made it possible to observe that some cracks had now propagated through the metallic matrix (Figure 2.4.9(d)).

Drawing on these results, the Type 1 and Type 2 AE signals were related to different damage mechanisms occurring in 1.2379 samples as the applied stress increased. The Type 1 signals corresponded to the breakage of carbides in the microstructure, i.e. nucleation of cracks, while the Type 2 signals were produced by the subsequent propagation of these cracks through the metallic matrix.

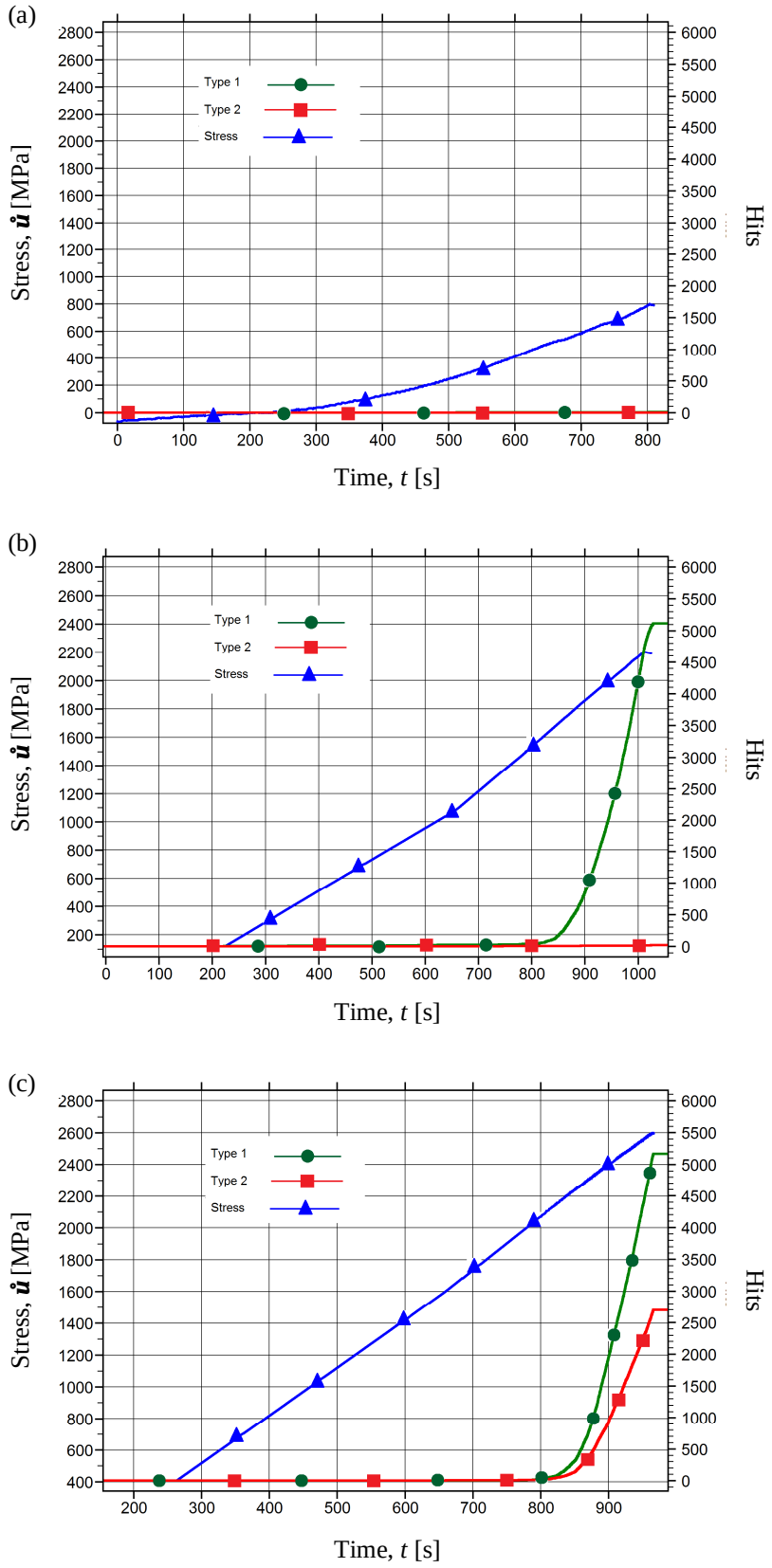

Figure 2.4.8. Applied stress and AE signal results (in terms of the cumulated number of located hits) of monotonic stepwise tests in 1.2379 vs time. (a) 800 MPa. (b) 2200 MPa and (c) 2600 MPa.

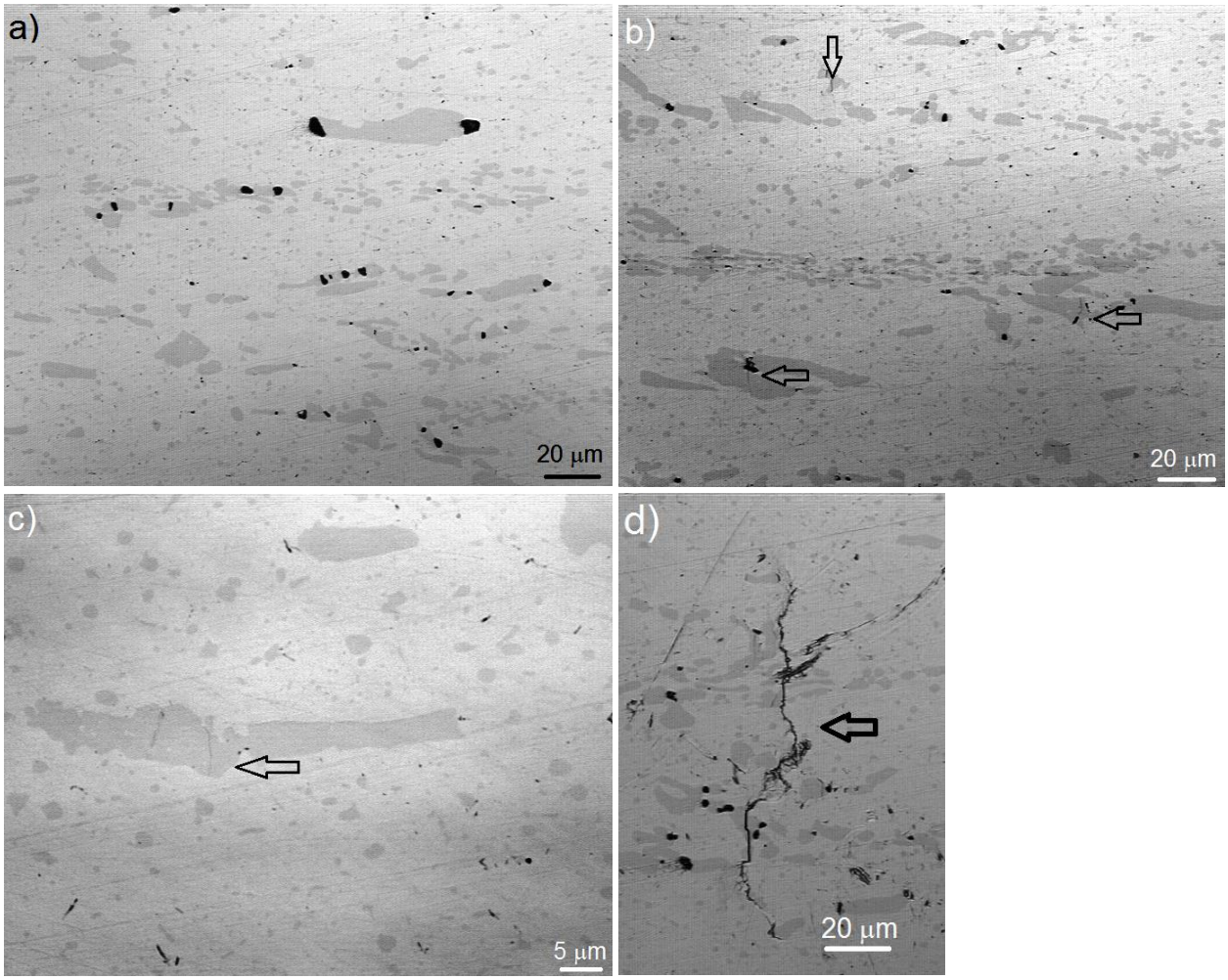

Figure 2.4.9. Images of the micro-structure of 1.2379: (a) 800 MPa, (b)-(c) 2200 MPa and (d) 2600 MPa.

2.4.3.4. Relationship between AE signals and micro-damage during bending tests of HWS under monotonic loading

In HWS only a few AE signals could be detected when performing the same analysis as in 1.2379, even when the acquisition threshold established for noise amplitudes was reduced to a lower value (30 dB). Figure 2.4.10(a) and Figure 2.4.10(b) show the cumulated number of hits as a function of the applied stress for stepwise tests of HWS at 3300 and 4100 MPa respectively. In these figures it can be seen that the first signals were recorded at 1700 MPa but just a few hits

were detected and they were mostly Type 1 signals. With only these small amounts of signals being detected, and given the very small microstructural size of HWS, no cracks could be observed on the surface at 3300 MPa (as shown in Figure 2.4.11(a)). However, when the load was increased to 4100 MPa, there were just a very few small cracks nucleated in the microstructure, both at broken primary carbides and at inclusion particles, as shown in Figures 2.4.11(b) and 2.4.11(c).

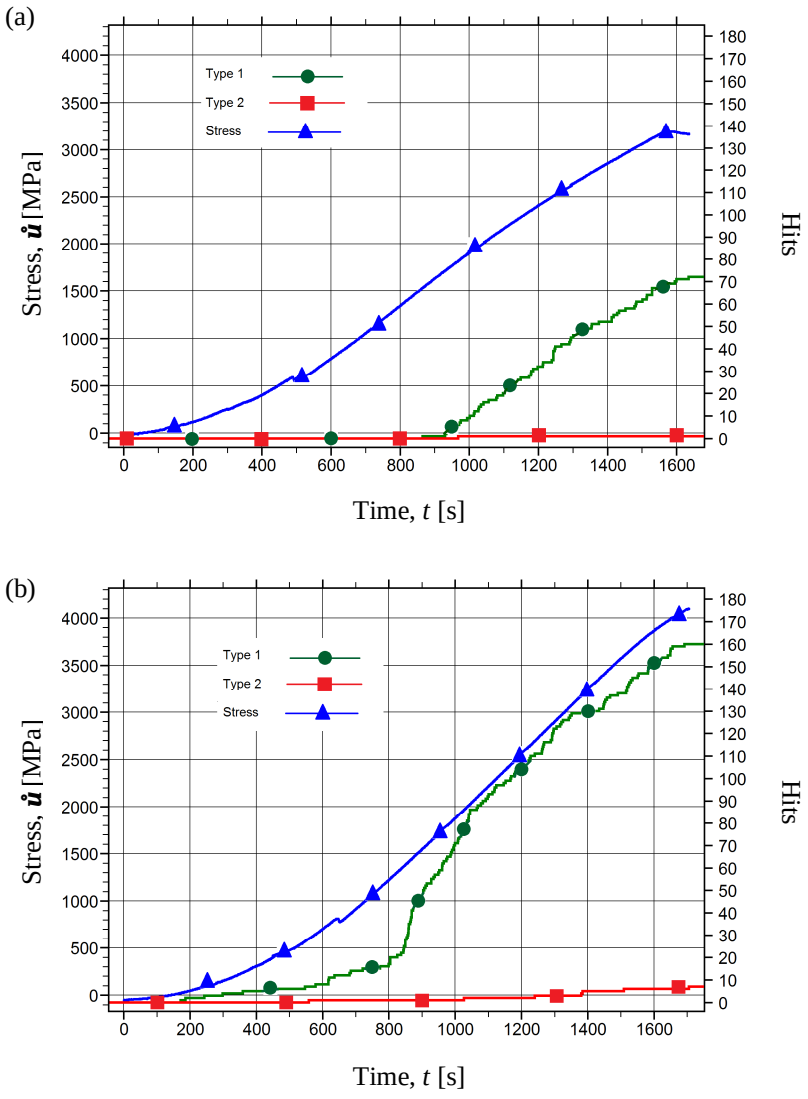

Figure 2.4.10. Applied stress and AE signal results (in terms of the cumulated number of located hits) of monotonic stepwise tests in HWS vs. time: (a) 3300 MPa and (b) 4100 MPa.

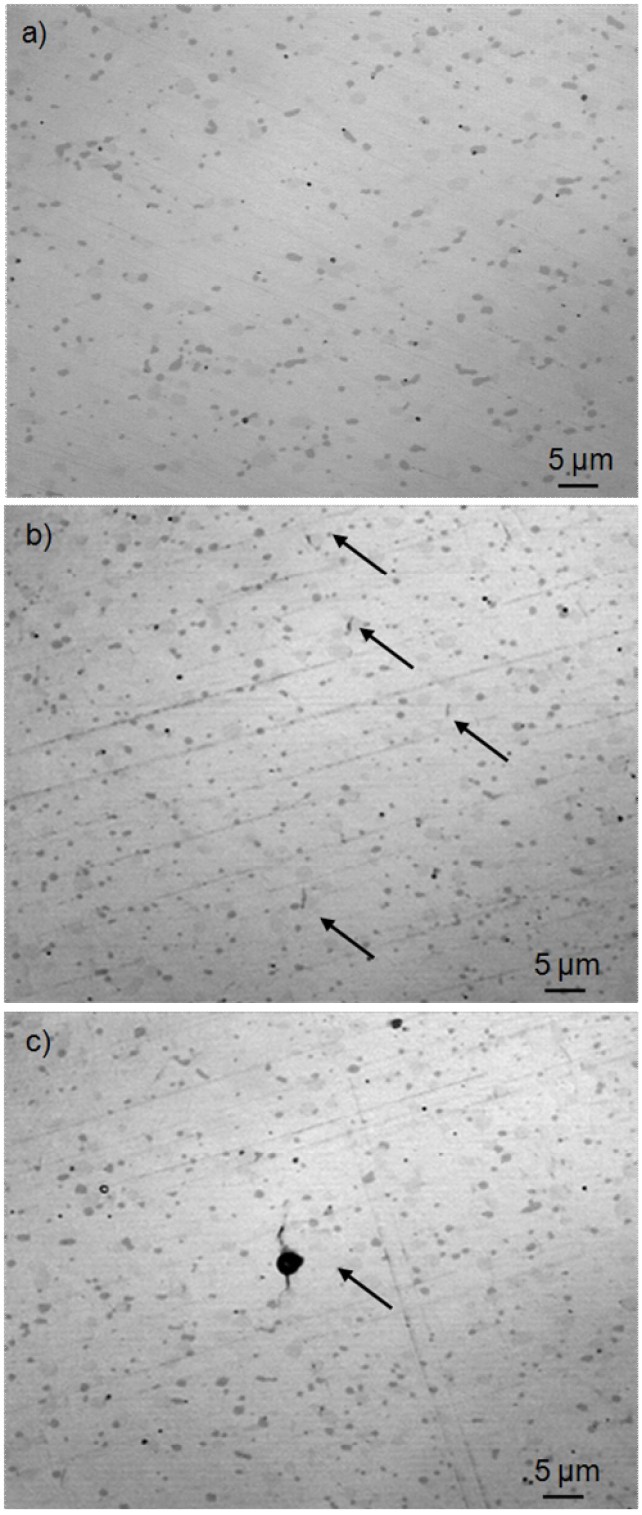

Figure 2.4.11. Images of the microstructure of HWS: (a) loaded at 3300 MPa, and (b)-(c) loaded until 4100 MPa.

2.4.4. Discussion

The data shown above these lines demonstrated that the AE technique, coupled to the bending tests under monotonic conditions, was able to provide accurate information regarding the acting micro-mechanical and damage mechanisms of 1.2379, the ingot metallurgic steel. In this case, the nucleation and propagation of cracks in the microstructure was well identified by means of two different types of AE signals reporting respectively, the breakage of carbides in the microstructure, i.e. the nucleation of cracks, and the moment when these cracks left the carbide and grew through the metallic matrix, i.e. the propagation of cracks. Therefore, this technique provided a unique and very accurate tool to determine the threshold stresses at which carbides started to break and thus, the stresses at which the first cracks were nucleated.

In case of HWS, the PM steel, it was found that even though the first signals started at 1700 MPa, only very few hits were registered compared to the high amounts obtained with 1.2379. These signals corresponded to the Type 1 previously defined and therefore, in correlation to what it was observed in 1.2379, some cracks were expected to have nucleated in the microstructure. However, no damage could be identified on the surface until a stress of about 4000 MPa was applied. At that moment, very small cracks were detected in primary carbides and inclusions. It is worth pointing out that practically no Type 2 signals were recorded before the final fracture of the sample, nor any propagation of cracks. This meant that the very high fracture resistance of HWS was mainly due to the contribution of a very high resistance to crack nucleation, but that the propagation of the nucleated cracks to final fracture took place very rapidly (in a very brittle-like manner).

In order to shed light on these phenomena, especially on the differences between the two steels, the concepts of Linear Elastic Fracture Mechanics (LEFM) were used. A basic equation of LEFM is shown in Eq. 2.4.1, where K is the acting stress intensity factor, Y a geometrical correction factor calculated after Newman and Raju [3], $\boldsymbol{\mathring{u}}$ the applied stress and a the crack length:

$$K = Y \cdot \sigma \cdot \sqrt{a} \qquad \text{(Eq. 2.4.1)}$$

Under such high applied stresses, as those sustained by HWS (e.g. 4000 MPa), it is reasonable to say that even if a very small crack is nucleated at a carbide in the microstructure (with an a value of 5 ε m for example), K of this crack can already attain values close to those of the fracture toughness of the material, K_{IC}, and hence, fracture may be imminent (for a = 5 ε m, $\boldsymbol{\mathring{u}}$ = 4000 MPa and Y = 1.2, K = 11 MPa·m$^{1/2}$ while K_{IC} is 21 MPa·m$^{1/2}$). Furthermore many cracks are nucleated at such stress levels and thus, coalescence of these cracks is prone to occur and rapidly lead to fracture.

In 1.2379 the first cracks were nucleated at much lower stress values (e.g. 1500 MPa) in the large primary carbides embedded in this steel (higher a values, e.g. 15 ε m), but as shown in Table 2, the K_{IC} of 1.2379 is higher than that of HWS (28 vs 21 MPa·m$^{1/2}$ respectively). Thus, cracks may propagate to longer lengths before critical failure takes place (K assuming a = 15 ε m, $\boldsymbol{\mathring{u}}$ = 1500 MPa and Y = 1.2 is equal to 7 MPa·m$^{1/2}$ and K_{IC} 28 MPa·m$^{1/2}$), and they would be easier to be identified both by visual inspection of the surface and by means of AE techniques. In addition, the much larger primary carbides of 1.2379 compared to HWS would lead to the propagation of a relatively large number of cracks on the surface (where the stresses during the three points bending test are maxima) instead of perhaps only a single crack inside the material (as could have been the case if there were a sufficiently large inclusion in the interior of an HWS

sample). Therefore, cracks in 1.2379 would always be observed by surface inspections, while those of HWS would not.

In any case, the results obtained in the present study suggested that further work should be devoted to characterizing the fracture phenomena in steels with very fine microstructures, such as powder metallurgy tool steels. The findings of this investigation were not enough to clarify whether cracks really nucleated in the microstructure of this PM steel at stresses around 1700 MPa, or whether the AE technique introduced in this work was insufficient to identify the initial stress level for crack nucleation in HWS samples.

Only a very little AE activity was detected in the tests on HWS steel, and this has been related to the small sizes of the nucleated cracks. This brings to mind the question whether the HWS steel may have been producing events that were below the detection threshold of the system.. Further improvements to the present work will consider the use of sensors specially adapted for low amplitude signals in the testing of HWS, so that even smaller events in the microstructure can be captured and analyzed.

2.4.5. Conclusions

The coupling in this study of AE and CM techniques with bending fracture tests provided helpful results for understanding in great detail the failure mechanisms of tool steels under such applied loading, as well as the interactions of their microstructural constituents. An ingot metallurgy steel and a powder metallurgy steel, analyzed by this means, had very different microstructural features such as the size, geometry and distribution of the primary carbides embedded. In the first of the tool steels studied, DIN 1.2379, two different AE signal wave

patterns were identified during a fracture test. With the help of CM, these signals were respectively assigned to crack nucleation in primary carbides (Type 1), and the propagation of these cracks through the metallic matrix (Type 2). The second of the studied materials, HWS steel manufactured by powder metallurgy, had a very fine microstructure with very small carbides distributed homogeneously in the matrix. In this steel, some Type 1 AE signals started to be detected at a certain applied load, but no damage could be observed at the surface of the sample until much higher applied stresses were applied. Type 2 AE signals were practically nonexistent in this material moreover, no propagating cracks were observed with CM. A fracture mechanics analysis made it possible to understand why such different behaviors were observed in these two materials. However, further work is required to rationalize the AE observations in HWS, and for that, new and more sensitive tests are planned in order to ensure a more accurate characterization of the phenomena taking place in the microstructure.

2.4.6. References

[1] Picas, I.; Hernández, R.; Casellas, D.; Valls, I.; Strategies to increase the tool performance in punching operations of UHSS. *Proceedings of the IDDRG Conference,* Graz (Austria), 2010, pp. 325-334.

[2] Fukaura K, Ono K (2001) Acoustic emission analysis of carbide cracking in tool steels. J. Acoustic Emission 19:91-9

[3] Newman JC, Raju IS (1984) Stress intensity factor equations for cracks in three dimensional finite bodies subjected to tension and bending loads. NASA Technical Memorandum 85793.

Chapter 3: Damage induced by spherical indentation test

3.1. Introduction

Failure detection in tools is a fundamental issue in manufacturing processes, as their premature failure is one of the most important factors ï and directly reflected ï in the price of manufactured parts. Thus, understanding fracture events in tools is crucial for foreseeing tool lifetime and further developing tool steels with an improved mechanical performance [1,2].

Spherical indentation, also known as Hertzian indentation [3, 4], is a widely-applied test due its experimental simplicity and the small sample volume required for the study of contact mechanics. The spherical indentation technique allows the simulation of a typical ñbluntò in-service condition [5], where the stress field distribution beneath the contact may be similar to those observed in shaping tools. The advantage of spherical indentation over other sharp indentations is the complete evolution of damage modes, as a progressive transition from initial elastic to final full plastic contact. This behavior makes the Hertzian indentation technique a useful tool in assessing damage mechanisms (e.g. cracks) which may occur in the elastic field, plastic field or the transition between both.

Furthermore, indentation tests can be monitored by means of AE as a useful in-service damage detection technique [6,7]. The AE technique is based on capturing on the surface of a specimen or component the transient elastic waves that are generated when a release of energy is produced within a material caused by a structural alteration, such as a crack or a dislocation [8]. This technique is the most common way of on-line monitoring of brittle coating failure in Scratch and Micro-Indentation testing [9,10]. However, most commercially-available instruments present poor information since they only supply an integrated RMS signal, which is sensitive to friction and poses difficulties in detecting low-medium elastic energy events that occur [9], for instance, carbide cracking in tool steels.

Spherical indentation tests monitored by AE have been widely used in different materials to identify the typical cone or radial cracks produced by the test [4]. It is the first fracture mechanism that occurs during the Hertzian loading of brittle materials. Ceramics have been analysed by AE to detect the initiation and propagation of ring cracks [11-13]. The behavior and failure mechanisms of coated samples with different substrate and coating mechanical properties have been studied by means of AE [9,14] and even metal foams for the automotive and aerospace industry [15]. In general, all these studies deal with homogeneous materials; Padture [16] presents the different crack propagation between the homogeneous and heterogeneous structure of silicone carbide when fatigue spherical contact is applied. Nevertheless, Guiberteau et al. [17] performed AE-monitoring on a spherical indentation test to investigate the effect of grain size in deformation and microfracture in polycrystalline alumina. The results reveal differences from an ideally brittle response which are associated with the generation of a deformation-microfracture damage zone in the confined region of strong compression and shear stresses beneath the indenter. The fully-developed damage zone is made up of an accumulation of microstructurally-discrete events, each consisting of some kind of intergrain shear faulting

accompanied by intergrain microcracking. This cumulative damage zone is quite different from the continuous Hertzian cone fracture that occurs in the weak tensile region outside the contact circle in classically homogeneous brittle materials. The results also confirmed that higher size grain ceramics are more sensitive to these micro-fractures by shear stress.

Tool steels have a non-homogeneous microstructure, and carbide cracking is the origin of cracks in these steels. Thus, obtaining information about carbide cracking during the indentation test prior to the appearance of cracks in the metallic matrix would be efficient in studying tool behavior. Some works have studied the mechanical properties of tool steels and coated tool steels by spherical indentation and other indentations methods [18-22]. Most of them focus on detecting cracks and not on microscopic damage such as broken carbides or precipitates. For this purpose, micro- or nano- indentation tests are performed which break them by directly applying the load on the carbide; see, for example, references [23,24]. To the best of the authorsô knowledge, the fracture detection of these hard particles by AE produced during spherical indentation has not yet been analysed. In the previous chapter, AE monitoring on three-point bending tests have been performed to determine the stress level at which primary carbides of some cold-work tool steels begin to break. In that chapter, the carbide cracking mechanism was due to tensile stress. Although the information obtained is useful for studying the properties of carbides, tool-shaping is subject to more complex loading conditions [25] more similar to that obtained by Hertzian indentation.

This chapter describes an AE-instrumented spherical indentation test to identify the breakage of carbides while the indentation stress remains lower the radial crack stress. According to the results obtained in other materials [26,27], carbide fractures are expected due to the shear stress

produced under the indenter contact. The article assesses the contact response of commercial tool steel under monotonic load up to 3000 N (elastic field) and 5000 N (plastic field).

3.2. Spherical indentation test

The problem of elastic contact between two bodies has been widely studied in literature [4,28-30] due to the interest of such theoretical and practical applications. Considering a frictionless contact of a rigid material sphere with a radius *R*, at normal load *P*, on a flat continuum specimen (Figure 3.1), if the load reaches a critical value P_c, circular cracks with a radius r_0 (slightly larger than radius *a* of the contact between the ball and the material) are formed. The field is initially elastic. From a critical load, circumferential or cone cracks on the specimen surface (ñbrittle modeò) or a subsurface deformation zone (ñplastic modeò) appear. This research is focused on the subsurface damage and therefore the basic features of the stress fields associated with this region are outlined here.

The test makes it possible to follow the entire evolution of damage modes, as a progressive transition from initial elasticity to plasticity (Figure 3.2). When an elastic sphere is pressed against the surface of an elastic material, the maximum shear stress of the specimen occurs at the axis of the load at a depth of $\approx 0.5 \cdot a$ below the contact surface (Figure 3.1):

$$\tau_{max} = 0.48 \cdot p_0 \qquad \text{(Eq. 3.1)}$$

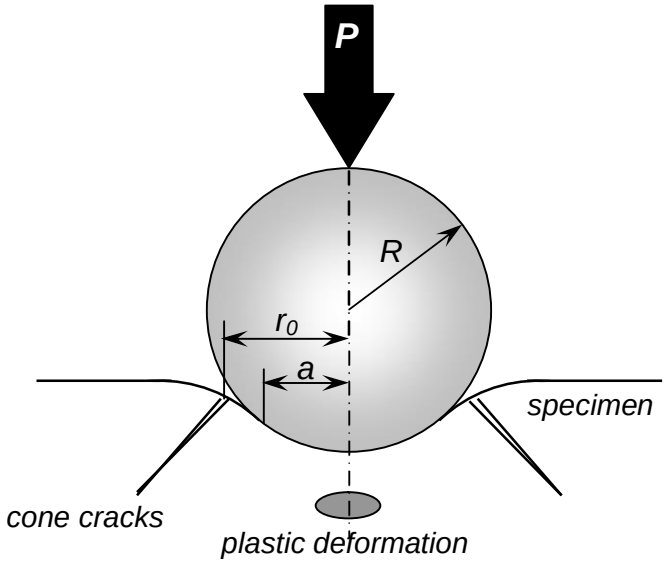

Figure 3.1. Hertzian contact of sphere on flat specimen. Deformations are exaggerated for clarity. *a* is the contact radius, r_0 is the crack radius at the surface of the specimen, *R* is the radius of the ball indenter and *P* is the indentation load.

In an elasticï plastic material, yielding first occurs below the surface where the shear stress is maximum. At this point, when the yield is incipient, the applied load *P* is identified with the yield load P_Y and the Hertzian solution still holds [3] (Figure 3.2). In small application loads the tool steel response could be assumed as having an elastic or ñpseudo-elasticò behavior because it exhibited a total recovery in depth penetration upon unloading. Within this context, the basic Hertzian solution was used to predict the linear elastic relation of the indentation stress-strain curve using the following equation [4]:

$$p_0 = \frac{3 \cdot E}{4 \cdot \acute{} \cdot s} \cdot \frac{a}{R} \qquad \text{(Eq. 3.2)}$$

where: *E* is the Young´s modulus of the cold-work tool steel and *s* is a dimensionless coefficient ($s = (9/16)[(1 \quad \gamma^2) + (1 \quad \gamma'^2)E/E']$ and υ and $\upsilon\hat{o}$ are the material and indenter Poisson´s ratio, and $E\hat{o}$ is the Youngôs modulus indenter. Eq.3.2 is the fundamental equation of

the Hertzian theory relating indentation stress (p_0) and indentation strain (a/R) in the elastic range.

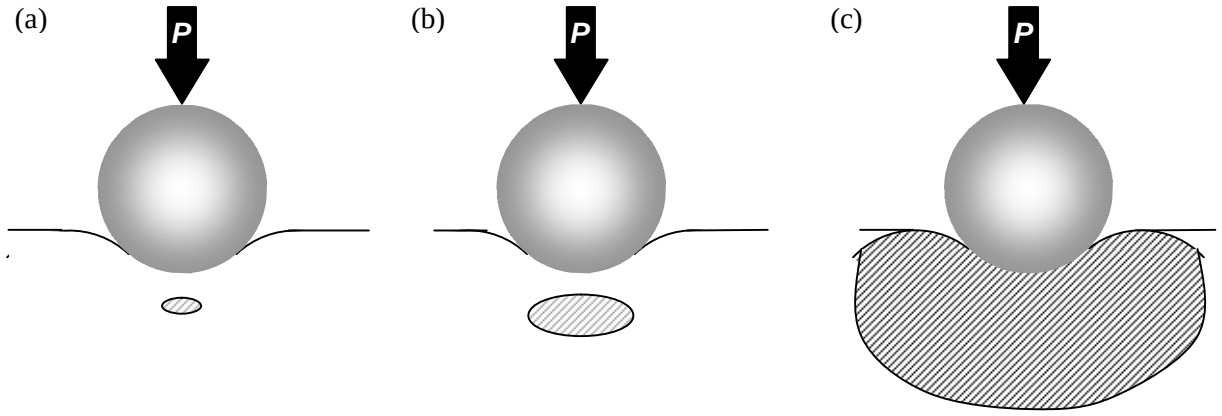

Figure 3.2. Schematic of the evolution in the deformed zone under the indentation for: (a) $p_0 = p_y$, (b) $p_0 > p_y$ and (c) $p_0 >> p_y$.

3.3. Experimental method

3.3.1. Material

Commercial cold-work tool steel was selected for the study. It is a ledeburitic steel obtained by ingot metallurgy routes. The main elements forming founded in its chemical composition are shown in Table 3.1. Heat treatment was applied to the samples in order to obtain a hardness level of 60 ï 62 HRC. This steel presents considerable toughness and a remarkably high compressive strength together with good wear resistance.

Table 3.1. Main alloying elements in the chemical composition of the studied steel (in weight percent %).

C	Cr	Mo	V	W	Others
1.2 ï 1.3	8.0 ï 9.0	2.0 ï 3.0	1.0 ï 1.5	-	+ Nb +Al

This steel presented a total percentage of 7.9 % primary carbides of the following types: 6.10% are M_7C_3, 0.80% are MC and 1.00% are M_6C (see Figure 3.3). In Table 3.2 the mean carbide sizes and morphologies are shown for M_7C_3, MC and M_6C. The size distribution of the primary carbides was determined by means of image analysis using a minimum of 15 images. Backscatter detection was employed to contrast carbides and metallic matrix and classify carbides with different chemical compositions. Images were randomly taken at 500X. The size of primary carbides was determined in terms of the equivalent diameter, *ECD*, minimum diameter, D_{min} and maximum diameter, D_{max}. The *ECD* is the diameter of a circle that has an area equal to the area of the carbide. D_{min} and D_{max} of a particle for angles in the range 0º through 179º with step width 1º. The morphology was assessed by means of the aspect ratio, *AR*, sphericity, γ, and shape factor, *SF*. *AR* is the maximum ratio of width and height of a bounding rectangle of the particle. Sphericity is described as the ćroundness of the particle by using central moments, being 1 for a spherical particle while for all other particles it is smaller than 1. More information about these values and how they were measured can be found in [31].

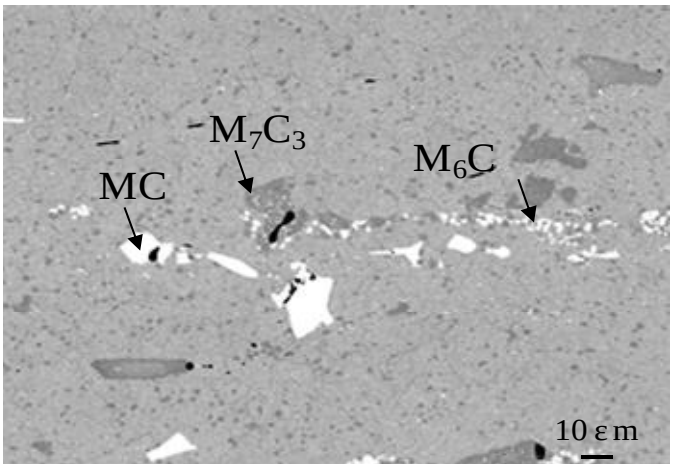

Figure 3.3. Backscatter diffraction images showing the carbides identified in the microstructure.

Table 3.2. Mean carbides size and geometry in terms of *ECD*, D_{min}, D_{max}, *AR*, γ and *SF*.

Carbide	*ECD* [εm]	D_{min} [εm]	D_{max} [εm]	*AR*	γ	*SF*
M_7C_3	11.2 ± 0.7	10.3 ± 6.6	21.6 ± 13.0	2.5 ± 1.2	0.2 ± 0.2	0.3 ± 0.2
MC	7.8 ± 2.8	7.3 ± 3.1	13.7 ± 4.9	2.2 ± 1.1	0.3 ± 0.2	0.3 ± 0.2
M_6C	1.0 ± 0.7	0.8 ± 0.7	1.3 ± 1.3	1.7 ± 0.7	0.4 ± 0.3	0.9 ± 0.3

3.3.2. Specimens

Prismatic specimens of dimensions 40x30x20 mm were grinded and polished on one side (indentation face).

3.3.3. Spherical indentation

Indentation tests under monotonic conditions were performed in a servohydraulic testing machine (MTS Landmark 370.02 100Hz) and were focused on obtaining the indentation stress-strain curves and determining the critical load for the damage emergence at the sub-surface of steel. In doing so, normal loads (*P*), between 3000 N and 5000 N, were imposed by means of trapezoidal waveform at a loading rate of 20 $N \cdot s^{-1}$ and applying the full test force during 20 s. The indenter was a sphere of AISI 52100 steel with a curvature radius of 14 mm. Indenter properties correspond to: 758 ± 13 HV1 hardness, 210 GPa Youngôs modulus and 0.33 Poisson ratio. The indenter balls were continually inspected and, if required, replaced to avoid the flattening in the contact area.

Contact radius *a* at each given load *P* was estimated from the residual impression measurement. The transition from elastic to plastic deformation was experimentally estimated by

applying low loads (between 2000 and 5000 N) on the surface of specimens sputter-coated with gold, and employing only the residual imprints obtained from an indenter with a curvature radius of 14 mm. In this case, although elastic recovery causes the depth of the residual imprint to be different from the one existing when fully loaded, the radius of the contact impression remains virtually unchanged [3]. Thus, the contact radius can be measured from the imprint in gold coated specimens after unloading through confocal Laser scanning microscopy (CLSM).

In addition, to visualise the residual depth, emergence profiles were acquired by means of confocal microscopy (Sensofar Plµ 2300). Metallographic characterisation was done by means of a sequential polishing process, from the surface of the residual imprint to the sub-surface damage.

3.3.4. Acoustic Emission

Commercial AE equipment (by Vallen Systeme Gmbh.) was used for signal detection and analysis. Two small magnetic AE sensors were secured to the specimens in order to detect the AE signals (Figure). The sensors were the resonant type (VS700 D) with a frequency range of between 100 ï 800 kHz and a peak frequency of 600 ï 800 kHz (flat range). Two pre-amplifiers with a gain 34 dB of the same brand were used (EAP4). The signals were recorded and analysed using a four-channel analyser system (AMSY-5). The system allowed waveform detection and storage.

The position of the sensors was finally established on the lateral side of the specimen (Figure 3.4), where the signal-to-noise ratio was highest. Sensors attached to the upper flat side of the specimen were less sensitive and more influenced by frictional noise.

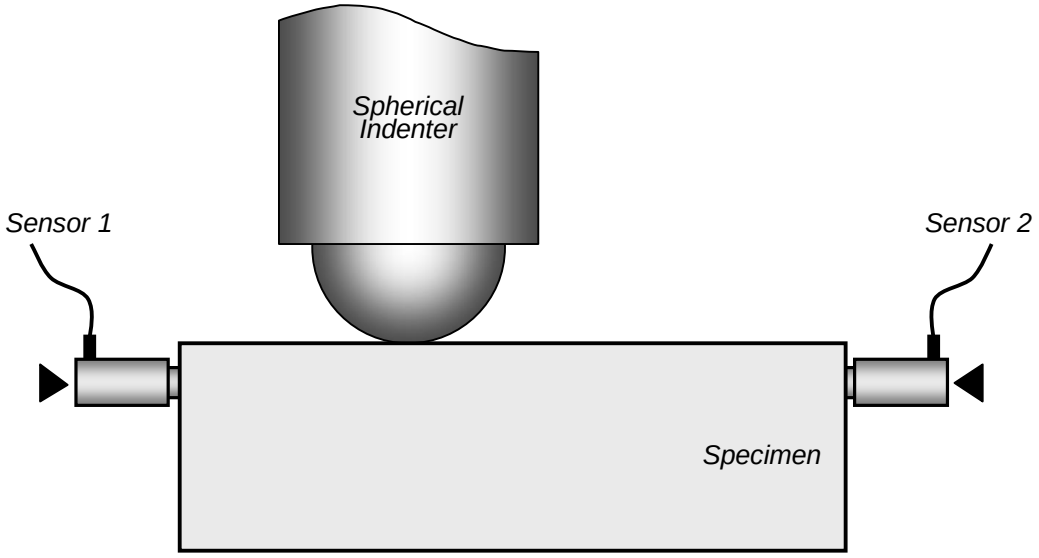

Figure 3.4. Schematic diagram for spherical indentation test.

3.3.5. Filtering noise

The test environment was noisy, and the AE signals were usually weak. Consequently, noise identification and valid signal discrimination is critical for successful AE results [32,33]. The most important source of unwanted signals was the hydraulic system of the testing machine (flow noise, friction and vibration of the valves), and they were transmitted to the specimen through the gripping system. Physical filtering was performed covering the gripping parts in contact with specimen with PVC film. Additionally, digital filters of 95 ï 850 kHz were applied in order to eliminate most of the mechanical noises of the servohydraulic system.

Some preliminary measurements of the background noise were conducted in order to determine the threshold level. The sensors were attached to the specimen and AE activity was detected with amplitudes below 43 dB; thus, the threshold level was fixed at 46 dB.

3.4. Results and Discussion

3.4.1. Damage induced by spherical indentation

Figure 3.5 shows the indentation stress-strain curve, showing both the experimental and theoretical (Eq. 2) results obtained using the measured contact radius (a), the experimental indentation stress or mean contact pressure (p_0) and strain (ε) where p_0 equals $P/\pi a^2$ and ε equals a/R, [28].

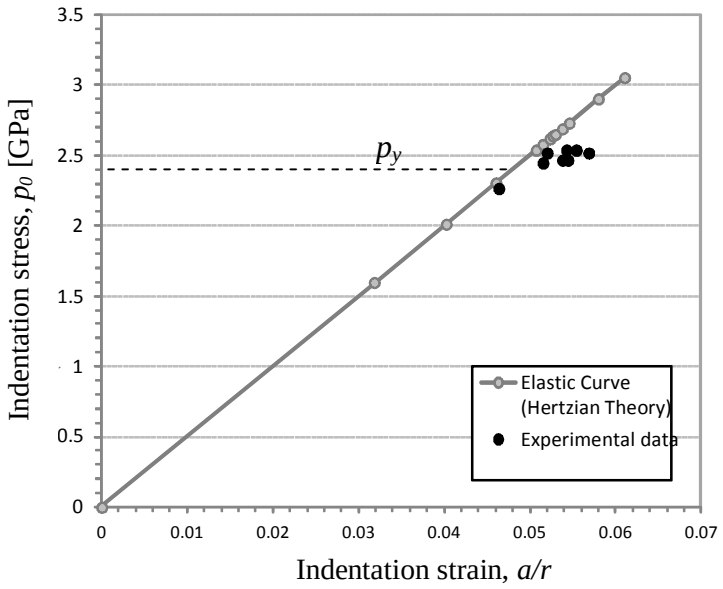

Figure 3.5. Spherical indentation stress-strain curve for plastic transition.

As the load increases above P_Y, the yield zone expands and this relationship can change radically. The value of P_γ is found by measuring the impressions profile of the specimens sputter-coated with gold for different loads until plastic deformation, if any. Figure 3.6 illustrates the evolution of the impression profile for the tool steel. In this case, the tool steel surface was deformed elastically at low indentation pressure, and as the stress increased, the residual depth

was evidenced. Transition from elastic to plastic deformation was observed at stresses of ~2.4 GPa, similar to other cold-worked tool steels reported in previous studies [34].

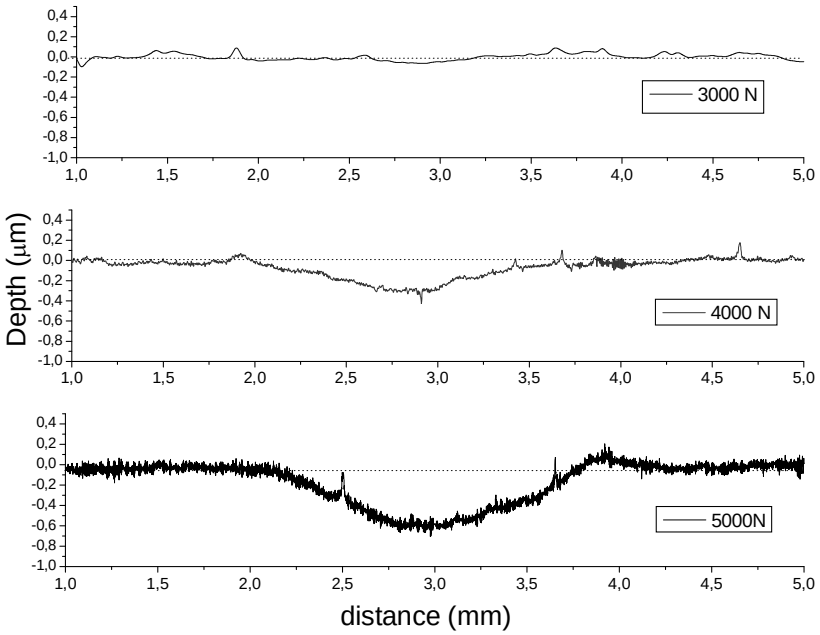

Figure 3.6. Remnant indentation depth profiles and imprints in cold work tool steel. Specimens sputter-coated with gold.

Following the results obtained, two different load condition indentations were decided: a maximum load of 3000 N to remain within the elastic range with total recovery and a second test up to 5000 N to ensure the appearance of permanent deformation. Under these conditions, the physical damage mechanisms expected in this material are carbide breakage, plastic deformation and/or crack nucleation or propagation in the metallic matrix [26,27].

3.4.1. Acoustic emission results

The waveforms shown in Figure 3.7 give information about the events that take place in the material. When a crack occurs within the material, quasi-instantaneous explosion-like energy releases propagating stress waves in all direction. Figure 3.7(a) and Figure 3.7(b) show the

waveform of events occurring during the loading and unloading of indentation tests respectively. The waveforms present a short duration and thus they are clear discrete burst hits, as shown in Figure 3.7(a) and 3.7(b), which indicate the existence of well-defined local instabilities in the material. Only when the test load exceeds 3000 N do some low amplitude continuous signals appear which are related to the plastic deformation process (Figure 3.7(c)).

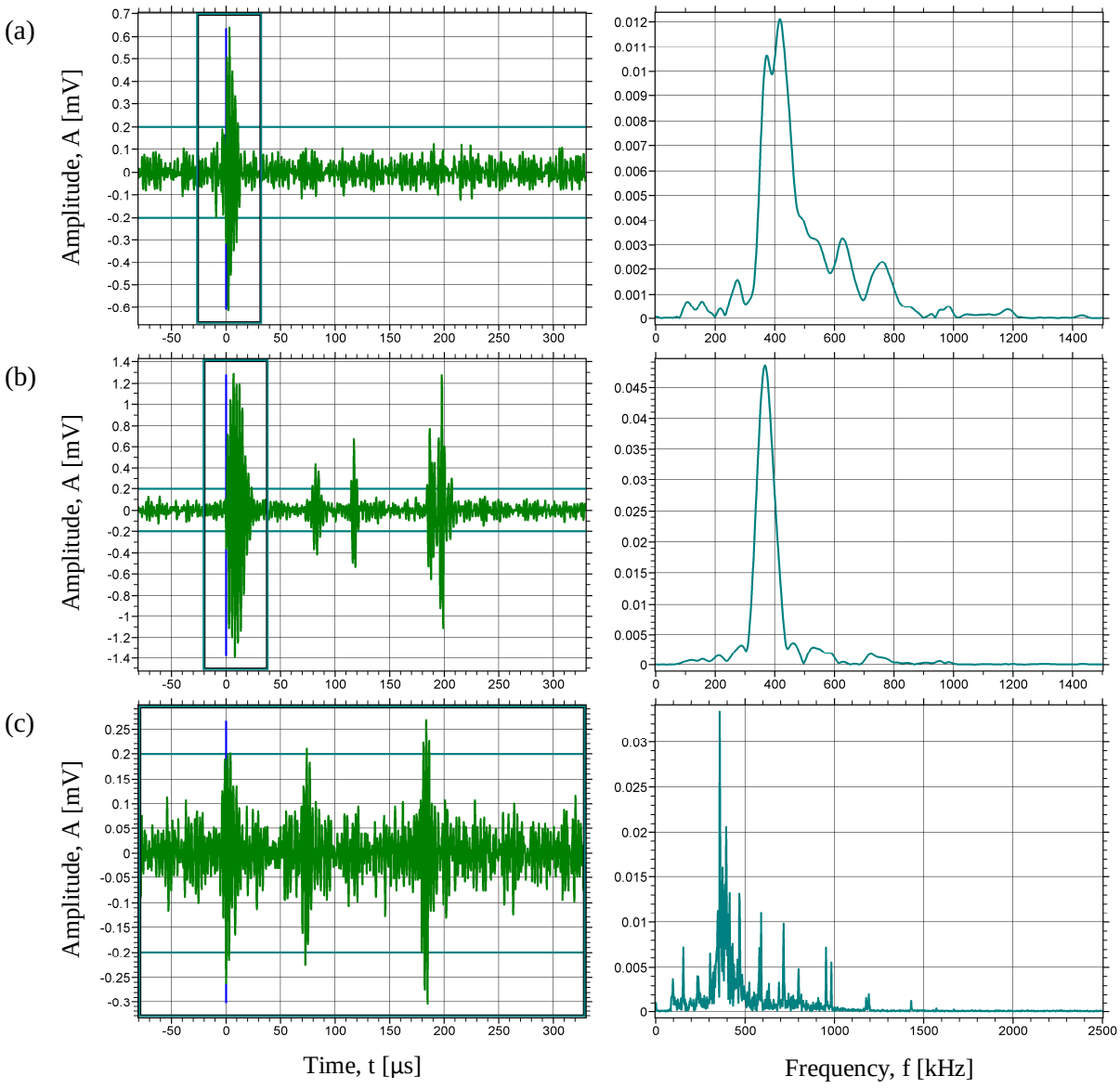

Figure 3.7. Waveforms and FFT of different events. (a) an event during loading, (b) an event during unloading the specimen and (c) continuous type signals that appear when the load exceeds the elastic field; these signals are related with plastic deformation.

Table 3.3 summarises the loading that induced AE burst activity for some of the indentations during loading; the mean contact pressure (p_0) and the maximum shear stress produced at the subsurface of the specimen are also calculated with Eq.3.2 and Eq.3.1 respectively.

Table 3.3. Load and stress values at which AE burst signals appears for four indentations up to 3000 N and four up to 5000 N.

Max.Load	Indentation	*P* [N]	*a* [εm]	p_0 [GPa]	τ [GPa]
3000 N	1B	2902	637.10	2.28	1.09
	2B	496	353.56	1.26	0.61
		555	367.06	1.31	0.63
		2875	635.12	2.27	1.09
	3B	2294	589.08	2.10	1.01
	4B	118	219.08	0.78	0.38
	5B	892	429.96	1.54	0.74
		2235	583.98	2.09	1.00
		2645	617.71	2.21	1.06
5000 N	4A	2190	580.04	2.07	1.00
	5A	1370	496.08	1.77	0.85
	6A	2091	517.16	2.04	0.98
		4570	741.22	2.65	-
	7A	264	286.53	1.02	0.49
		2433	600.74	2.15	1.03
	8A	171	247.92	0.89	0.43
		981	443.81	1.59	0.76
		2889	636.15	2.27	1.09

Figure 3.8 shows the AE activity during spherical indentation tests for specimens loaded up to 3000 N (elastic behavior of the material was expected). AE hits are represented as a dot by their amplitude (green S1 and red S2). The AE activity appears in some load values as an isolated,

rapid event clearly detected by both sensors. These signals are burst type, as figure 7(a), and they appear in all the tested specimens during loading.

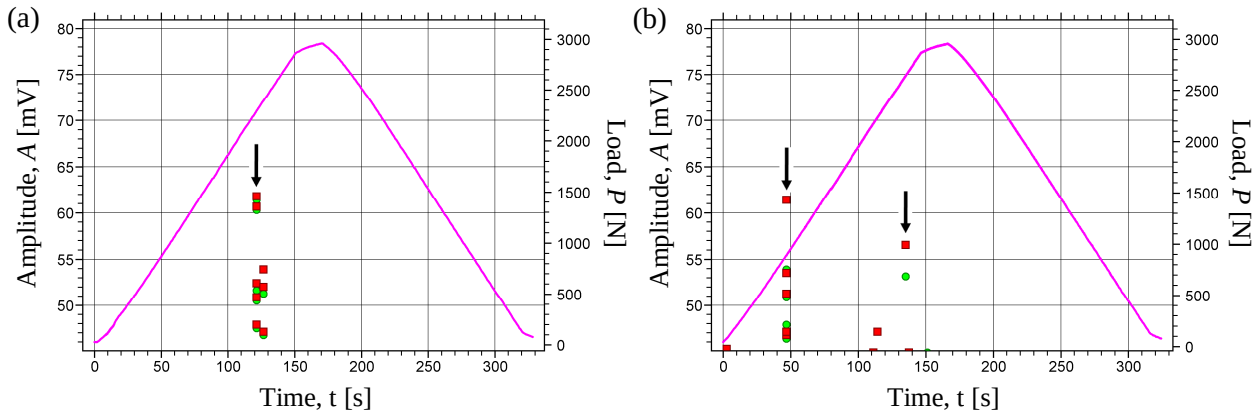

Figure 3.8. Indentations P_{max} = 3000N. (a) Indentation *3B* (b) Indentation *5B*. Green points correspond to sensor 1 (S1) and red points to sensor 2 (S2).

Figure 3.9 shows some results obtained for loads up to 5000 N. In this case, plastic deformation is present in the material. The AE activity detected can be classified into two types: i) burst type signals, as in Figure 3.7(a) and 3.7(b); and ii) continuous AE activity of long duration and low amplitude (Figure 3.7(c)), which appears at loads higher than 3000 N and it remains during the full test load. This behavior may be related to the plastic deformation of the material due to the absence of this AE activity for loads below the plastic yielding onset, as shown in Figure 3.8. Also, some AE activity was found during the unloading. The most important effect produced by the change in the stress component corresponds to the damage mechanisms. Studman and Field [35] observed the presence of órадial cracksô in the periphery of the indentation print in carbon steels. They were attributed to hoop stresses. In fact, the authors deduced from experimental tests that these stresses tend to be higher during unloading. In the same way, Abudaia et al. [36] support this theory with experimental tests and a finite element model. Thus, during unloading, the stress field changes and may provoke more carbide cracking.

Another possibility for these unloading signals is that the carbide damage is produced during loading without emitting AE due to the compression field, and during unloading the stress relaxation permits the release of AE energy.

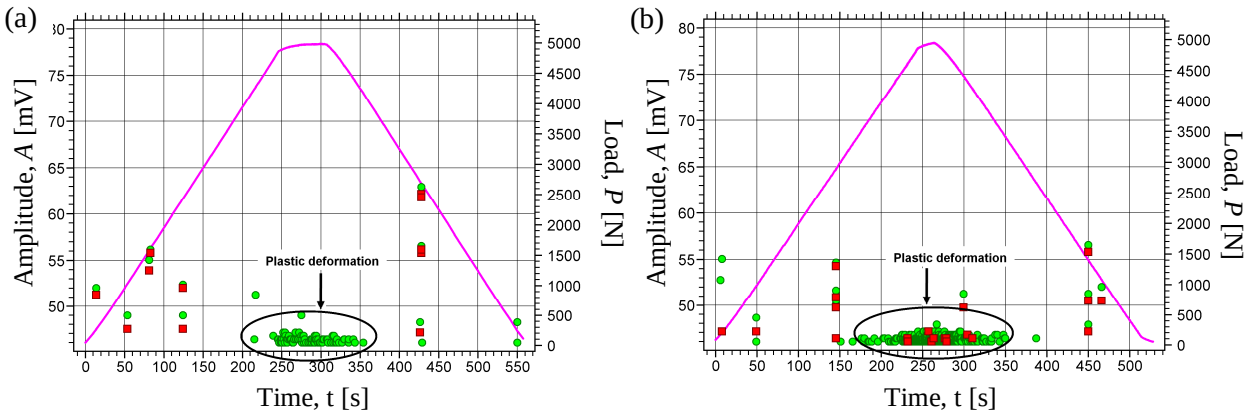

Figure 3.9. Indentations P_{max} = 5000N. (a) Specimen *7A* (b) Specimen 8A. Green points correspond to sensor 1 (S1) and red points to sensor 2 (S2).

Differences in events detection between loads could be related to the influence of microstructural features since they determine the amount of stresses magnified in the carbide region with respect to macroscopically-applied stress [37]. Hence, the fracture strength of the carbides, $\mathring{\boldsymbol{u}}^{RC}$, of this steel can vary quite a lot because of the presence of carbides of different sizes, shapes, morphologies and arrangements.

Picas [31] measured the fracture strength of primary carbides, $\mathring{\boldsymbol{u}}^{RC}$, in this steel and the values are summarised in Table 3.4. To determine the fracture stress, some prismatic specimens were submitted to stepwise bending tests, inspecting the tensile surface in each step. Thus, this stress value is assumed to correspond to the fracture strength of carbides under monotonic tensile loading. In this regard, $\mathring{\boldsymbol{u}}^{RC}$ of M_7C_3 and MC carbides are 500 ï 700 MPa and 1300 ï 1500 MPa respectively. The shapes of the M_7C_3 carbides are rather irregular and their size is quite high.

The MC carbides are rounder and more regular than the M_7C_3, and that is why they show a higher $\mathring{u}^{RC}$. The M_6C were too small and it was impossible to break them.

The AE burst-signals obtained correspond to carbide breakage, but in this case their fracture is produced by shear stress, not by tensile stress. If a volume element is considered beneath the contact surface, this is submitted to hydrostatic stresses. Figure 3.10 schematises the Hertzian field in this zone, and $-\mathring{u}_1$ and $-\mathring{u}_2$ represent the principal compression stresses. These components are generally unequal, thus a shear stress component acts on planes inclined to the principal axis, attaining a maximum value $\frac{1}{2}\cdot(\mathring{u}_1 - \mathring{u}_3)$. As was previously reported, the maximum shear stress in the Hertzian field occurs at $\approx 0.5\cdot a$ below the contact surface and its value is defined in Eq.3.1. This maximum shear stress is calculated for each load that produces AE for each specimen in Table 3.3.

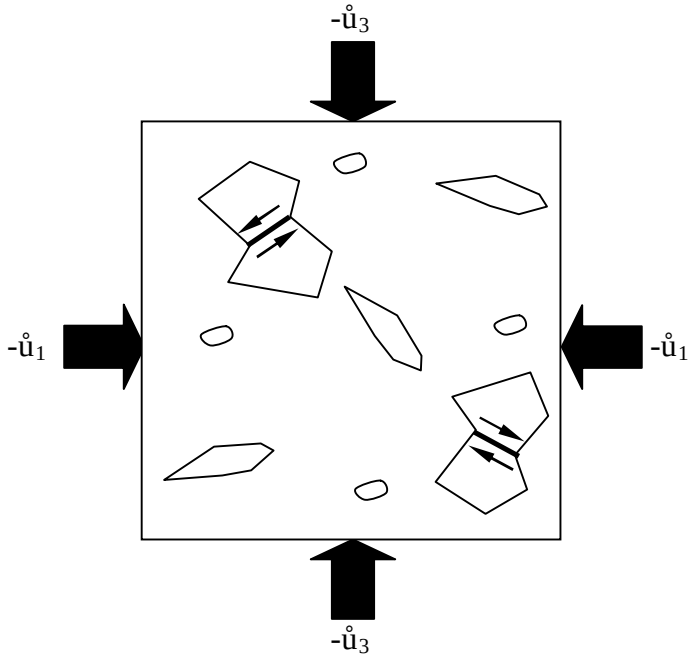

Figure 3.10. Schematic deformation-microfracture damage in tool steel. The volume element is subjected to compressive stress ï $\mathring{u}_1$ and ï $\mathring{u}_3$ along the contact axis below the spherical indenter. The shear stresses (arrows) initiate the breakage of carbides.

Therefore it is impossible to compare the applied maximum shear stress, τ, during spherical indentations with the carbide fracture stress, $\mathring{u}^{RC}$. Hence, the fracture shear stress of these carbides, τ^{RC}, is estimated based on the fracture tensile stress, $\mathring{u}^{RC}$. With this aim, following the failure theory of von Mises [38] τ^{RC} :

$$\tau^{RC} = \frac{\sqrt{3}}{2} \cdot \sigma^{RC} \qquad \text{(Eq. 3.3)}$$

Table 3.4 presents $\mathring{u}^{RC}$ and the estimated τ^{RC}. The expected τ^{RC} for M_7C_3 are 0.43 ï 0.61 GPa and 1.1 ï 1.3 GPa for MC. Observing the shear stress level related to AE during the loading (Table 3.3) it can be concluded that the AE signals are related to the breakage of both primary carbides caused by the shear stress produced on the subsurface of the specimen.

Table 3.4. Fracture stress of carbides: tensile fracture stress, $\mathring{u}^{RC}$, and shear fracture stress, τ^{RC}.

Carbide	$\mathring{u}^{RC}$ [MPa]	τ^{RC} [MPa]
M_7C_3	600 ± 100	520 ± 87
MC	1400 ± 100	1212 ± 87

After unloading, the samples were cut and sequentially polished to inspect the indented surface. Figure 3.11 shows the microscopic images of two indentation samples loaded up to 3000 N. In the images the M_7C_3 and the MC carbides can be seen; the first ones are the big white ones and the smaller darker ones are the MC carbides. These samples were loaded up to 3000 N and AE activity appeared during loading. Both images show cracks in both carbides (represented as white arrows for M_7C_3 and black for MC).

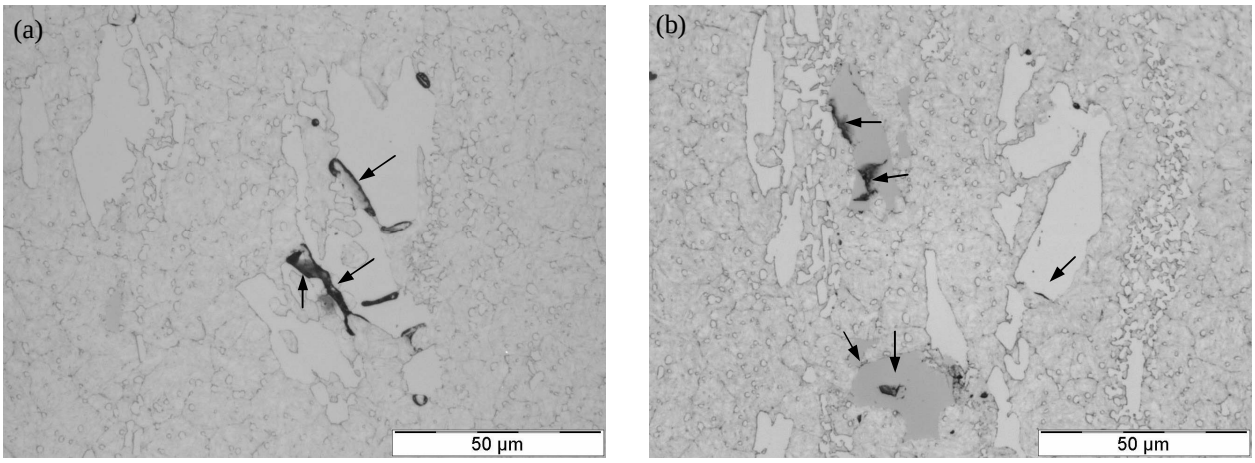

Figure 3.11. Images of the microstructure of the indented plane up to 3000 N (indentation 5B): (a) White carbides correspond to M_7C_3 and (b) darker ones to MC.

3.4. Conclusions

According to the experimental results obtained by means of coupling AE to spherical indentation tests, and the microstructural observation, the following conclusions can be drawn:

- AE is a useful tool for on-line incipient damage during spherical indentation tests. Thus, Hertzian tests monitored by AE enables the carbide breakage to be detected while the metallic matrix is under the elastic or plastic field, before the appearance of radial cracks on the surface of the specimen.
- Incipient damage in the microstructure was detected by AE. This technique was used to detect cracks during the indentation test and also allows the nucleation of these cracks to be detected.
- The stress levels at which the carbides were broken were determined by AE. These stresses were correctly correlated by the calculated/estimated fracture stress of carbides, in the case of M_7C_3 and MC.

- When an elastic field was generated by spherical indentation, the initial damage in tool steels is due to the carbide breakage caused by shear stress produced below the indentation contact.
- Incipient plastic deformation in the specimens was detected, and continuous AE signals were related with plasticity.

3.5. References

[1] Advanced High Strength Steel (AHSS). Application Guidelines. Version 4.1. International Iron & Steel Institute. Committee on Automotive Applications, June 2009. www.worldautosteel.org.

[2] Picas, I.; Hernandez, R.; Casellas, D.; Valls, I.; Strategies to increase the tool performance in punching operations of UHSS. R. Kollek (Ed.), Proc IDDRG, Graz, Austria (2010), pp. 325-334.

[3] L. Johnson: Contact Mechanics, Cambridge University Press, Cambridge, United Kingdom, 1985.

[4] Lawn, B.R.; Indentation of ceramics with spheres: a century after Hertz. *Journal of the American Ceramic Society*, Vol. 81 (1998), pp.1977ï 1994.

[5] Lawn, B.R. and Wilshaw, T.R.; Indentation fracture: principles and applications. *Journal of Materials Science,* Vol. 10, Nr. 161, pp. 1049-1081, June 1975.

[6] Padture, N.P. and Lawn, B.R.; Toughness properties of a silicon carbide with an in-situ induced heterogeneous grain structure. *Journal of the American Ceramic Society,* Vol. 77, Nr. 10, pp. 2518-2522, Oct. 1994.

[7] Faisal, N.H.; Ahmed, R.; Reuben, R.L.; 2011; Indentation testing and its acoustic emission response: applications and its emerging trends. Vol. 56, Nr. 2, pp. 98-142, March 2011.

[8] Scruby, C.B.; An introduction to acoustic emission; *Journal of Physics E: Scientific Instruments;* 1987, Vol.20; Nr.8; pp.946-953; doi: 10.1088/0022-3735/20/8/001.

[9] von Stebut, J.; Lapostolle, F.; Bucsa, M.; Vallen, H.; Acoustic emission monitoring of single cracking events and associated damage mechanism analysis in indentation and scratch testing; *Surface and Coatings Technology,* Vol. 116-119, pp. 160-171, Sept. 1999.

[10] von Stebut, J.; Multi-mode scratch testing ï A European standards, measurements and testing study. *Surface and Coatings Technology,* Vol. 200, Nr. 1-4 Special Issue; pp. 346-350, October 1, 2005.

[11] Wereszczak, A.A. and Johanss, K.E.; Spherical indentation of SiC, in Advances in Ceramic Armor II: Ceramic Engineering and Science Proceedings, 2008, Vol. 27, Issue 7 (eds. L. Prokurat, A. Wereszczak and E. Lara-Curzio), John Wiley & Sons, Inc., Hoboken, NJ, USA. Doi: 10.1002/9780470291368.ch4

[12] Bouras, S.; Zerizer, I.; Gheldane, F; Bouazza, M.T.; Bouzabata, B.; Study of the resistance to crack propagation in alumina by acoustic emission. *Ceramics International,* Vol. 34, pp. 1857-1865, 2008.

[13] Wereszczak, A.A.; Daloz, W.L.; Strong, K.T.; Jadaan, O.M.; Effect of Indenter Elastic Modulus on Hertzian Ring Crack Initiation in Silicon Carbide. International Journal of Applied Ceramic Technology, 2011, Vol.8, pp. 885ï 894. doi: 10.1111/j.1744-7402.2010.02522.x

[14] Gallego, A.; Gil, J.F.; Vico, J.M.; Ruzzante, J.E.; Piotrkowki, R.; Coating adherence in galvanizad steel assessed by acoustic emission wavelet ananlysis. *Scripta materialia*; 2005, Vol.52, pp. 1069-1074.

[15] Kádár, C.; Chmelik, F.; Lendvai, J.; Bacsán, N.; Rajkovits, Z.; Acoustic emission response of metcomd b foams during indentation. *Kovové Materiály*, Vol. 42, Nr. 4, pp.265-274, 2004.

[16] Padture, N.P. and Lawn, B.R.; Contact fatigue of a silicon carbide with a heterogeneous grain structure. *Journal of the American Ceramic*, 1995, Vol. 78, Nr.6, pp. 1431-1438.

[17] Guiberteau, F.; Padture, N.P.; Lawn, B.R.; Effect of grain size on hertzian contact damage in alumina. *Journal of American Ceramic Society*, Vol. 77, Nr. 7, pp. 1825-1831, July 1994.

[18] Nolan, D.; Leskovsek, V.; Jencko, M.; Estimation of fracture toughness of nitride compound layers on tool steel by application of the Vickers indentation method. *Surface & Coatings Technology*, Vol. 201, Nr. 1-2, pp. 182-188, Sept. 2006

[19] Verleene, A.; Dubar, M.; Dubar, L.; Dubois, A.; Oudin, J.; Determination of a hardening behavior law for a cold forging TiN-coated tool steel. *Surface and Coatings Technology*, Vol.127, Nr. 1, pp. 52-58, May 2000

[20] Attar, F. and Johannesson, T.; Adhesion evaluation of thin ceramic coatings on tool steel using the scratch testing technique. *Surface and Coatings Technology*, Vol. 78, Nr. 1-3, pp. 87-102, Jan. 1996.

[21] Larsson, M.; Olson, M.; Hedenqvist, P.; Hogmark, S.; Mechanisms of coating failure as demonstrated by scratch and indentation testing of TiN coated HSS. *Surface Engineering*, Vol. 16, Nr. 5, pp. 436-444. 2000

[22] Lai, F.D. and Wu, J.K.; Structure, hardness and adhesion properties of CrN films deposited on nitrided and nitrocarburized SKD 61 tool steels. *Surface and Coatings Technology*, Vol. 88, Nr. 1-3, pp. 183-189, Jan. 1997.

[23] Casellas, D.; Caro, J.; Molas, S.; Prado, J.M.; Valls, I.; Fracture toughness of arbides in tool steels evaluated by nanoindentation; *Acta Materalia;* August 2007; Vol.55; Nr. 13; pp.4277-4286.

[24] Dyjak, P. and Singh R.P.; Acoustic emission analysis of nanoindentation-induced fracture events. *Experimental Mechanics,* 2006, Vol. 46, pp. 333-345. DOI 10.1007/s11340-006-7303-x.

[25] Hernandez, R.; Riera, M.D.; Casellas, D.; Valls, I.; Casas, B.; Prado, J.M.; Tool steel selection for cold forming of high strength steels based. Materials Science and Technology (MS&T). Automotive: Advanced High-Strenth and other speciality sheet steels products for automotive industry. Detroit (Michigan, USA), September 2007, pp. 235-243.

[26] Stachowiak, G.W. and Batchelor, A.W.; Engineering tribology, 3rd edition, Ed. Elsevier Butterworh-Heinemann, Burlington, MA, USA, 2005, (pp.571-593).

[27] Mishnaevsky Jr., L.; Lippmann, N.; Schmander, S.; Micromechanisms and modeling of crack initiation and growth in tool steels: role of primary carbides. *Zeitschrift fuer metallkunde/Materials Research and Advaccned Techniques,* Vol. 94, Nr. 6, pp. 676-681, June 2003.

[28] Fischer-Cripps, A.C. and Lawn, B.R.; Indentation stress-strain curves for óquasi-ductileô ceramics. *Acta materialia,* Vol. 44, Nr.2, pp. 519ï 527, Feb.1996.

[29] Zhang, H. and Fang, Z.Z.; Characterization of quasi-plastic deformation of WCï Co composite using Hertzian indentation technique. *International Journal of Refractory Metals & Hard Materials,* Vol.26, Nr.2, pp. 106ï 114, March 2008.

[30] Tarrés, E.; Ramírez, G.; Gaillard, Y.; Jiménez-Piqué, E.; Llanes, L.; Contact fatigue behavior of PVD-coated hardmetals. *International Journal of Refractory Metals & Hard Materials,* Vol. 27, pp. 323ï 331, 2009.

[31] Picas Anfrús, Ingrid. Mechanical behavior of tools for shearing Ultra High-Strength Steels: influence of the microstructure on fracture and fatigue micro-mechanisms of tool steels and evaluation of micro-mechanical damage in tools. PhS. Dissertation. Universitat Politecnica de Catalunya, 2012. http://hdl.handle.net/10803/112059

[32] Huang, M.; Jiang, L.; Liaw, P.K.; Brooks, C.R.; Seeley, R. ; Klarstrom, D.L.; Using acoustic emission in fatigue and fracture materials research, *Journal of Materials*, Vol.50, Nr.11 (web publication) (1998).

[33] Martinez-Gonzalez, E.; Picas, I.; Romeu, J.; Casellas, D.; Filtering of acoustic emission signals for the accurate identification of fracture/ mechanisms in bending tests. *Materials Transactions*, Vol. 54, Nr. 7, pp. 1087-1094, 2013.

[34] Ramirez, G.; Mestra, A.; Casas, B.; Valls, I.; Martinez, R.; Bueno, R.; Góez, A.; Mateo, A.; Llanes, L.; Influence of substrate microstructure on the contact fatigue strength of coated cold-work tool steels. *Surface and Coatings Technology*, Vol.206, pp.3069-3081, 2012.

[35] Studman, C.J. and Field, J.E.. The indentation of hard metals: the role of residual stresses. *Journal of Materials Science*, Feb. 1977, Vol. 12, Nr.2, pp. 215-218.

[36] Abudaia, F.B.; Evans, J.T.; Shaw, B.A.; Spherical indentation fatigue cracking. *Materials Science and Engineering A*, Vol.391, pp. 181-187, 2005.

[37] Rammerstorfer, F.G.; Plankensteiner, A.F.: Fischer, A.D.; Antretter, T.; Hierarchical models for simulating the mechanical behavior of heterogeneous materials: an approach to high speed tool steels. *Materials Science and Engineering* A, Vol.259, pp. 73-84, 1999.

[38] L. Ortiz Berrocal. Resistencia de materiales. Ed. Mc.Graw-Hill (3rd ed.), 2007. ISBN 978-84-481-5636-6.

Chapter 4: Conclusions and Contributions

4.1. Conclusions

In this research AE measurements were successfully applied to detect and identify damage mechanisms in tool steels. The AE measurement procedure has been calibrated for two mechanical tests: fracture test (three-point bending test) and indentation test (spherical indentation).

The fracture tests provoke cracks due to tensile stress. The damage starts with the nucleation of cracks (cracking carbides and local plastic deformation) and afterwards, the cracks grow through the metallic matrix following the broken carbides. The purpose of the research is to present a filtering process that will detect each stage of the fracture: the carbide crack (nucleation), the stage where the crack passes through to the steel matrix and the eventual catastrophic failure.

The spherical indentation tests for the creation of a more complex distribution of stresses in an affected part of the specimen. An elastic field was created in the specimen under the ball indenter applying low level loads. Nevertheless, AE activity was detected in this elastic field,

and these signals were related to the breaking of carbides in the zone of maximum shear stress. An important feature of this test is that the carbide crack is produced without plastic deformation, so the damage signals were clearly identified with the carbide breakage.

Successful AE monitoring must always recognize the presence of noise (extraneous or interfering acoustic signals carrying no relevant data in relation to the investigated process). In both tests the identification of noise sources was essential, and they were isolated or inhibited.

4.2. Contributions

A new acquisition and filtering configuration in fracture tests to eliminate spurious signals due to contact damage between the specimen and the machine supports

In the three-point bending test, the damage mechanisms of interest induced by flexion were also accompanied by another kind of damage due to the test configuration. The high contact pressure between the supports and the specimen surface cause contact damage. This secondary effect is difficult to isolate using classical localization methods if the dimensions of specimen are small, due to the proximity between this mechanism and the ones in question (in the center of the specimen, they occur exactly on the opposite sides of the width). Specifically, it is found that the signal caused by the damage induced by the supports is stronger at the beginning than the one caused by the cracking of carbides and crack propagation, which is the real fracture mechanism in the steels under study. The coexistence of both signals seriously hampers the correct identification and evaluation of the fracture mechanisms. A new filtering method is presented to eliminate the signals related with the contact damage of the raw data.

Identification of different damage mechanisms in specimens with small dimensions

AE waveforms have information about the source that generates it and the medium through which they travel. The small dimensions of specimens produce interfered waveforms that are difficult to interpret. Many reflections of the stress waves are added to the signal in an almost-instantaneous way. Proper interpretation of the AE response during the test was difficult using the whole waveform features. A new analysis of acquired data based on frequency features of the very first cycles of each waveform is proposed in this thesis to classify the different sources of the signals. This classification makes it possible to identify different the signal sources. Thus, it is possible to follow the evolution of the damage mechanisms, which one appears first and at which level of load it appears. The AE results obtained for different tool steels in this thesis confirm the previous works that identify carbide breakage as the cause of the nucleation of cracks in these steels; the growth of these cracks through the metallic matrix has also been identified.

Early identification of carbide breaking

AE monitoring of the mechanical tests, both the fracture and the spherical indentation, permits more precise information to be obtained about the damage that takes place. Superimposing AE with the stress-strain data provides accurate information about the precise instant at which an event takes place. Thus, in these tests it is possible to identify the stress level at which the carbides start to break more accurately than with other conventional techniques.

Results of mechanical tests monitored by means of AE

In both the monitored tests, spherical indention and bending tests, the tool steels presented the breakage of carbides as an incipient damage stage even during the elastic field. Thus, very initial damage occurs in the specimen during the elastic range, and therefore when the specimen is unloading the recovery of the microstructure is not complete, as might be expected. The importance of this point is that during correct loading in-service, tools can present micro-damages which may act as the origin of fatigue cracks.

Reduction of tasks and time in mechanical fracture research

The tool steels under study are very fragile materials. The calibration of an AE system coupled to the fracture test permits the previous prediction of the fracture of the specimen. From the standpoint of materials research, this is a significant improvement in the fracture test. Following the acquired AE signals, the test can be stopped as soon as the first damage occurs, in order to analyze the microstructure in the microscopy or the evolution of cracks can be studied using the AE information. This makes it possible to stop the fracture test in each jump of the crack and photograph or analyze it and then continue loading the specimen. This procedure was used during the experiment to obtain the microscopic images of a crack in its final stages, maintaining the specimen integrity.

The same improvement may be useful in the case of the indentation test, as the AE indentations can be used in unloading the test, to obtain specimens with very incipient damage or with the first induced cracks.

Chapter 5: Future developments

5.1. Future developments directly related to the presented research

The usefulness of AE for the further study of tool steels has been proved. In this thesis, the study of the behavior of these materials was focused on monotonic loads. However, the response that they exhibit when subjected to varying stresses (fatigue) is necessary in order to continue to improve knowledge about the matter.

A predictive maintenance tool using AE could be designed for performance tools. In the automotive industry, for example, performance tools such as punches are crucial parts of the manufacturing process. Currently, AHSS are used to shape these tools and the fragility of these steels referred to above leads to unexpected failures in tools which stop production. In-service monitoring could control the crack length in the tools by means of the AE signal features, allowing for the planned maintenance and changing of tools. It should be noted that all these tools operate under cyclic loading.

Some fatigue tests have been conducted during this study. Three-point bending tests were performed with cyclic loading. The aims of these tests were to find a relationship between the

crack length and AE signal features and prevent the catastrophic failure of the specimen. Some previous results were obtained, and they are consistent with the results presented by other authors in some materials (including some steels). The set-up of these tests required many hours, and some difficulties arose which should be overcome. Mainly, two problems were detected: i) excessive cycling frequency due to the characteristics of the testing machine and ii) the high randomness of the specimen behavior. Some specimens endured only a few minutes of testing while others resisted for hours. Also, the cracks were difficult to follow since they appeared at any point of the tensile surface. This is because grinding small defects acting as a stress concentrator and constitutes the origin of the crack. It would therefore be necessary to repeat the test with notched specimens to control the evolution of the crack from a known point.

In ductile steels, some authors have associated the crack length with the signal counts. Relating some feature of the acquired signals with the length of cracks in tool steels would make it possible to predict the number of cycles remaining to reach the critical length of the crack (in accordance with Parisôs law). With AE activity, this predictive law can be easily applied from the instant that crack appears and it may therefore be useful for predicting the fracture of the specimen.

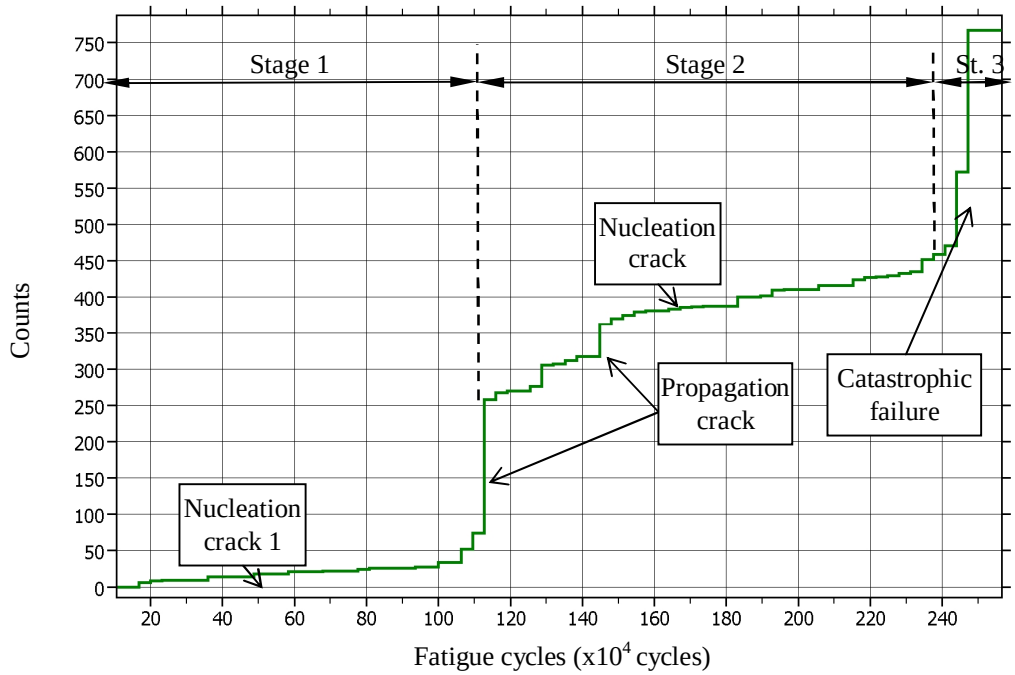

Figure 5.1. Cummulative AE counts versus fatigue cycles during the fatigue three-bending test.

Coupling the AE to the mechanical test allows accurate information to be obtained in real time about the material behavior that would not otherwise be possible, as has been demonstrated in the fracture and spherical indentation test. Consequently, using AE during other common mechanical tests could be a useful tool to ensure the accuracy of the test results. During this research work, the AE technique was applied to micro- and nano- indentation tests and scratch tests. The results are preliminary, but they seem interesting. Continuing with these tests, it is necessary to improve and adapt the signal filtering process, lowering the threshold level to detect very incipient changes in the material.

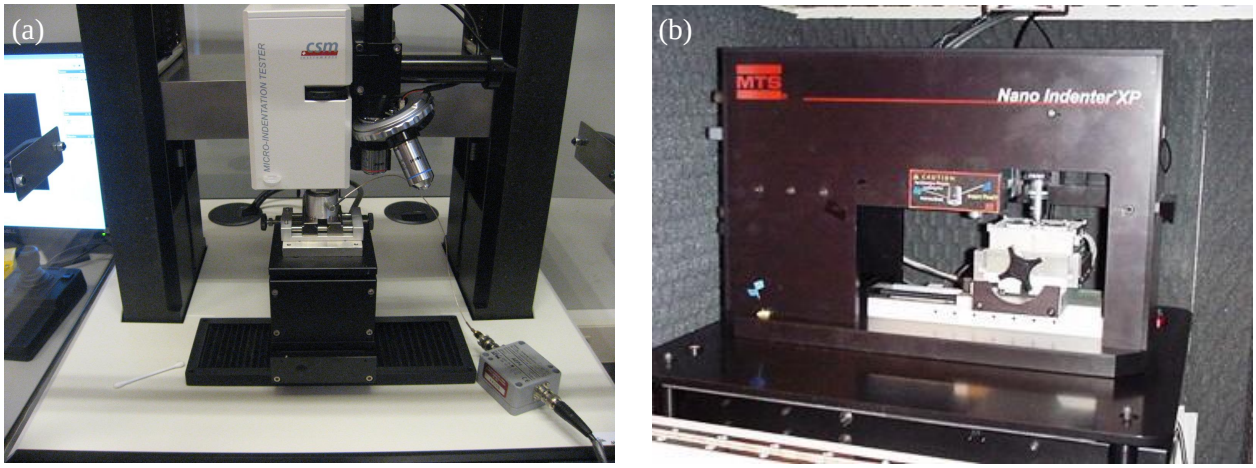

Figure 5.2. (a) Micro-indentation test monitored by means of AE and (b) Nano-indentation test by means of AE.

A future development is to apply the AET to the predictive maintenance of tools. Some very preliminary tests have been done in laboratory punches.

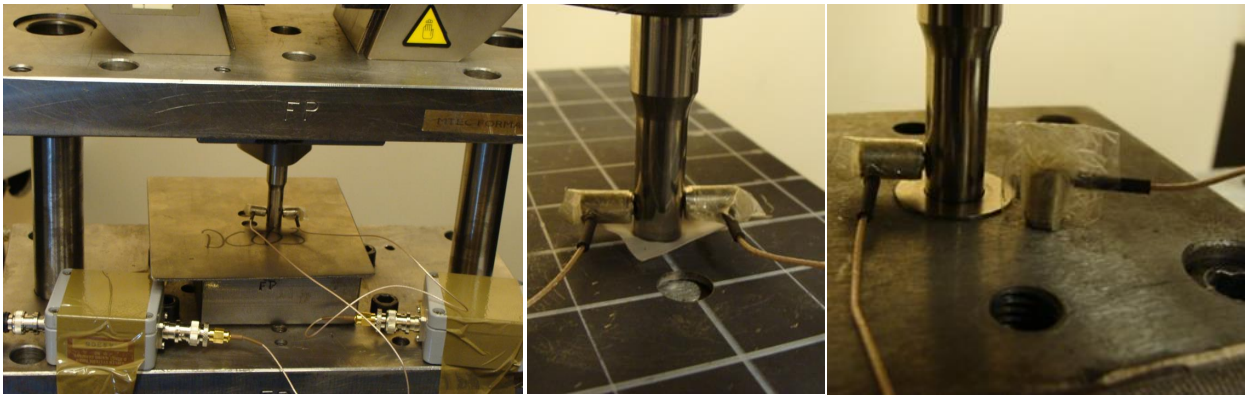

Figure 5.3. Some pictures of a laboratory punch monitored by means AE.

5.2. Other future developments

AE is useful for detecting changes in the material while they occur. This characteristic enables it to be applied in different fields where incipient damage must be detected. Two lines of future work are highlighted below, as they have now been started with successful results:

- Incipient cracks in gear teeth.
- Biomaterials.

5.2.1. Incipient cracks in gear teeth

The first application is the detection of cracks in mobile parts of machines. Some work has been carried out to detect incipient cracks in the tooth of a gear loading by variable bending in laboratory tests (mimicking the behavior of a tooth in service). Although the work is at an early stage, the start of the crack can be thus detected with sensors mounted on the gear and on the shaft that supports it. Progressing in this way, and studying the transmission paths of AE waves, the detection sensors could be removed from the gear. The purpose would be the failure detection of mobile parts by mounting the AE sensors on the fixed parts of the machine such as the bearing supports or the machine casing. This would mean an advance in the preventive maintenance of gearboxes or machine elements which are expected to fail, for the purpose of planning their replacement or repair.

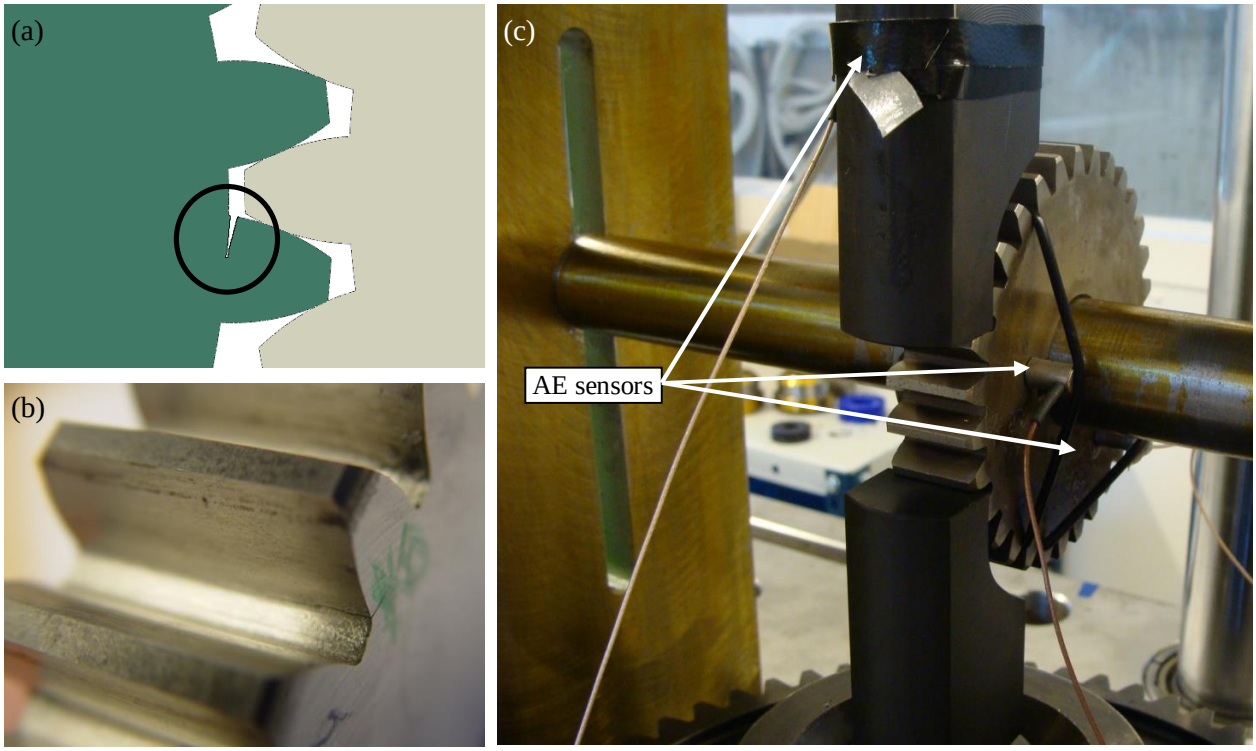

Figure 5.4. (a) Simulated fatigue crack in the tooth of gear, (b) Fatigue crack in the tooth due to a test and (c) Set-up configuration of the fatigue tests with gear teeth monitored by means of AE.

5.2.2. Biomaterials

The second application, which is currently in operation, addresses the study of biological materials. Basically, two types of materials have been tested: bones and the human esophagus, in collaboration with research group GRABI *(Impact biomechanics research group)*.

Bone tests

With the aim of improving seatbelt designs, a study of human rib behavior will be conducted. This is a large study for a wide range of ages. The project consists of determining an experimental stress-strain model for human ribs covering individuals of all ages and sex. The

experimental procedure consists of: tensile tests applied to *coupons* (small specimens of cortical bone extracted from the rib) and three-point bending tests applied to whole human ribs. The deflections are obtained from the images of a high-speed camera filming the tests and the force using load cells. The complex bone formation process makes difficult to detect the incipient fiber breakage from the stress-strain curve. For this purpose, the tests are monitored by AE. The AE activity allows the level of stress (or force) that causes damage to the rib to be identified. Currently, these tests have been performed on pork ribs and the positive results obtained encourage us to continue with human ribs.

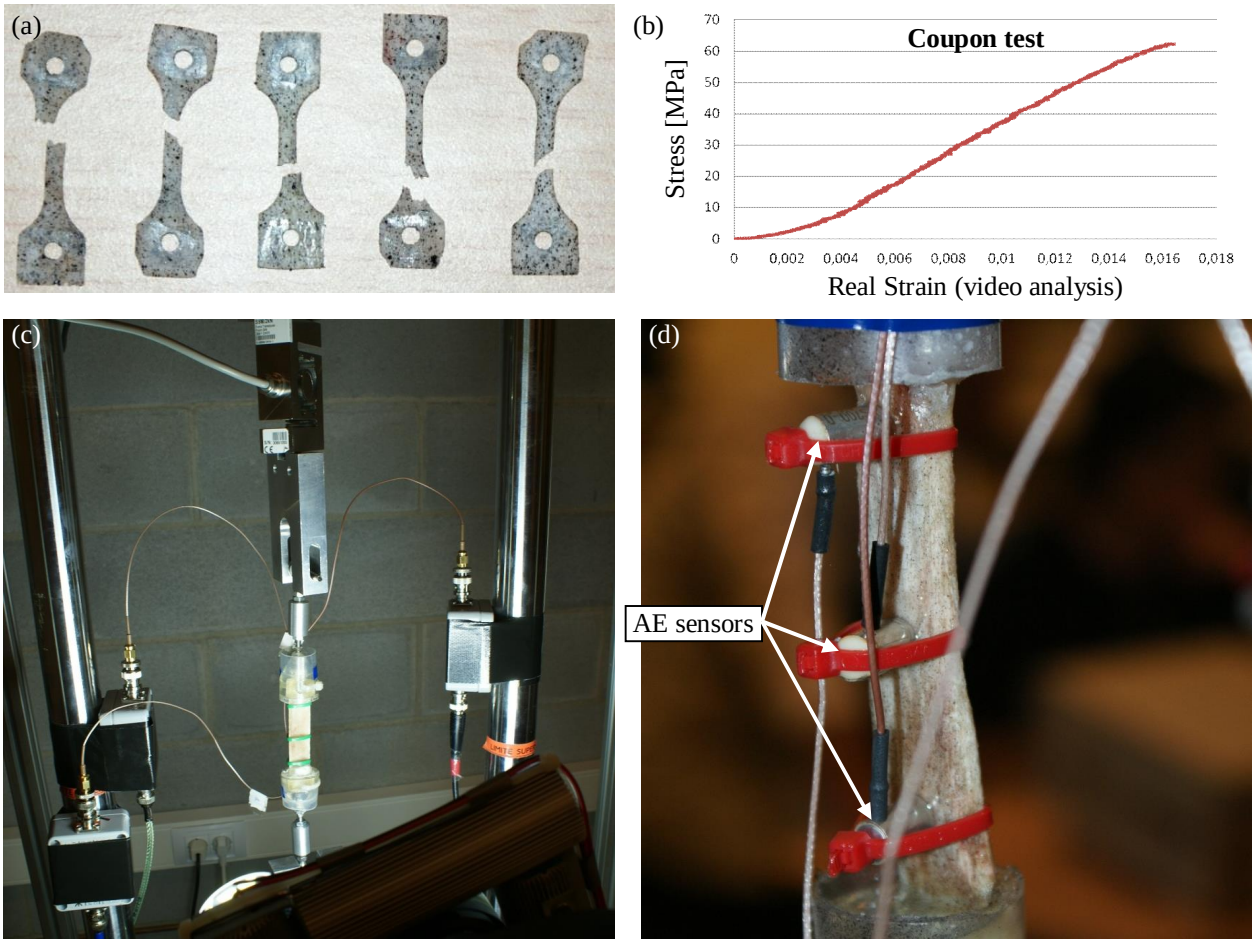

Figure 5.5. (a) Tested coupons, (b) real strain vs. stress of a coupon, (c) tensile test of a pork rib monitored by acoustic emission and (d) detail of the AE sensors attached to the rib.

Esophagus tests

Stenosis is the obstruction of a human duct. In the case of esophagus stenosis, keloids grow on the internal walls of the esophagus which block the esophageal transit. In the most severe cases, the internal opening may be less than one millimeter in diameter. The treatment in such cases consists of inserting a plastic cone or a balloon into the esophagus to break these fibers and reopen the duct. The lack of knowledge about the resistance of the esophagus is a problem in therapy. Physicians can only rely on their experience and intuition during this process. In some cases, mechanical treatment may damage the healthy part of the esophagus. In these particular cases, 50% of the patients die, since the surgery needed to repair it is very complicated and normally there is not enough time.

With the aim of studying the resistance of the esophagus and improving treatment results, David Sanchez Molina is writing his doctoral thesis about this topic. At present some of the tests have been monitored with AE, and the positive results indicate that the cracking of the fibers in this tissue can be detected by means of AE. Future work will be developed in this field.

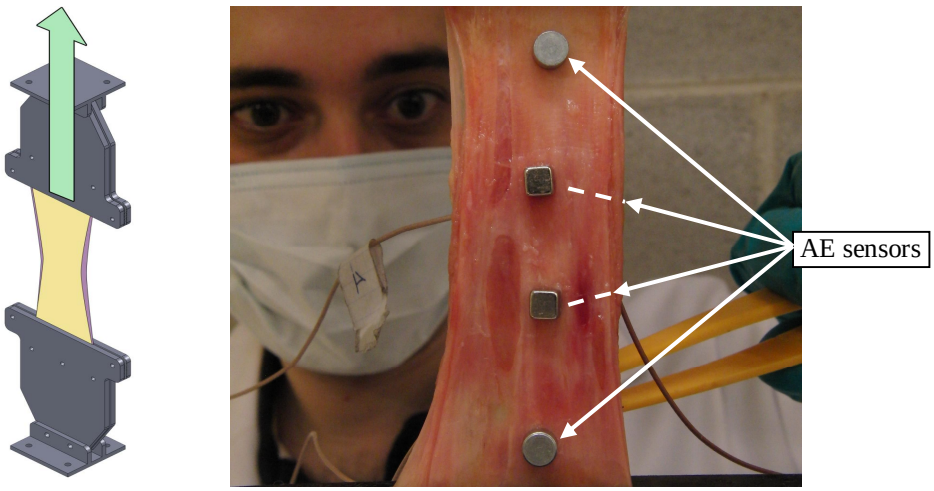

Figure 5.6. Tensile testing of an esophagus monitored by AE.